Department of Internal Medicine I, University Hospital Ulm,

Prof. Dr. Seufferlein

Hepcidin knockout mice as a model of iron-overload associated liver disease

Dissertation presented to the Medical Faculty of Ulm University

to obtain the degree Doctor of Human Biology

Mariia Lunova

Leninakan, Armenia

2013

Current Dean: Prof. Thomas Wirth

Thesis reviewers:

1st reviewer: PD Dr. Pavel Strnad

2nd reviewer: Prof. Thomas Simmet

Date of doctorate awarded: 08.11.13

Table of contents

Abbreviations

ALD	Alcoholic Liver Disease
ALC	Alcoholic Liver Cirrhosis
ALT	Alanine Transaminase
AP	Alkaline Phosphotase
AST	Aspartate Transaminase
ATP	Adenosine triphosphate
BSA	Bovine Serum Albumin
BPT	Bathophenantrolinedisulfonic acid disodium salt hydrate
cDNA	Complementary Deoxyribonucleic Acid
CTGF	Connective Tissue Growth Factor
DAB	Diaminobenzidine
DMT1	Divalent Metal Transporter 1
DNA	Deoxyribonucleic Acid
dNTP	Deoxyribonucleotide
ECM	Extra Cellular Matrix
EPON	Epoxy Resin
ER	Endoplasmatic Reticulum
Fe-S	Iron-Sulfur
FeNTA	Iron III Nitrotriacetic Acid
FTH1	Ferritin Heavy Polypeptide 1
H_2O_2	Hydrogen Peroxide
H&E	Haematoxylin and Eosin
HCV	Hepatitis C Virus
HDAC2	Histone Deacetylase 2
HGF	Hepatocytes Growth Factor
HH	Hereditary Hemochromatosis
HNE	4-hydroxynonenal
HSC	Hepatic Stellate Cells
Hsc70	Constitutively Expressed Chaperone 70
Hsp60	Heat Shock Protein 60
HRP	Horseradish Peroxidase
ICAM	Intracellular Adhesion Molecule
IHC	Immunohistochemistry

KO	Knockout
LC3	Light Chain 3
MCP1	Monocyte Chemoattractant Protein 1
MDA	Malondialdehyde
NTBI	Non Tranferrin Bound Iron
PAGE	Polyacrylamide Gel Electrophoresis
PBS	Phosphate Buffered Saline
PCR	Polymerase Chain Reaction
PDGF	Platelet Derived Growth Factor
POD	Peroxidase
PSR	Pico Sirius Red
PVDF	Polyvinylidene Difluoride
RNA	Ribonucleic Acid
ROS	Reactive Oxygen Species
RT	Room Temperature
SDS	Sodium Dodecyl Sulphate
SD	Standard Deviation
SEM	Scanning Electron Microscope
SH	Secondary Hemochromatosis
TBA	Thiobarbituric Acid
TBST	Tris Buffered Saline containing 0,1% Tween
TEM	Transmission Electron Microscope
TEMED	1,2-Bis(dimethylamino)ethane
TdT	Terminal Deoxynucleotidyl Transferase
TF	Transferrin
TFR1	Transferrin Receptor 1
TFR2	Transferrin Receptor 2
TGFß	Transforming Growth Factor ß
TS	Transferrin Saturation
WB	Western Blot
WT	Wild Type

1 Introduction

1.1 Iron homeostasis

Iron is an essential element which plays an important role in growth and survival, since it is necessary for various cellular processes such as DNA synthesis and repair, regulation of transcription, mitochondria respiration, or oxidative phosphorylation, and other enzymatic functions [1]. It is also required for iron sulphur clusters synthesis (iron sulphur clusters participate in electron transport, catalysis and regulatory processes of the cell) [2], haem synthesis and ferritin production [1,3]. The most important function of iron is to accept and donate electrons, thereby enabling oxygen transport [1,4] and generation of adenosine triphosphate (ATP). The human body contains 4 – 5 g of iron [5] which is found mainly as haem in haemoglobin of erythroid cells (> 2 g) or myoglobin in muscles (about 300 mg). Macrophages from spleen, liver, and bone marrow harbour the transient iron fraction which totals approximately 600 mg, while approximately 1000 mg of iron is stored in parenchymal cells in the form of ferritin [6]. Among the parenchymal cells, liver hepatocytes represent the major iron – storing cells. 1 – 2 mg of the iron is lost every day through excretion via urins, faces, sweat etc as well as physiological blood loss [7]. Lost amount of iron needs to be replaced with iron absorbed from intestine [8]. In fact, intestinal iron uptake represents the only way to regulate iron metabolism and this regulation is executed by hepcidin, the central iron regulator.

1.2 The role of hepcidin in iron homeostasis

Hepcidin was first isolated from plasma and urine filtrates by A. Krause in 2000 [9] and C. H. Park in 2001 [10,11]. The gene encoding hepcidin (HAMP) resides at chromosome 19q13 and encodes an 84 amino acid long precursor termed preprohepcidin. After two cleavage steps, the final 25 amino acid long hepcidin is found. Hepcidin exerts its function through binding and subsequent internalization and degradation of ferroportin, the only

known iron exporter [12]. Thereby iron export from the intestine into blood, the release of iron from macrophages and hepatocytes (Figure 1.1) [13]. Liver hepatocytes represent the predominant source of hepcidin synthesis and hepcidin production is regulated by iron demand [14]. In case of iron abundance, hepcidin concentration increases and limits further iron absorption [15,16]. On the other hand, in case of iron deficiency, hepcidin expression decreases and thereby permits an unrestricted release of iron from the intestine to the plasma [16,17,18,19,20]. However the regulation of hepcidin expression is very complex and increases in response to many processes such as infection and inflammation (via IL – 6 STAT3 signalling pathway) or hypoxia [21].
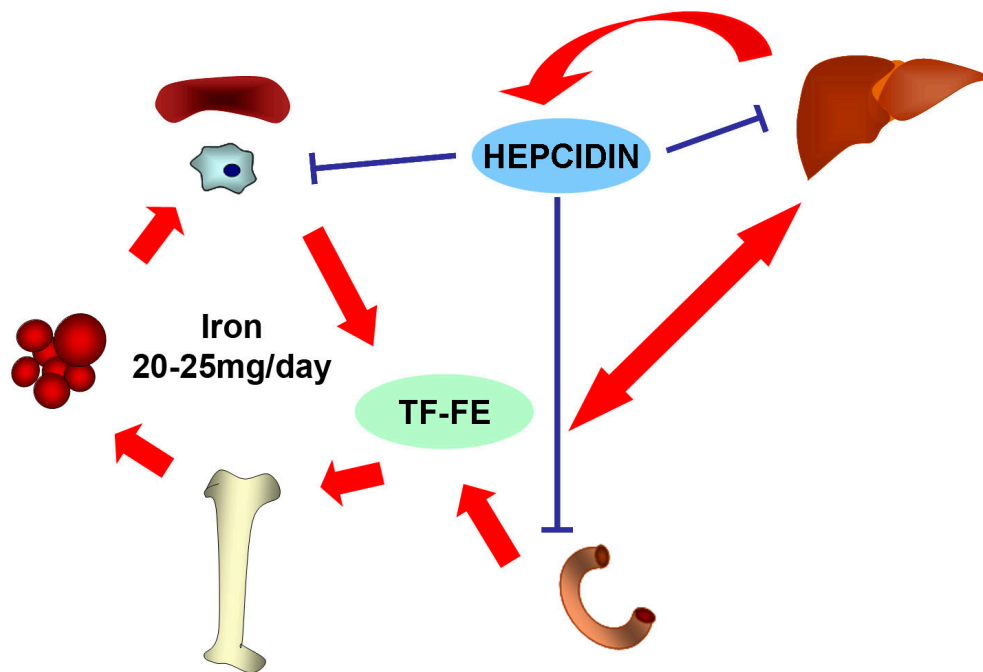
Figure 1.1. Iron distribution in human body. Human body contains about 4 – 5 g of iron. The majority of the iron is found in haemoglobin of circulating red blood cells. Approximately 20 – 30 % of body iron is stored in hepatocytes and reticuloendothelial macrophages bound to ferritin or hemosiderin. Hepcidin is the major regulator of iron metabolism which controls iron release from intestine, macrophages, and hepatocytes.

1.3 Hepcidin – Ferroportin interaction and cellular iron release

It has been shown that binding of hepcidin to ferroportin leads to phosphorylation, internalization, ubiquitination, and finally to lysosomal degradation of ferroportin [22,23]. The 5 N – terminal amino – acid of hepcidin residues are needed for this interaction [22,24,25]. In situations of high hepcidin production, iron is located within the enterocytes and is lost through desquamation of cells into the gut lumen. Ferroportin is also expressed by macrophages and, thereby, hepcidin plays a key role in iron recycling [26]. To that end, senescent red blood cells are phagocytosed by macrophages, iron liberated from haem, and this iron is brought back to the bloodstream via ferroportin, where it is bound to transferrin and redistributed into different tissues. Ferroportin is also found in hepatocytes, the liver parenchymal cells [27]. In summary, hepcidin regulates the amount of ferroportin and release of iron from multiple different cells; and patients in whom the hepcidin – ferroportin interaction is disrupted due to ferroportin mutation, Kupffer cells contain increased amount of iron (Table 1.1).

1.4 Iron overload disorders. Role of hepcidin in iron overload

1.4.1 The role of hepcidin in iron overload disorders

Multiple human conditions result in a dramatic iron overload, which is typically caused by a dysfunction in hepcidin signalling, inappropriately low hepcidin production and/or exogenous iron supply mainly due to repeated blood transfusions. Such an iron overload can damage multiple tissues and lead to many symptoms such as: diabetes, cardiomyopathy, arthritis, bronze pigmentation of the skin, and liver cirrhosis [28]. Mutations in hepcidin or several hepcidin – related genes including HFE, TFR2, and HJV lead to an inherited iron overload and this group of diseases is termed hereditary hemochromatosis (HH). To that end, under normal conditions, the membrane proteins HFE, TFR2, and HJV form a multi – protein membrane complex required for hepatic production of iron hepcidin [29]. Consequently, a defect in HFE [30], TFR2, and HJV

leads to diminished hepcidin expression and results in iron overload (Table 1.1) [28,31].

Mutations in HFE are the most common form of HH accounting for > 85 % of HH cases, with mutations in HJV or hepcidin resulting in particularly severe diseases [28]. Secondary or acquired iron overload usually develops as a result of repeated blood transfusions [32], and/or due to non – physiologically low hepcidin production in hepatic disorders such as hepatitis C or alcoholic liver disease [33,34]. Every millilitre of transfused blood adds about 0,47 mg of iron [35]. In addition, anemia is known to decrease hepcidin production thereby triggering absorption of iron from intestine [19,32]. Therefore, patients with multiple blood transfusions eventually develop iron overload.

Table 1.1. The role of hepcidin in selected human disorders. Black font HH; Blue font SH.

Disorder	Gene name; chromosomal location	Gene function	Hepcidin and consequences
Hereditary Hemochromatosis Type I	HFE; 6p21.3	Interaction with transferrin receptor 1; uptake of transferrin bound iron; modulation of hepcidin expression	**Low** or inappropriately normal; iron overload in liver, endocrine glands, heart
Juvenile Hereditary Hemochromatosis Type II A	HJV; 1q21	Co – receptor of BMP, interacts with BMP6; modulation of hepcidin expression	**Low** or inappropriately normal; iron overload in liver, endocrine glands, heart
Juvenile Hereditary Hemochromatosis Type II B	HAMP; 19q13.1	Up – regulation of iron release by enterocytes, macrophages, and placental cells.	**Hepcidin dysfunctional** iron overload in liver, endocrine glands, heart
TFR2 related Hereditary Hemochromatosis Type III	TFR2; 7q22	Possibly uptake of iron by hepatocytes; precise role of TFR2 remains unclear	**Low** or inappropriately normal; iron overload in liver, endocrine glands, heart
Ferroportin disease Type IV	SLC40A1; 2q32	Ferroportin – iron transporter, regulated by hepcidin. Export of iron from enterocytes, macrophages, placental cells, or hepatocytes	Depending on the mutation site, may lead to iron – deficiency or iron overload
Iron – refractory iron deficiency anemia	TMPRSS6; 22q12.3	TMPRSS6 gene, which encodes the serine-protease matriptase 2 [36] an inhibitor of hepcidin production	**High** level of hepcidin; iron deficiency
Hypotransferrinemia	Transferrin (TF); 3q22.1	Binds and transport iron from the intestine, reticuloendothelial system, and liver parenchymal cells to all proliferating cells in the body	**Low** level of hepcidin, anemia, iron overload in liver and heart
β – Thalassemia intermedia	β – Globin; 11p15.5	Mutant β - globin causes sickle cell anemia	**Low** level of hepcidin due to anemia
Chronic Hepatitis C, alcoholic liver disease		Inappropriately low hepcidin production	Hepcidin level **decreased**
Anemia of inflammation		Inappropriately high hepcidin production due to IL – 6 signalling	**High** level of hepcidin, despite anemia and hypoferremia
Anemia of chronic kidney diseases		Hepcidin inappropriately high due to ongoing inflammation	**High** level of hepcidin, despite anemia and hypoferremia
Alcoholic Liver Cirrhosis		Inappropriately low hepcidin production	Hepcidin level **decreased**

1.4.2 Hereditary hemochromatosis (HH)

The most common inherited disorder of iron metabolism is the HH type I. It constitutes an autosomal recessive disease with mutation in HFE gene. HFE is located at chromosome 6p and encodes an atypical major histocompatibility complex (MHC) class I type molecule [31,37]. Majority of patients with type I HH have point mutation in exon 4 of HFE gene that results in substitution of tyrosine for cysteine at position 282 of HFE protein (C282Y) [28,37]. Other patients are compound heterozygote for C282Y / H63D HFE mutations which result in a mild phenotype. Homozygous C282Y mutation represents one of the most common inherited disorders and are found in people of Northern European origin [38,39]. In the US HFE C282Y mutation is responsible for 80 – 90% of hemochromatosis cases [40]. While homozygotes for C282Y mutation frequently all develop a multiple organ iron overload as a marker [41], the percentage of the disease (i.e. occurrence of clinical symptoms) is relatively low [42]. Similarly, HFE C282Y mutation leads to marked iron overload in mice, however it does not typically lead to tissue damage under basal conditions [43]. The H63D variant is even more common and is found in 15 – 40 % of Caucasians, however homozygous presence of H63D variant is not sufficient to cause disease development [44]. On the other hand, compound heterozygotes C282Y / H63D may develop a disease although the phenotype is milder than the one seen in homozygous HFE C282Y carriers [45]. Reports of several groups show that the disease development in HFE C282Y carriers correlates with the extent of iron overload, albeit this correlation is imperfect [46,47]. The second most common HH form is due to homozygous mutation in the gene encoding the transferrin receptor 2 (TFR2) and was first described in 2000 by Camaschella [48]. Although the role of TFR2 in iron mechanism is incompletely understood, current evidence suggests that TFR2 is involved in cellular iron regulation rather than in iron uptake [49]. TFR2 related hemochromatosis shows relatively late development (3rd – 4th decade of the life) and can lead to heart disease, endocrine disorders

as well as liver damage [50,51]. The most severe type of HH is also known as a juvenile hemochromatosis (JH). It represents an autosomal recessive disorder with severe iron accumulation and disease development in 15 – 20 years old subjects [52]. In addition to elevated transferrin saturation (TS), serum iron, and serum ferritin levels, the patients display impotence and cardiomyopathy. JH might be caused by mutations in the gene coding for HJV (more common, type 2A HH) or HAMP (less common, type 2B HH) [52,53]. In agreement with that, HJV as well as hepcidin knockout mice develop severe iron overload phenotype [54]. Mutations in ferroportin gene (SLC40A1) causes HH type IV which is also known as 'ferroportin disease' [55]. The phenotype of 'ferroportin disease' typically includes elevated serum ferritin level and low or normal transferrin saturation. Dependent on the position of ferroportin mutation, these mutations can lead either to diminished ferroportin levels resulting in macrophages iron overload or to hepcidin resistance (i. e. elevated ferroportin levels) with hepatocellular iron overload [22,25,56]. 'Ferroportin disease' is inherited in autosomal – dominant manner, is typically less severe than HFE but display a large variability dependent on the underlying mutation [57].

1.4.3   Secondary hemochromatosis (SH)

The term Secondary Hemochromatosis (SH) describes a heterogeneous group of disorders, in which the development of iron overload is not due to an inherited mutation in a gene involved in iron methabolism. ß-thalassemia represents probably the best known cause of SH and with at least 60000 individuals being born every year [58,59]. ß-thalassemia arise ß – globin gene which results in its reduced synthesis, ineffective erythropoiesis and deregulation of iron metabolism lead to iron overload due to the need for multiple blood transfusions and increased intestinal iron absorption. Together with the massive haemolysis, iron overload causes accumulation of Non Transferrin Bound Iron (NTBI) which contributes to the observed damage in multiple tissues such as spleen, liver

(predominantly hepatocytes), and bone marrow [60,61]. Several researchers showed that despite the presence of iron overload, hepcidin remains low in patients with ß – thalassemia probably because of the anemia which inhibits hepcidin production [62]. Of note, a crossbreeding of thalassemia mice with homozygous Tmprss6 significantly improved the phenotype of the mice and increased their life span [63]. Another two common disorders which are associated with hepatic iron overload are chronic Hepatitis C Virus (HCV) infection [33] and Alcoholic liver disease (ALD) [34,64]. HCV and ALD represent two abundant chronic liver diseases which may lead to development of liver cirrhosis and hepatocellular carcinoma thereby causing a significant mortality and mobility. It has been reported by Friedmann in 1988 that patients with ALD have twice increased intestinal iron absorption which leads to elevation of serum iron markers even at early age and iron accumulation in liver (predominantly periportal hepatocytes and later in Kupffer cells) [34]. Iron accumulation in ALD is typically relatively mild, but increase with development of cirrhosis. The pathomechanism of iron accumulation in patients with ALC is not completely understood, but it seems to be due to inappropriately low hepcidin expression [65,66,67]. Several researchers showed that alcohol consumption decreases hepcidin levels mainly due to an inhibition of transcriptional factor known to regulate hepcidin expression [65,66,67]. Several studies suggest that iron overload contributes to progression of ALD likely due to the facts that both iron and alcohol leads to generation of Reactive oxygen species (ROS) and thereby to activation of hepatic stellate cells (HSC) with subsequent fibrogenesis [68,69]. In contrast to ALD, the iron accumulation in HCV - infected patients starts approximately at the age of 40 years. Several groups reported that HCV - infected patients displaying hepatic iron overload developed a more severe liver damage [33,64]. Similar to ALD, iron accumulation in hepatocytes of HCV - infected patients is likely due to hepcidin suppression. Hepatic iron overload is thought to lead to generation of ROS as well as to mitochondrial damage [70].

1.5 Iron redistribution and storage

1.5.1 Plasma iron and mechanism of cellular iron uptake

To avoid toxic reactions, most of iron in the blood is bound to plasma proteins. Transferrin (TF) represents the major iron carrier, while minute iron amount is also bound to albumin or citric acid [71]. The major function of TF is to transport iron through the body. Transferrin is a glycoprotein with homologous N – and C – terminal iron binding domains and is synthesized mainly in the liver. Under normal conditions, about 30 % of plasma TF is loaded with iron. To that end, TF – binding is also crucial for cellular iron uptake. The TF – iron complex binds to Transferrin Receptors 1 (TFR1) (Figure 1.2) [72,73] which is expressed on all dividing cells. In contrast to TFR1 transferrin receptor 2 (TFR2) [74] is expressed primarily in the liver and binds to TF – iron (Fe III) complex with much lower affinity [75]. The precise role of TFR2 is unknown, but it seems to be involved in iron sensing rather than iron uptake. Upon binding to TFR1, TF – bound iron (Fe III) is taken up by the cell via receptor mediated endocytosis (Figure 1.2) [76]. Within the endosome, the internalized iron is released from TF, a process which requires an ATP – dependent acidification of endosome as well as reduction of Fe III to Fe II [77,78] . The reduction of FeIII to FeII is mediated by ferrireductase STEAP3 [79]. The ferrous iron is then transported into the cytoplasm by Dvalent Metal Transporter 1 (DMT1) [80]. At acidic pH the apotransferrin (i. e. TF which lost its iron) remains bound to TFR1 and is brought back to the cell surface. After a switch to neutral pH, apotransferrin separates from TFR1 and is releases into extracellular milieu where it can bind the next iron ion [79,81].

Under normal conditions most of plasma iron is bound to TF, and only small fraction remains as NTBI [82]. In case of plasma iron overload, capacity of TF to bind iron is exceeded which leads to high level of NTBI [82,83]. Additionally, free iron is toxic since it produces reactive oxygen species and NTBI serve as an important marker of potentially toxic iron [82]. The precise composition of NTBI is unknown, but they include iron bound

to albumin or small organic acids such as citric [78]. The uptake of NTBI is incompletely understood but seems to involve DMT1 [84,85] (Figure 1.2) and stimulator of iron transport (SFT) which is found on plasma membrane of hepatocytes. Accordingly, expression of DMT1 and SFT is increased in situation of iron overload [84,85,86,87].
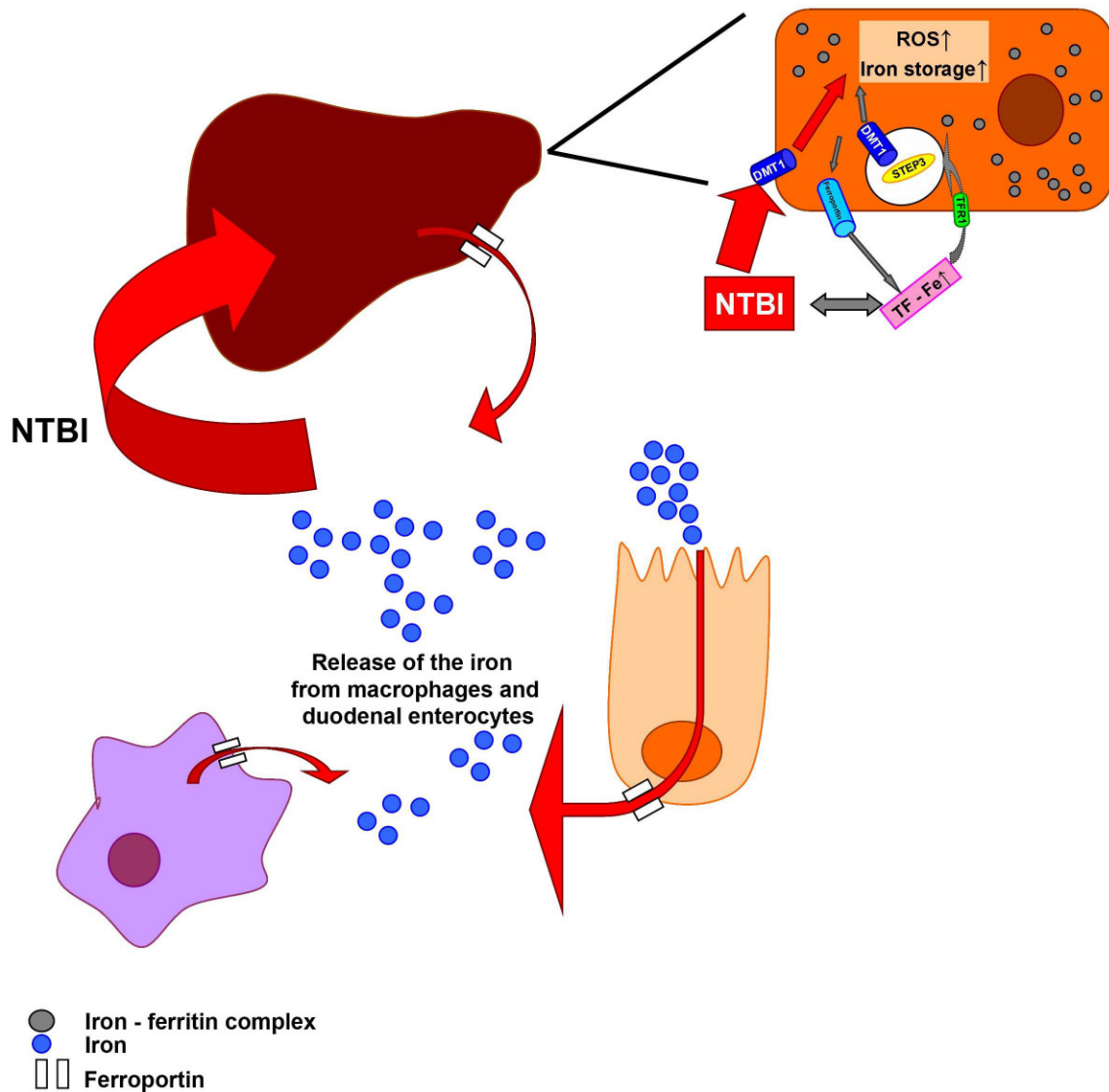
Figure 1.2. Pathogenic model of hepcidin deficient hemochromatosis. Loss of hepcidin signalling leads to development of hemochromatosis (for instance, Hemochromatosis Type 1, 2A and 2B) due to uncontrolled iron absorption by intestine. Elevated iron amount leads to increased amount of NTBI which are taken up and stored by liver hepatocytes. Heavy iron accumulation within the liver may lead to iron toxicity due to production of ROS and disruption of lysosomes. These processes may in term cause apoptosis or other forms of cellular death.

1.5.2   Storage of intracellular iron

Intracellular iron has to be stored in nontoxic form to prevent formation of ROS, but at the same time has to be available for all cellular needs. The most abundant iron storage form constitutes the binding to ferritin (Figure 1.2) [88]. Ferritin is a ubiquitously expressed protein of 450 kDa consisting of 24 subunits which are both of the light (L, 19 kDa) and heavy type (H, 21 kDa) [89]. Up to 4500 iron atoms bound to oxygen can be stored within ferritin, which forms a shell around the iron. Ferritin production is regulated by iron content and hepatic ferritin amount correlates with body iron levels [90]. Under normal conditions, hepatocytes are the major iron – storing and ferritin – synthesizing cells [88]. The majority of this protein is located within the cell, but a small part of ferritin is glycosylated and secreted into the circulation [88]. Of note, serum ferritin constitutes a useful parameter to estimate the body iron stores. The serum ferritin binds iron, but does not significantly affect iron trafficking throughout the body. Extracellular ferritin is quickly removed from the plasma by the liver via binding to a specific ferritin receptor and subsequent endocytosis [91]. Although the majority of the ferritin is taken up by hepatocytes, hepatic stellate cells (HSC) are also able to take up ferritin [88]. Mitochondrial ferritin represents another iron – sequestering protein localizing to mitochondria [92]. Overexpression of mitochondrial ferritin leads to iron sequestration within mitochondria, decrease in cytosolic ferritin and an increase in TFR1 expression [92]. Another important iron storage complex is hemosiderin (see Figure 1.2). Once the liver becomes iron overloaded, ferritin molecules are proteolytically degraded and form hemosiderin aggregates which are able to store even more iron [89]. Iron is also found in iron – sulfur (Fe-S) proteins [2]. This general term describes a family of metalloproteins such as ferredoxins, NADH dehydrogenases, cytochrome c reductase, and nitrogenase, which all contain Fe–S clusters in their structure. Fe–S proteins are found in cytoplasm, mitochondria, endoplasmatic reticulum (ER) and nucleus and assist in many important

cellular functions such as catalysis, electron transport, DNA/RNA synthesis and repair, and iron as well as haem metabolism [2,3].

1.6 Iron toxicity via reactive oxygen species (ROS). Mechanism of oxidative liver fibrosis development

Liver iron is usually stored in the form of ferritin within lysosomes and the cytoplasm as well as in the form of mitochondrial ferritin within mitochondria. In situation of iron overload, lysosomal iron is also stored in the form of hemosiderin [93,94,95,96]. Such an lysosomal iron accumulation is found in hemochromatosis patients [97] and these lysosomes are proins to generation of free iron which leads to oxidative stress and may result in apoptosis [96,98]. Free iron is an established transition metal which catalyses the formation of the highly reactive hydroxyl radicals (*OH) via Fenton and Haber – Weiss reactions [99,100].

$$H_2O_2 + O_2{}^{*-} \xrightarrow{Fe} OH^- + OH^* + O_2 \quad \text{Fenton and Haber – Weiss reaction}$$
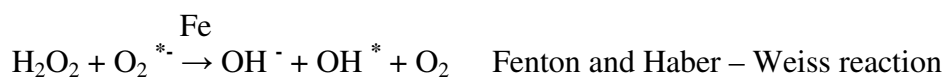
This is why cellular organelles produce ROS as a consequence of unbalanced iron overload. To prevent cellular damage, the ROS have to be detoxified with enzymes such as superoxide dismutase, catalase, and glutathione peroxidases [96,101]. In this protective response, an overwhelming ROS lead to oxidative damage of cellular organelles and membranes causing a leakage of enzymes. It also results in oxidation of amino acids and in DNA strand breaks [70,100]. In particular, hydrogen peroxide in combination with lysosomal free iron leads to lysosomal membrane damage [95,102]. At the same time, iron overload results in mitochondrial dysfunction and inhibition of mitochondrial electron transport chain via peroxidation of cytochrome C oxidase and increase in mitochondrial DNA damage [102]. OH^* groups react with polyunsaturated fatty acids and that leads to generation of lipid radicals as well as formation of peroxyl radicals in the presence of oxygen (Figure 1.3).
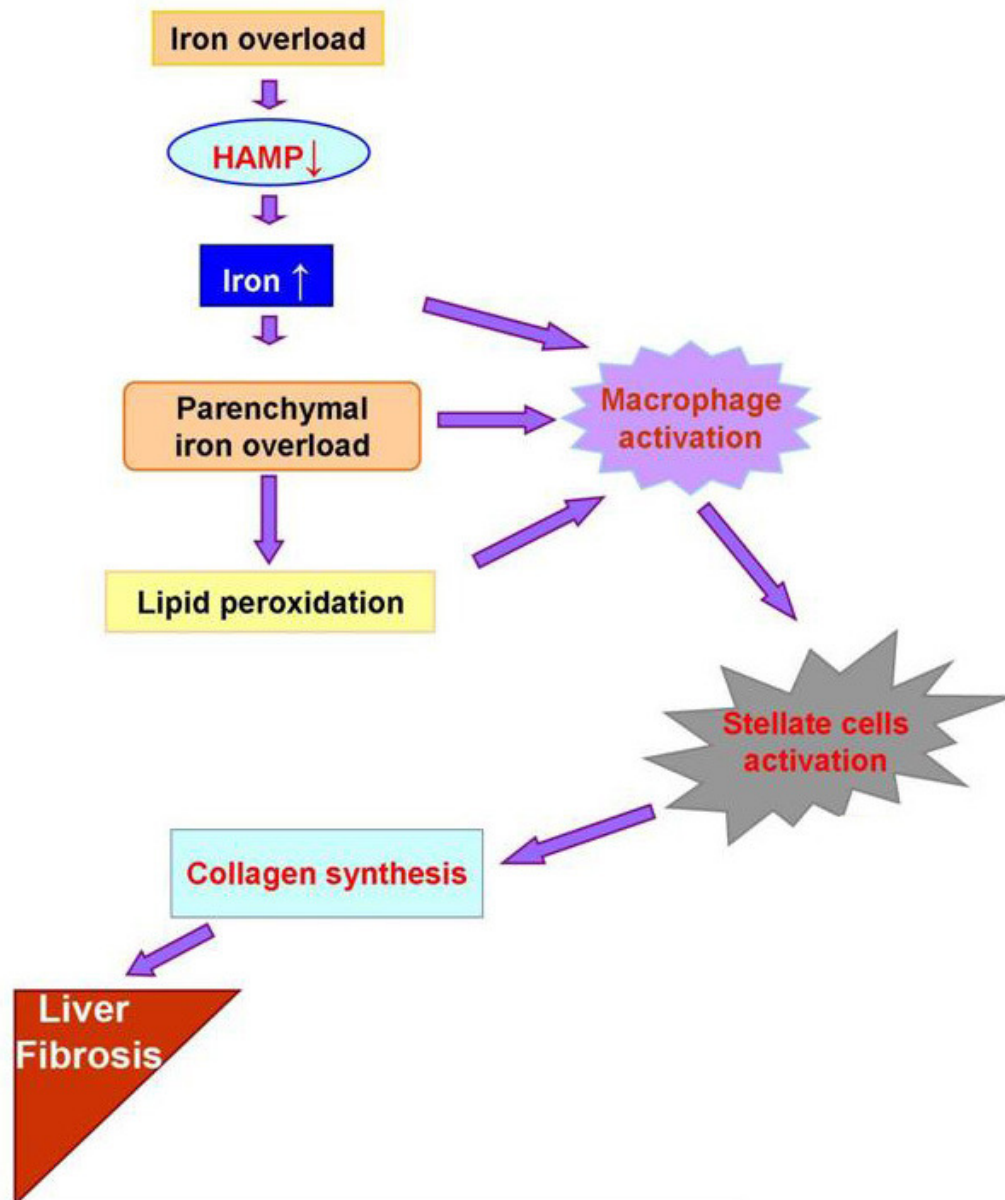
Figure 1.3. Potential mechanism of iron associated liver damage. Inappropriately low concentration of hepcidin leads to iron overload. The liver is the major iron storage organ and hepatocytes are able to store large quantities of iron in a chemically inert form. When this storage capacity is exceeded, unbound iron leads to ROS generation, lipid peroxidation, and subsequent activation of macrophages (both resident termed as Kupffer cells and monocytes recruited from blood stream). Macrophages in term stimulate activation of stellate cells via generation of proinflammatory cytokines. The active stellate cells start to produce collagen and thereby lead to development of liver fibrosis.

The iron induced ROS initiate a cascade of reactions with lipids which leads to generation of end – products such as Malondialdehyde (MDA) or 4-hydroxynonenal (HNE). The presence of MDA in tissues can be detected due to their reactivity with thiobarbituric acid (TBA) which results in formation of fluorescent product [102,103]. Moreover, end – products of lipid peroxidation may react with DNA thereby forming DNA adducts. Last but not least, protein carbonylation, oxidation of amino acids in proteins, inactivation of specific enzymes via oxidation of co – factors. The presence of oxidative stress does not only cause cellular damage, but also leads to inflammation with recruitment of resident macrophages (Kupffer cells) and blood stream macrophages (mononuclear cells) [93,104]. Activated macrophages produce various signalling molecules such as adhision molecules (intracellular adhesion molecule - ICAM), growth factors (hepatocytes growth factor – HGF), profibrogenetic stimuli (connective tissue growth factor – CTGF, platelet derived growth factor – PDGF), cytokines and chemokines (monocyte chemoattractant protein - MCP – 1, transforming growth factor beta TGFß) [105,106,107]. The messenger molecules induce activation of HSC which start producing expression of extracellular matrix (ECM) proteins such as collagen type I/III and fibronectin [108] and thereby lead to development of liver fibrosis [103].

2 Aims of the study

While there is a large body of evidence demonstrating that iron overload precipitates the development of human liver diseases, the underlying pathomechanisms remain incompletely understood. This is in particular due to the fact that there is a lack of animal models leading to development of liver damage as a consequence of chronic iron overload. To overcome this problem, was explored the usefulness of hepcidin knockout animals fed with iron-rich diet as such a model.

Hepcidin knockout mice were chosen given that (i) hepcidin represents the key regulator of iron homeostasis; (ii) hepcidin expression is inappropriately low in multiple human conditions and (iii) mutations in hepcidin lead to particularly severe disease.

By employing this model, there is a hope to gain further insight into the following basic questions of iron biology:

- Is the lack of hepcidin in combination with iron-rich diet sufficient to precipitate the development of liver injury?

- How is the iron storage and trafficking in the liver altered in situations of chronic iron overload?

- What are the precise mechanisms of iron-overload induced tissue damage?

3   Material and methods

3.1   Animal experiments

To study the consequences of multivisceral iron overload, were used previously described hepcidin knockout (KO) mice on C57BL/6N background [54]. Genotyping was performed as previously described [109] with primers given in Table 2.1. To induce iron overload, hepcidin KO mice and their non-transgenic littermates were fed 3 % carbonyl iron - containing diet (Ssniff, D12450B including 3 % Iron carbonate, Sigma) starting at the age of 28 days. The diet was pre-mixed and ordered as pellets (Sniff). Mice fed standard diet (Ssniff, D12450B) were used as controls. Mice were sacrificed at indicated time-points by CO_2-inhalation, blood was obtained by cardiac puncture for measurement of serum parameters and liver was rapidly removed and cut into pieces that were: 1) immediately fixed in 10 % formalin for histological/immunohistochemical (IHC) analysis, 2) snap-frozen in liquid nitrogen for protein analysis, or 3) submerged into RNAlater stabilization reagent (Ambion) for mRNA analyses. The animal experiments were approved by the state of Baden-Württemberg in Germany and the University of Ulm animal care committee and were conducted in compliance with the German Law for Welfare of Laboratory Animals.

3.2   Deoxyribonucleic acid (DNA) isolation

DNA was isolated from mouse tail tips and genotyping has been performed using the DNeasy Blood and Tissue kit (Qiagen). Briefly, the tail tips were digested in a mixture of proteinase K and buffer ATL at 56°C over night. To ensure an optimal binding of DNA to the column, 200 µl buffer AL and then 200 µl 96 – 100 % ethanol (Sigma) were added, samples were thoroughly vortexed after each step and placed onto DNeasy Mini spin columns. During subsequent centrifugation, DNA selectively bound to the column and the flow-through was discarded. To wash the column, 500 µl of AW1 buffer and then 500 µl of AW2 was used, each step followed by a centrifugation. To remove the washing buffer

AW2 completely, the collection tube was replaced with fresh one after first centrifugation and columns were centrifuged once more at 20000 g for 1 minute. To elute DNA from this column, a low - salt elution buffer AE (provided in the kit) with basic pH was used.

3.3 Mouse genotyping

Hepcidin KO and their non-transgenic littermates were genotyped using polymerase chain reaction (PCR). To that end, were used previously described primers [54]- see table 2.1 for details. PCR reaction was carried out with the GoTaq Green Master Mix (Promega) which includes Taq DNA Polymerase, dNTPs, and the appropriate reaction buffers.

Reaction mix:

GoTaq Green Master Mix, 2x   25µl

Primer, each 10µM   0.5µl

DNA template   2.5µl

Nuclease-free water   16.5µl

The reaction mix was placed into PCR tubes and the reaction was started with an initial denaturation of DNA at 94°C for 4 minutes. After that, 40 PCR cycles were performed, such consisting of (i) a denaturation step at 94°C for 30 seconds; (ii) an annealing step at 54°C (optimal primer melting temperature) for 30 seconds, these step enabled this primers to bind to single strand DNA; (iii) extention step performed at 72°C (optimal working temperature for Taq DNA Polymerase) for 30 seconds (extension time is dependent on DNA length and Polymerase, under normal conditions this time is about 10 second per 100bp of DNA). To ensure that all single strands of the DNA fully extended, the final extension was performed at 72°C for 10 minutes and the DNA fragments were stored at 4°C.

3.4 Agarose gel electrophoresis

To estimate the size of DNA products, agarose gel electrophoresis was performed. This method allows separating the molecules based on their size. To that end, negatively charged DNA molecules move through agarose matrix due to an applied electric field. Shorter molecules move faster than longer and migrate further. After PCR amplification, 9μl of the sample was mixed with 1 μl of 6 x DNA Loading Dye (Fermentas) and loaded on 1.5 % agarose gel (Biozym; this gel concentration was used to allow detection of this expected relatively small DNA fragments). For detection of DNA fragments, 0.0005 % ethidium bromide (Sigma) was added. This dye intercalates between two DNA strands and omits fluorescence under UV light. Electrophoresis was performed in TAE buffer at 130 V for 45 minutes. Gene Ruler 50 bp (Fermentas) was used to identify the DNA fragment size.

3.5 Western Blot

All procedures concerning protein isolation and latter application were performed on ice. To avoid the protein degradation, livers were homogenized in 3 % sodium dodecyl sulphate (SDS) homogenisation buffer (buffer described below). After homogenisation, the tissue lysates were centrifuged (14000 rpm, 1 minute) to remove non - solubilized debris. To ensure that samples reach sufficient density to sink to the bottom of the well, liver tissue homogenates were diluted 1 : 2 with 4 x loading buffer which contains glycerol. Protein concentration was determined using the Bio - Rad DC protein assay (Bio - Rad Laboratories). This colorimetric method is based on binding of the dye Coomassie Briliant Blue G – 250 to basic and aromatic amino acid residues which results in a shift in absorbance maximum from 465 to 595 nm. Equal amounts of protein were separated by 10 % SDS-polyacrylamide gel electrophoresis (PAGE, see figure 2.1). Briefly, denatured proteins bind to SDS to ensure relatively constant negative charge and are therefore separated based on their molecular weight. The gels consisted of stacking gel which has large pores and enable concentration of proteins in a thin zones and a resolving gels (10 %

gel was used in most gels), which leads to a separation of proteins based on their size. The electrophoresis was performed at 70 V for 30 minutes (migration thorough stacking gel) and after that at 110 V for 1 hour (migration through resolving gel) using Bio - Rad system. After the electrophoretical separation, the negatively charged proteins were transferred onto PVDF membrane (0.45 µm pore size, Millipore) using constant current of 0.2 A for 80 minutes and a wet - blot apparatus (Bio - Rad). To reduce nonspecific binding to the membrane, PVDF membranes were blocked 1 hour at room temperature with 5 % Milk powder (Roth) dissolved in Tris Buffered Saline containing 0.1% Tween (TBST) buffer. To detect the proteins of interest, the membranes were incubated with primary antibody (diluted in blocking buffer) at + 4°C overnight. Afterwards, at least 5 washing steps (5 minutes each) with TBST buffer were performed to remove the unbound antibody before the membranes were incubated with secondary antibody (diluted in 5 % blocking buffer) for 1 hour at room temperature. After 5 TBST washes, these membranes were incubated with enhanced chemiluminescence reagent (GE Healthcare/Amersham Biosciences). This reagent containing substrate for horse radish peroxides (HRP) and the enzyme coupled to secondary antibodies. The reaction between HRP and this substrate leads to formation of hydrogen peroxide which oxidizes luminal and therefore leads to an emission of light. The antibodies (Abs) used were anti Hsp 60 (heat shock protein 60, Stressgen), cathepsin B (Santa Cruz), cytochrome C (Santa Cruz), FTH1 (ferritin heavy polypeptide 1, Cell Signaling), ß - tubulin (Sigma), HDAC2 (histone deacetilase 2, Cell Signaling), D237 (obtained from MB Omary, University of Michigan) [110], LC 3 (light chain 3, Novus Biological), p62 (Progen), and Hsc70 (constitutively expressed chaperone protein 70, Stressgen).
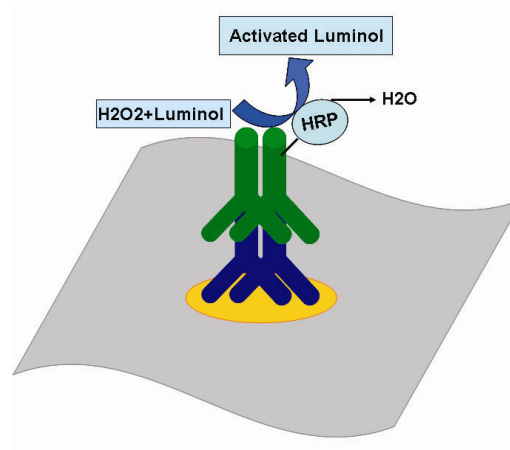
Figure 2.1. Schematic of protein detection by Western blotting. Using SDS - gel electrophoresis, proteins were separated based on their molecular weight. After that, proteins were transferred onto PVDF membrane (gray) and detected by a combination of protein specific primary (blue) and species – specific secondary (green) antibody. The secondary antibody was conjugated to an enzyme named horseradish – peroxidase (HRP). After addition of the substrates, HRP catalyzed the production of H_2O_2 which leads to luminal oxidation and subsequent light emission.

3.6 Subcellular fractionation

To better understand where the iron accumulated inside of the cell, subcellular fractionation was performed. This method allows separating nucleus, mitochondria, lysosomes, autophogosomes, and cytoplasm. Subcellular fractionation was performed as it was described previously by Wattiaux et al [111]. Briefly, the livers were harvested and washed twice with cool (4°C) phosphate buffered saline (PBS Dulbecco, Biochrom) to remove red blood cells. The livers were homogenized in 0.25 M sucrose (Sigma) using a teflon homogenizer (Mikro-Tissue homogenizer) with a ratio between buffer volume and liver weight of 7 : 1. To remove cell debris, the mixture was filtered through two layers of cheesecloth. The flow-trough was collected in tube and centrifuged at 4°C, 2000 g for 5 minutes, and then supernatant was collected in separate tube and kept on ice as supernatant 1. To clear the nucleus fraction from the other fractions, pellet 1 was resuspended in ½ volume of 0.25 M sucrose (Sigma) and centrifuged at 4°C, 2000 g, 5 minutes leading to a separation into supernatant 2 and pellet 2. Both supernatants were put

26

together for latter fractionation and pellet 2 was saved as nuclear fraction. To precipitate further cellular organelles, the supernatant was centrifuged at 17000 g for 12 minutes at 4°C, after which the supernatant was saved as cytoplasm and the pellet 3 was used for isolation of the remaining cellular organelles. For this purpose, a Nycodenz gradient centrifugation was used (Figure 2.2), which allows separating cellular parts according to their size and weight (smaller cellular parts are found in lower density and bigger cellular parts in higher density fraction). To do so, the pellet 3 was mixed with 1.9 ml of sucrose and 2.8 ml of 85.6 % nycodenz (Progen) in water (pH = 7.2) and (see Figure 2.2) transferred to the bottom of an ultracentrifugation tube (Beckmann Coulter). The nycodenz gradient was prepared 2 hours in advance and stored at 4°C. The gradient centrifugation was performed on ultracentrifuge with SW41 rotor for 3 hours at 25000 rpm 4°C. Afterwards, the different layers were carefully collected.
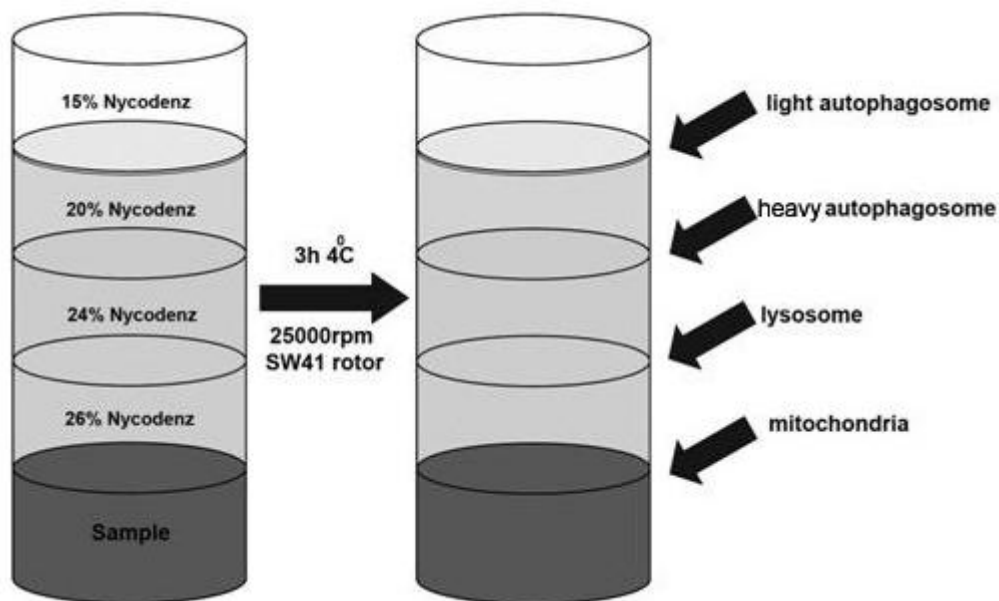
Figure 2.2. Schematic view of subcellular fractionation method based on Nycodenz density gradient. This method allows separation of organelles based on their size. For instance, smaller and lighter particles and found in the lower density layer and vice versa.

3.7   Hydroxyproline assay

To detect collagen amount in liver tissue samples hydroxyproline assay was performed. Hydroxyproline is an amino acid modification found almost exclusively in collagen and plays a key role in collagen stability. Hydroxyproline in liver samples was measured colorimetrically as described [112]. Briefly, liver tissues samples were weighted and homogenized in water. The lysates were hydrolysed in 6 N HCL at 110°C for 18 hours, then filtered to remove debris and evaporated by speed vacuum centrifugation. The pellets or 0.5 – 20 µg of trans-4-hydroxy-L-proline standards (Sigma) were dissolved in 50 µl of distilled water. The oxidation of the samples was performed via addition of 450 µl of 56 mM chloramine –T trihydrate (Sigma) in acetate buffer (pH = 6.5) and incubation for 25 minutes at RT. The detection of hydroxyproline is based on formation of the pyrrole - type chromophore with absorbance at wave length of 562nm. To form the compound, 500 µl of Ehrlich solution was added and this mixture was incubated at 65°C for 20 minutes. After incubation, the samples were measured at 562 nm. The results are presented as means ± standard deviation (SD).

3.8   Serum enzymes concentrations and serum iron parameters

The serum levels of alanine aminotransferase (ALT), aspartate aminotransferase (AST), alkaline phosphatase (AP), serum ferritin, and serum iron were analyzed in the local clinical chemistry department. Data are shown as means ± SD.

3.9   Tissue staining

The harvested livers were fixed in 10 % buffered formalin at RT overnight, embedded in paraffin, sectioned (3 µm), and stained with Haematoxylin and Eosin (H&E), Perls' Prussian Blue as well as Sirius Red staining or were used for immunohistochemistry (IHC).

3.10 Perls' Prussian Blue staining

Formaldehyde fixed liver tissue sections were washed twice with xylol (VWR Prolabo) 10 min each time to remove paraffin and then hydrated with a descending ethanol series (100 %; 96 %; 90 %; 80 % and 70 % - 2 minutes each). Afterwards, the slides were washed with deionized water 3 times for 5 minutes each. To produce blue iron complex liver slides were incubated 30 minutes in a mixture of 2 g of potassium hexacyanoferrate(II) trihydrate (Sigma) dissolved in distilled water and then mixed with 2.7 % HCL in water for pH adjustment. As a next step, the slides were washed in deionized water and stained at RT for 5 minutes with 0.5 % Eosin G-solution (Merk) for visualisation of basic parts of the cell (for instance cytoplasm). After that, slides were washed with deionised water, dehydrated in a graded ethanol series (70 %; 80 %; 90 %; 96 % and 100 % each 1 min) and incubated in xylol for 10 minutes. The slides were covered with glass coverslip using the Entellan medium (Merk).

3.11 Picro-Sirius-Red (PSR) staining

Picro-Sirius-Red (PSR) staining was used for visualization of the fibrotic matrix. Paraffin fixed liver tissues were deparaffinized with xylol and then hydrated with different concentrations of ethanol (100 %; 96 %; 90 %; 80 % and 70 %). Tissue was incubated in water for 5 min and placed into iron haematoxylin solution (Merk) for 10 minutes for visualisation of nuclei. After that, the slides were washed with tap water. A mixture of 500 ml Picric acid solution 1.2 % (Chroma) and 0.5 g of Direct Red 80 (Sigma) was used to stain the fibrotic areas. The staining was performed for 1 hour at RT and samples were washed in deionized water afterwards. Subsequently, the probes were dehydrated via an ascending ethanol series and covered with glass coverslip. Fibrosis score of the livers was evaluated using an established Scheuer scoring system [113].

3.12 Haematoxylin and Eosin staining (H&E)

For overall histological assessment, H&E staining was used. The tissue was deparaffinized in xylol and hydrated with serial dilutions of ethanol (100 %; 96 %; 90 %; 80 % and 70 %). After that, probes were incubated in deionised water for 1 minute at RT. To visualise the nuclei, slides were incubated with haematoxylin solution (Dako) for 5 minutes. After removing the stain via washing with tap water for 5 minutes, samples were placed into 0.5 % Eosin G-solution (see above) for 5 minutes (cytoplasm staining) and were washed with deionised water afterwards. Stained slides were dehydrated with serial dilutions of ethanol and xylol and covered with glass coverslip using Entellan medium (see above).

3.13 Immunohistochemical staining

Immunohistochemistry staining was performed with a mouse ABC Staining System (Vectastain ABC Kit, Vector Laboratories) as described previously [114]. To that end, deparrafinized, hydrated sections were boiled in Antigen Retrieval Solution (Vector Laboratories) and preincubated with 3 % hydrogen peroxide solution (H_2O_2) (Fischer) for 10 minutes to remove endogenous peroxidase activity. To reduce unspecific background staining, slides were incubated with a blocking buffer containing bovine serum albumin (BSA, fraction V) (Serva). After exposure to BSA-containing buffer for 20 minutes, the slides were incubated with primary antibody D237 for 1 hour, washed 3 times with TBST, and incubated with biotinylated secondary antibody for 30 minutes (all at RT). For detection of the specific signal, a chromogenic reporter - AB enzyme reagent (Vector Laboratories) was used. To that end, the slides were incubated with AB enzymes reagent for 30 minutes and washed with TBST. This enzyme reacts with a substrate Vector Nova Red (Vector Laboratories, INC) to yield an intensively colour product that can be analyzed with a microscope. The slides were than dehydrated with graded ethanol series (70 %; 80 %; 90 %; 96 % and 100 % each 1 minute) and incubated with xylol for 10 minutes. The slides were covered with glass coverslip using the Entellan medium (Merk).

3.14 DNA damage staining

DNA damage staining was performed with "In situ Cell Death Detection Kit, POD" from Roche (TdT – mediated dUTP Nick End Labeling). Oxidative damage is known to cause single strand breaks and fragmentation of DNA. The terminal deoxynucleotidyl transferase (TdT) detects these nick ends and ligates fluorescein labelled nucleotides to the free 3'- OH – ends of the DNA fragments. The fluorescein – nucleotide adducts are then recognized by an HRP – conjugated antibody and after addition of substrate visualised in light microscopy.

The staining was performed on paraffin embedded liver sections. Sections were deparaffinized in xylol and hydrated with serial dilutions of ethanol (100 %; 96 %; 90 %; 80 % and 70 %). Then, probes were incubated in deionised water for 1 minute at RT. After that, sections were washed in PBS for 30 minutes and put for 10 minutes into blocking solution containing 3 % hydrogen peroxide in methanol to inhibit the endogen peroxide. Subsequently, probes were shortly washed with PBS, incubated 2 minutes on ice with permeabilisation solution (0.1 % Triton X – 100 / 0.2 % sodium citrate) and another washing step with PBS was performed. One slide was used as a negative control and labelled with 50 µl of Label solution (supplemented in kit), the other slides were treated with mixture of 45 µl Label solution and 5 µl Enzyme solution (the enzyme terminal deoxynucleotidyl transferase (TdT) catalyzes the template – independent polymerization of deoxyribonucleotides to the 3"- end of single and double strand DNA) and incubated at 37° C in a dark, humidified chamber for 1 hour. Slides were washed with PBS 3 times and then were incubated with 50 µl of Converter – POD (peroxidase) for 30 minutes at 37° C in a humidified chamber. After washing with PBS, tissue slides were treated with DAB solution as a POD substrate for several minutes, until the brown colour was detected under light microscope, washed with PBS and then rinsed shortly with 70 % ethanol to reduce

DAB (diaminobenzidine) staining. After that, slides were washed one more time with tap water and were covered with medium and coverslip.

3.15 Electron microscopy staining (EM)

EM was prepared using standard procedure described previously by Walther et al 2003 for visualisation of the cellular organelles and iron distribution in the cell [115]. Liver tissues with thickness of approximately 0.2 – 0.4 mm were placed in the cavity of supporting aluminium plate and surrounded by 1 – hexadecane upon application of a second covering plate. The prepared sample – sandwiches were immediately high pressure (> 2000 bar) frozen in liquid nitrogen using Balzers HPM 010 apparatus with in which they were stored until next step. To bring the samples to RT and make a chemical stabilisation of tissue a few soft rising temperature steps were performed: the samples were replaced for 12 hours into – 90° C with water - free acetone mixture (Acetone, 2 % of Osmiumtetroxid, 1 % of Uranylacetate and 1 % of Methanol and 5 % of water), then – 60° C for 6 hours and – 30° C for 3 hours. After that, samples were brought to RT and infiltrated with epoxy resin (Epon). This preserves the tissue sample in a snapshot of its solution state. The image was created on FEI 300 kV "Titan" Raster-Transmissions Electron microscope using a beam of electrons.

3.16 Determination of nonheme hepatic iron

Hepatic iron content was measured as described previously [116]. Firstly, liver tissue were dried at 120°C for 24 hours and weighted. Subsequently, they were hydrolysed in 1 ml of 100 mM citric acid (Calbiochem) at 60°C for 4 hours. To detect total iron, 500 µl of the samples were mixed well with 500 µl of 100 mM citric acid, 50 µl of L-ascorbic acid (Sigma) which can reduce the iron (III) to iron (II) and then iron (II) react with 100 µl of 5 mM Bathophenanthrolinedisulfonic acid disodium salt (BPS, Sigma) which forms red colour complex with iron. The samples were mixed well and incubated for 30 minutes in the dark to develop the described red – compound iron - complex. The absorbance was

measured with a spectrophotometer at wavelength 535 nm. The data are presented as average ± SD.

3.17 Determination of Non Transferrin Bound Iron (NTBI)

To detect free iron NTBI measurement was performed. Determination of NTBI was done as described [117]. This method consist two steps: first – to produce the FeNTA (iron nitrilotriacetic acid) complex with NTBI and second – to detect the red iron complex with Bathophenanthrolinedisulfonic acid disodium salt hydrate (BPT) as described above. For formation of FeNTA complex, liver tissues were homogenized in water and mixed with 800 mM NTA (mixture of nitrilotriacetic acid disodium salt (Sigma) and trisodium salt (Sigma), pH = 7) in ratio 1:9. To clear the FeNTA from cellular debris and protein mixture, the samples were ultrafiltered using Amicon Ultra 0.5 Centrifugal Filter Unit with Ultracel - 30 membrane (Millipore) with centrifugal force of 3000 g for 1 hour at 4°C. The filtrates were mixed in ratio 1 : 1 with 5 mM MOPS (Sigma) buffer (pH = 7.4). For red complex formation, 50 µl of 120 mM sodium thioglycolate (TGA) (Sigma) in deionised water and 50 µl of 60 mM BPT (Sigma) in deionized water were added into solution and incubated for 30 minutes at room temperature. The complex was measured by spectrophotometer at 535 nm. The data were presented as average ± SD.

3.18 Ribonucleic acid (RNA) isolation

To ensure optimal RNA quality, tissue samples were stored in RNAlater stabilization reagent (Ambion) and the RNA was isolated with a RNeasy mini kit (Qiagen). To that end, ~20 mg of liver was homogenized in lysis buffer containing: 600 µl of RLT + 1 % ß - mercaptoethanol (Sigma). To remove cell debris, the lysate was filtered thought QIAshredder columns (Qiagen) at 14000 rpm for 3 minutes. The liquid was collected and mixed with 600 µl of 70 % ethanol to guarantee appropriate binding of RNA to the column. The complex was transferred onto RNeasy spin columns which bound RNA to their silica-based membrane. After discarding the flow-trough, columns were washed with

buffer RW1. To remove DNA contaminations, columns were incubated with a mixture of RDD buffer - DNase (RNase - Free DNase Set) in ratio 70 µl : 10 µl for 15 minutes at RT. After that, column was washed once with 350 µl of RW1 buffer and twice with 500 µl RPE buffer. To remove the RPE buffer completely, the column was placed onto a new collection tube after the last washing step and centrifuged once more at 14000 rpm for 1 minute. At the end, RNA was eluated with 30 µl of RNase free water provided in the kit. To increase RNA yield, the elution step was performed twice. The concentration of RNA was determined by measuring the absorbance at 260nm in NanoDrop 1000 spectrophotometer (Thermo Scientific). The purity of RNA was calculated as an absorbance ratio of 260 and 280nm.

3.19 Reverse transcription

Each 2 µg of isolated RNA was reverse transcribed using SuperScript II reverse transcriptase (Invitrogen). To that end, RNA was first mixed with 100 ng of random primers (Invitrogen), 0.5 mM of deoxynucleoside triphosphate (dNTP's) (5Prime) and DEPC treated water (Pyrogen free, Invitrogen) was added up to 13 µl of total volume. The mixture was incubated at 65°C for 5 minutes for denaturation of secondary RNA structure and quickly placed on ice to let the primers anneal to the RNA. Then, 2 µl of 0.1 M DTT (Sigma), 4 µl of 5 x First - Strand buffer (provided in kit) and 200 units of reverse transcriptase-SuperScript were added. The transcription was performed at 42°C for 50 minutes. Finally, to stop the reaction, the samples were heated to 70°C for 15 minutes.

3.20 Quantitative real - time PCR (RT – PCR)

Quantitative real – time PCR was performed with a Sequence Detection System (Applied Biosystems 7500 fast Real Time PCR system) using specific primers (Table 2.1) and DNA binding dye SYBR Green which binds to all double strand DNAs in PCR and emits fluorescent light. An increase of the DNA products during PCR leads to increase in intensity of fluorescence which is measured during each cycle of PCR and allows

quantification of the initial, target-gene specific, mRNA level. SYBR Green qPCR Master mix (Qiagen) which contains SYBR Green Dye, AmpliTag Gold Polymerase, and dNTPs with dUTP, was used for amplification and detection. The samples were pipetted into MicroAmp Fast Optical 96well Reaction Plate (Applied Biosystems) and were analyzed in duplicates. At least 4 individual mice were tested for each genotype. The mixtures were composed of 12.5 µl of SYBR Green Master Mix, 1 µl of 10 pM forward and reverse primers, 9 µl of DEPC treated water (Pyrogen free, Invitrogen) and 2.5 µl of cDNA (complementary deoxyribonucleic acid). The plate was sealed with MicroAmp Optical Adhesive Film (Applied Biosystems) to prevent evaporation of the samples. Samples were collected to the bottom of the plate via a centrifugation at 2000 g for 3 minutes and amplification of the product was done using following conditions: initial activation of the enzyme at 95^0C for 10 minutes; 45 amplification cycles each consisting of a denaturation step (95^0C for 15 seconds) and an combination of annealing and extention step ($60°$C for 1 minute). L7 ribosomal protein (Table 2.1) was used as an internal control and cDNA levels were normalized so that L7 expression was equal in all tested mice. Data were analysed using Excel and Statistics programs. After confirming that the amplification efficiency was approximately equal for all genes, the transcript levels relative to L7 were determined and reported as means ± SD.

3.21 Statistical analysis

The results were expressed as average ± SD. The Kruskal Wallis test (nonparametric statistic for multiple comparisons) was used for multi-group comparisons. Differences were considered statistically significant at $p < 0.05$.

3.22 Materials

Antibodies

For western blot (WB), all antibodies were diluted in 5% dry fat milk (milk powder, Roth) in TBST. Incubation with specific antibodies for WB occurred overnight at 4°C.

Secondary antibodies were diluted 1:10000 with 5 % dry fat milk in TBST. For immunostaining, incubations occurred with specific antibodies (diluted in 5 % BSA /TBST) for one hour at room temperature in dark chamber with humidified environment.

Antibody	Company	Cat. No.	Aplication
Hsp 60	Stressgen, Ann Arbor, USA	SPA-805	WB
Cathepsin B	Santa Cruz, Germany	sc-13985	WB
Cytochrome C	Santa Cruz, Germany	sc-13156	WB
Hsc70	Stressgen, Germany	SPA-819	WB
FTH1 (ferritin)	Cell Signaling, Germany	3998	WB
Histone diacetylase 2 (HDAC2)	Cell Signaling, Germany	2570	WB
LC3	Novus Biologicals, Germany	NB100-2220	WB
P62	Progen, Germany	GP62-C	WB
ß-Tubulin	Sigma, Germany	T8328	WB
D237 Keratin 18 (Asp 237)	obtained from MB Omary [110] 55148A, AnnaSpec		WB, IHC

Primers

Primer pairs were designed as 19-21 mer and produced at Biomers. net GmbH, Germany.

Table 2.1. PCR Primers (5'–3') for Genotyping and Real-Time qRT-PCR

Genotyping PCR		
Primer	**Forward**	**Reverse**
musHepc1KO-Scr-F1*	ggctgtagaggttctgctg	
musHepc1KO-Scr-F2*	gctgaagaacgagatcagc	aacagataccacactgggaa
musHepc1KO-Scr-R*		
Real-time qRT-PCR		
Primer	**Forward**	**Reverse**
musHamp	ctgtctcctgcttctcctcct	ggctgcagctctgtagtctgt
musMCP1	cgg ctg gag cat cca cgt gt	ctt tgg gac acc tgc tgc tgg t
mus collagen1a1	tgaagaactggactgtcccaacc	gggtccctcgactcctacatctt
mus TGFß	gcctgagtggctgtcttttga	gctgaatcgaaagccctgtatt
mus STEAP3	aactctgccctgattccaga	atagcagtgccttcgtggac
mus DMT1	catgctgacctctttcccag	ctggccagaataggttccag
mus L7	gaaaggcaaggaggaagctcatct	aatctcagtgcggtacatctgcct

* Genotyping of hepcidin knockout mice.

Kits

Item	Company
0,5% Eosin G-solution	Merck, Germany
Antigen Retrieval Solution	Vector Laboratories, INC., CA
Bio-Rad DC Protein Assay	Bio-Rad Laboratories, Hercules, CA
DNeasy Blood and Tissue Kit	Qiagen, Germany
ECL Western Blotting Detection Reagent	GE-Healthcare, Amersham Biosc.,Munich
Gene Ruler 50bp	Fermentas, Germany
GoTaq Green Master Mix	Promega, Germany
Haematoxylin solution	Dako, Germany
In Situ Cell Death Detection Kit, POD	Roche, Germany
RNase-Free DNase Set	Qiagen, Germany
RNeasy Mini Kit	Qiagen, Germany
SuperScript II Reverse Transcriptase	Invitrogen, Carlsbad
SYBR Green PCR Master Mix	Applied Biosystems, Germany
Vectastain ABC Kit	Vector Laboratories; Inc, Burlingame CA
Vector Nova Red	Vector Laboratories, INC., CA
Weigerts Iron haematoxylin solution	Merck, Germany

Chemicals

Item	Company, ordering number
Acetic acid 100%	VWR Prolabo, 20104.298, Germany
Acrylamide 30%	Roth, 3029.1, Germany

Agarose	Biozym, 840004, Germany, Lonza 50004
Albumin bovine factor V (BSA)	Serva, 11930, Germany
Ammonium persulphate	Sigma, A-3678, Germany
Bathophenanthrolinedisulfonic acid disodium salt	Sigma, 146617, Germany
Bathophenanthrolinedisulfonic acid disodium salt hydrate (BPT)	Sigma, B1375, Germany
Bromphenol blue sodium salt	Sigma, B5525, Germany
Chloramine-T trihydrate	Sigma, 31224, Germany
Citric acid monohydrate	Calbiochem, 231211, Germany
Coomassie Briliant blue R250	Sigma, B0149, Germany
Deoxynucleotides Set (dNTPs)	5Prime, 2900340, Germany
Direct red 80	Sigma, 365548, Germany
DL-Dithiothreitol (DTT)	Sigma, D9163, Germany
EDTA	Roth, 8043.1, Germany
Ehrlich's solution	Sigma, 03891, Germany
Entellan	Merk, 1.07961.0100, Germany
Ethanol	Sigma, 32.205, Germany
Ethidium bromide	Sigma, E1510, Germany
Glycerol	Roth, 7530.1, Germany
Hydrochloric acid (HCL) 35%	VWR Prolabo, 20252.290, Germany
Hydrogen peroxide (H_2O_2) solution 30%	Fischer, 55760, Germany
L-Ascorbic Acid	Sigma, 5960, Germany
Methanol	Sigma, 32213, Germany

Milk Powder	Roth, T145.2, Germany
MOPS(3-(N-Morpholino)propanesulfonic acid, 4-Morpholinepropanesulfonic acid)	Sigma, M1254, Germany
Nitrilotriacetic acid disodium salt	Sigma, N0128, Germany
Nitrilotriacetic acid trisodium salt	Sigma, N0253, Germany
Nonidet P40 (NP-40)	Roche, 11332473001, Germany
Nycodenz	Progen, 1002424, Germany
PBS Dulbecco	Biochrom, L182-50, Germany
Phenylmethanesulfonylfluorid (PMSF)	Sigma, P-7626, Germany
Potassium chloride	AppliChem, A2939, Germany
Potassium Deoxycholate	Sigma, D9750, Germany
Potassium hexacianoferrate (II) trihydrate	Sigma, P9387, Germany
RNAlater	Ambion, AM7024, US
Sodium dodecyl sulphate (SDS)	Roth, 2326,2, Germany
Sodium thioglycolate (TGA)	Sigma, T0632, Germany
ß-Mercaptoethanol	Sigma, M3148, Germany
Sucrose	Sigma, S-0389, Germany
TEMED (1,2-Bis(dimethylamino)ethane)	Sigma, T-7024, Germany
Trans-4-hydroxy-L-proline standard	Sigma, 54409, Germany
Tris	USB, 75825, Germany
Tween 20	Roth, 9127.1, Germany
Xylol	VWR Prolabo, 28975.325, Germany

Other

Item	Company, ordering number
AmiconUltra centrifuge tube	Millipore, 42422, Germany
MicroAmp Fast Optical 96well Reaction Plate	Applied Biosystems, 4346906, Germany
MicroAmp Optical Adhesive Film	Applied Biosystems, 4311971, Germany
PVDF membrane	Millipore, IPVH00010, Germany
Random primers	Invitrogen, 48190-011, Germany
SuperFrost Plus microscope slides	ThermoScientific, J1800AMNZ, Germany
D12450B with 3% carbonyl iron	Ssniff, Germany
Ultracentrifuge tubes	B2B/Beckmann Coulter, 344059, Germany

Laboratory equipment

Item	Company
7500 Fast Real-Time PCR System, with software Sequenction detection Software, Version 1.4	AppliedBiosystems, Germany
Block thermostate	Biostep GmbH, Jahnsdorf, Germany
Centrifuge 5417C	Eppendorf , Germany
Centrifuge 5417R	Eppendorf, Germany
Deep freezer	Heraeus, Kendro Lab products, Germany
DNAEngine Piltier Thermal Cycler	Bio-Rad Lab, USA
Gel electrophoresis equipment and accessories	Bio-Rad Laboratories, USA
Homogenisator	VWR 432-5032, Germany

Ice machine AF200	Scotsman, Germany
Microscope light	Leica Mikrosysteme Vertrieb GmbH, with sofware ''Leica application suite'' Wetzlar, Germany
MS3 Minishaker (Vortex)	IKA, Staufen, Works Inc., Germany
NanoDrop 1000	Thermo Scientific, Schwerte, Germany
pH-Meter DRI-Block	Biostep GmbH, Jahnsdorf, Germany
Photometer Ultrospec 1100 pro	GE Healthcare, München, Germany
Pipet boy	Hirschmann Lab equipment, Germany
Pipets	Eppendorf, Germany
Power supply	Bio-Rad Laboratories, USA
Scale PM 4000	Mettler-Toledo GmbH, Giessen, Germany
Sorvall Ultracentrifuge OTD 50B	DuPONT, Germany
Waterbath	Laboratory technology, Germany

General buffers

TAE Buffer pH 8:

40 mM Tris

20 mM acetic acid

1 mM EDTA

Homogenisation buffer:

SDS(Sodium dodecyl sulphate**)**   3 %

Tris pH 7,8   50 mM

Potassium chloride   150 mM

Nonidet P 40   1 %

Potassium deoxycholate   0.5 %

Spermidine	25 µg/ml

0,1 % Coomassie brilliant blue buffer :

Coomassie brilliant blue	1 g
Methanol	500 ml
Acetic acid	100 ml
Distilled water	400 ml

10 x TBS, pH=7,6:

Tris	24.2 g
NaCl	80 g
Distilled water till	1000 ml

1 x TBS:

10xTBS	100 ml
Distilled water	900 ml

TBST:

10x TBS	100 ml
Distilled water	900 ml
Tween 20	1 ml

APS (Ammonium persulphate) 10 %:

Ammonium persulphate	0.1 g
Distilled water	1000 µl

SDS (Sodium dodecyl sulphate)10 %:

SDS	10 g
Distilled water	100 ml

Resolving gel buffer:

Tris base	181.71 g
Distillate water	500 ml

pH to 8.8 (with HCL)

Distilled water till   1 L

Stacking gel buffer:

Tris base   60.5 g

Distillate water   600 ml

pH to 6.8 (with HCl)

Distilled water till   1 L

4 x SDS Loading Buffer(Laemmli buffer):

1M TrisCl(pH 6,8)   1.5 ml

1M DTT   3 ml

SDS   0.6 g

Bromophenol blue   0.03 g

100% Glycerol   3 ml

10 x Gel Running Buffer:

SDS   50 g

Tris Base   150 g

Glycine   720 g

Distillate water   4 L

Heat up at 70-80°C in a waterbath to dissolve the chemicals

Add distillate water till   5 L

10 x Transfer Buffer:

Tris base   30.48 g

Glycine   72.1 g

Add distillate water till 1L

1 x Transfer Buffer:

10xTransfer Buffer   100 ml

Methanol   200 ml

Distillate water   700 ml

10% SDS Resolving gel:

H_2O, ml	2.05
Resolving gel buffer, ml	1.3
30 % Acrylamide, ml	1.65
10 % SDS, µl	50
10 % APS, µl	25
TEMED, µl	7.5

Stacking gel:

H_2O, ml	1.5
Stacking gel buffer, ml	0.65
30 % Acrylamide, µl	375
10 % SDS, µl	25
10 % APS, µl	12.5
TEMED, µl	2.5

4   Results

4.1   Phenotypic analysis of Hepcidin 1 knockout mouse

To study the mechanism of iron overload associated liver injury, hepcidin knockout mice were used, given that hepcidin represents the central regulator of iron metabolism and human hepcidin mutations leads to a particularly severe disease [15,16]. To that end, we used previously described hepcidin knockout mice generated by replacing exons 1, 2 and part of exon 3 with hygromycin resistance cassette using homologous recombination in Embryonic Stem cells (Figure 4.1.A) [54]. Hepcidin heterozygous mice were bred together in order to obtain hepcidin knockout animals and their non - transgenic littermates. The genotyping was done via PCR (Figure 4.1.B) and the lack of hepcidin expression was confirmed by RT – PCR (Figure 4.1.C) analysis.
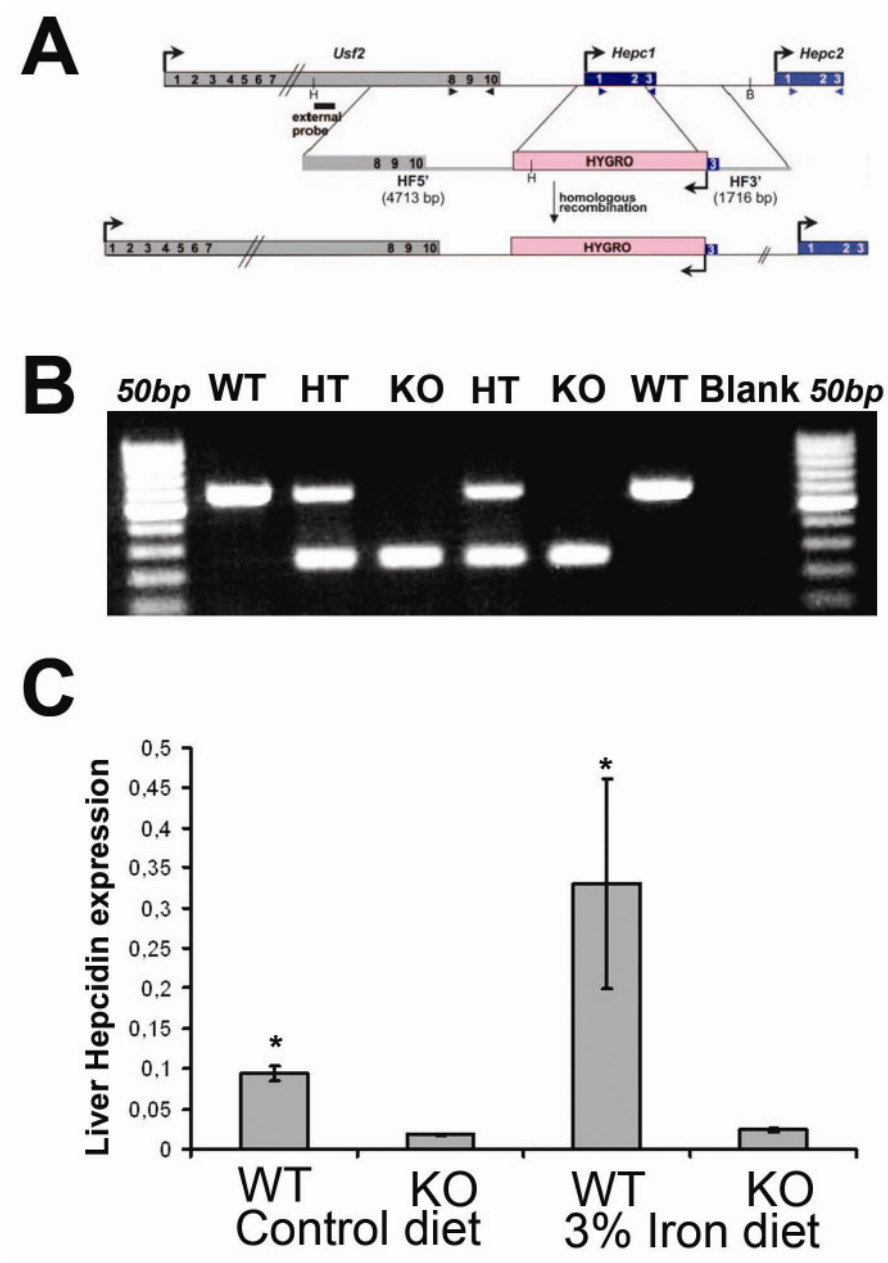
Figure 4.1. Genotypic analysis of Hepcidin 1 knockout mouse. A) Schematic presentation of generation hepcidin 1 knockout mouse. The gene locus containing Usf2, Hepc 1, and Hepc 2 genes is shown on the top, the targeting construct in the middle and the resulting – targeting allele at the bottom. The genes are depicted as colour boxes and arrows highlight the direction of transcription; modified from Lesbordes-Brion et al, 2006. B) Genotyping of transgenic mice via PCR. C) Determination of hepcidin transcript levels using real time RT – PCR. Results are expressed as mean ± SD (n = 5) p < 0.05.

4.2   Experimental iron overload model

To further increase the iron accumulation in hepcidin knockout mice feeding of them iron-rich (3 % iron carbonyl – containing diet) diet [118,119,120] was started at the age of 28 days (Figure 4.2.). Control animals were fed standard chow containing approximately 0.02 % of iron (Ssniff). To study the influence of iron overload on hepcidin level in hepcidin WT mice real time RT – PCR was performed (Figure 4.1.C). In six months old animals fed iron–rich diet, were observed significantly higher hepcidin transcript levels that in mice kept on control diet. Of note, the levels of hepcidin expression were negligible in hepcidin KOs regardless of the treatment regimen.
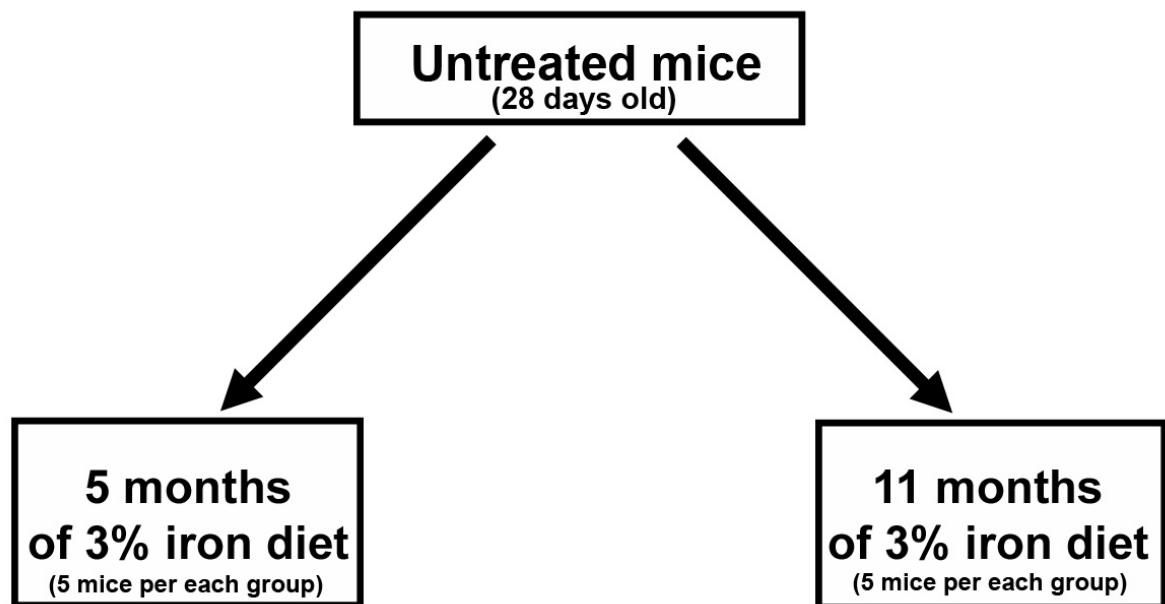
Untreated mice
(28 days old)

5 months of 3% iron diet
(5 mice per each group)

11 months of 3% iron diet
(5 mice per each group)

Figure 4.2. Schematic view of the chronic iron overload model. 28 days old hepcidin knockout and wild type mice were placed on 3 % iron – carbonyl containing (latter like iron-rich) diet or standard chow for 5 and 11 months after which they were sacrificed and analysed. At least 5 mice were used per each group.

4.3 6 months old hepcidin knockout mice on iron-rich diet display elevated transaminases levels

Liver injury was assessed by measuring serum ALT, AST, and AP levels (Figure 4.3. A,B,C). In mice fed standard diet, serum ALT, AST, and AP levels remained within the normal range for both genotypes. After 5 months of iron-rich diet, serum ALT, AST, and AP activity were moderately, but significantly increased in Hepcidin KO mice but not WT animals (Figure 4.3. A,B,C).
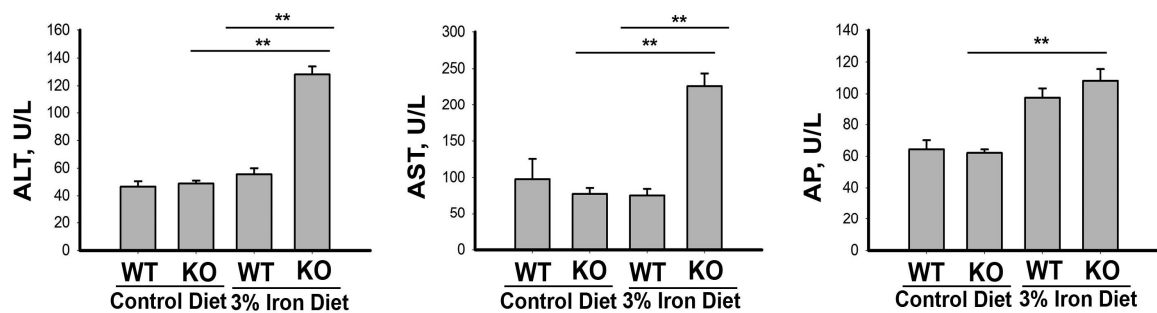

Figure 4.3. Hepcidin knockout mice display elevated transaminases levels after 6 months of iron-rich diet. ALT (A), AST (B), and AP (C) which were used as biochemical markers of liver injury display a moderate increase in hepcidin KO mice after 5 months of iron-rich diet. On the other hand, hepcidin KO mice kept on normal chow do not develop elevated transaminases. Results are shown as mean $\pm$ SD (n = 5). Double asterisk indicate results with $p < 0.05$.

4.4 Hepcidin knockout mice show elevated serum iron parameters

As reported previously [54], 6 months old hepcidin KO mice kept on standard diet display higher serum ferritin levels, while no differences were observed in serum iron (Frigure 4.4.). On the other hand serum ferritin levels were comparable in 6 months old WT mice kept on iron–rich diet and hepcidin KOs on standard chow, whereas hepcidin KO mice on iron – rich diet showed clearly the highest serum iron and ferritin levels. Furthermore, the hepatic NTBI levels were analysed, given that NTBI represents the most reactive iron sub–pool. Among the mice on standard diet, hepcidin KO mice display significantly higher NTBI levels which were clearly higher than the levels seen in WT mice on iron–rich diet. Of note, feeding with iron–rich diet resulted in an approximately two fold increase of NTBI levels in hepcidin KO mice.
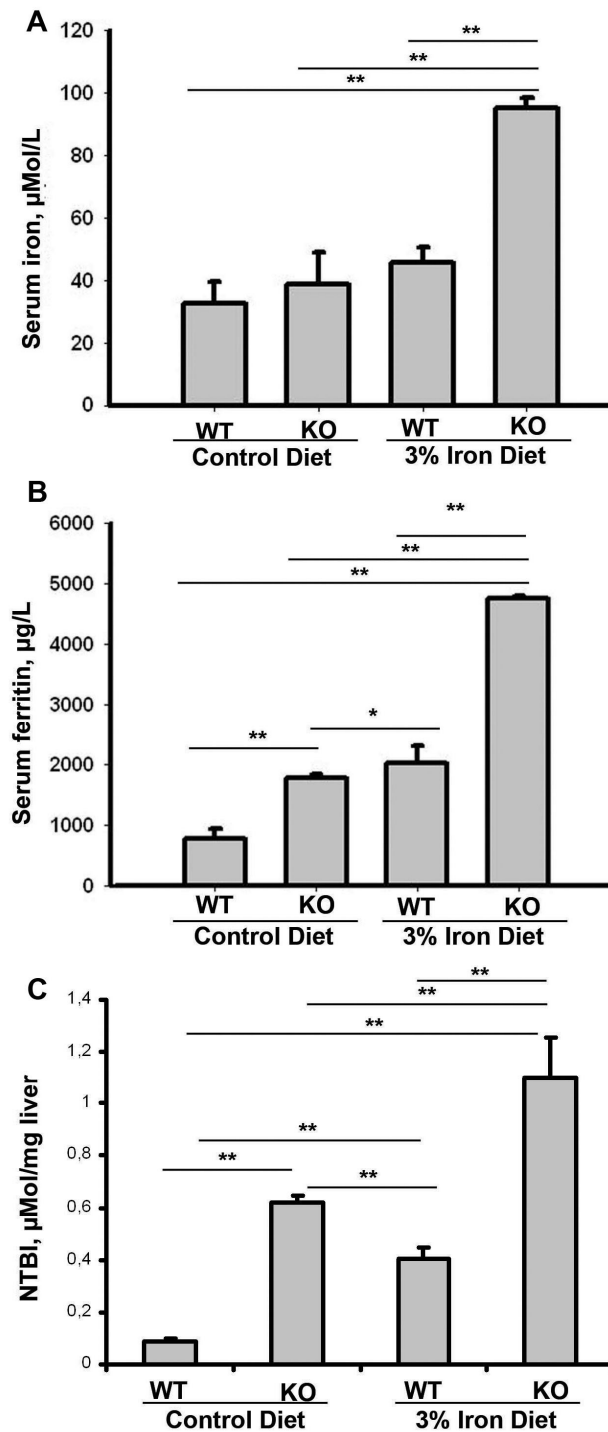
Figure 4.4. Hepcidin knockout mice show elevated serum iron parameters as well as hepatic NTBI levels. The graph summarizes findings obtained from 6 months old hepcidin WT and KO mice kept on normal and iron–rich diet. Note that serum iron (A) and ferritin (B) levels dramatically increased in hepcidin KO mice after treatment with iron-rich diet. C) Hepatic NTBI levels were significantly upregulated in hepcidin KO mice kept on normal diet and further increased in KOs fed iron-rich diet. Results are expressed as mean $\pm$ SD (n = 5) and double asterisk indicate results with $p < 0.05$.

4.5 Accelerated and ubiquitous iron accumulation in 6 months old hepcidin knockout mice fed iron–rich diet

To reveal the iron distribution in hepcidin knockout mice, Prussian Blue staining was performed. Hepcidin WT mice kept on standard diet showed no obvious iron accumulation (figure 4.5.A). In contrast to that, hepcidin knockout mice on standard diet displayed a marked iron overload throughout the liver (Figure 4.5.B). Hepcidin WT mice on iron–rich diet developed prominent iron accumulation in the periportal area (Figure 4.5.C). The highest iron accumulation was detected in hepcidin KO mice fed iron-rich diet (figure 4.5.D). These mice showed a fairly homogeneous iron distribution throughout the liver lobes, but in contrast to the other groups displayed often with rather fine iron staining big iron complexes. To determine the precise extent of iron accumulation total non – heme liver iron content was quantified (Figure 4.5.E). Hepcidin WT mice kept on standard diet harboured low amount of iron (level below 200 µg/mg tissue) comparable to the previously reported values [54]. On the other hand, hepcidin KO mice kept on standard diet displayed significantly increased iron content: 1444 ± 102 µg/mg (Figure 4.5.E) which was comparable to the amount of iron observed in WT animals on iron-rich diet: 1493 ± 136 (Figure 4.5.E). The highest liver iron accumulation was seen in hepcidin KO mice on iron-rich diet: 2543 ± 14 (figure 4.5.D,E). In summary, hepcidin KO mice displayed accelerated iron accumulation as well as altered iron distribution.
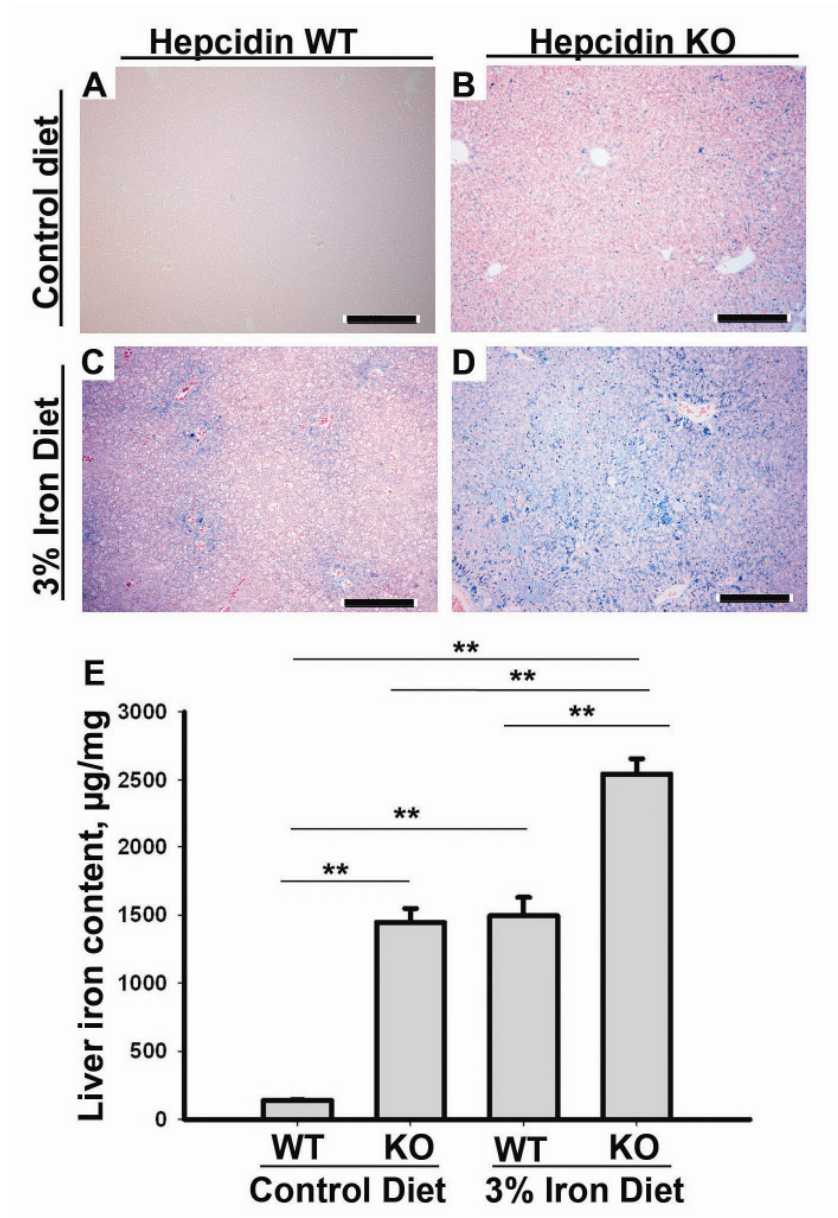
Figure 4.5. Accelerated and ubiquitous iron accumulation in hepcidin knockout mice. Hepcidin WT (A, C) and KO mice (B, D) were fed normal (A, B) or iron-rich diet (C, D) for 5 months. Scale bar 200 µm. E) Biochemical determination of non - heme liver iron content. Note, that hepcidin KO mice on iron-rich diet showed dramatic elevation of liver iron content. Results are expressed as mean ± SD (n = 5) and double asterisk highlights $p < 0.05$. Both, hepcidin KO mice on iron-rich and normal chow developed iron overload, but mice on iron-rich diet accumulated significantly more of iron in the liver. Furthermore, iron is distributed homogeneously throughout the liver in hepcidin KO mice and occasionally forms large complexes, while WT animals displayed fine and show primary periportal iron staining.

4.6   6 months old hepcidin knockout mice develop mild liver injury

In order to characterize the liver injury in hepcidin KO and WT mice, was performed H&E staining (figure 4.6.A-D). On normal diet, hepcidin WT as well as hepcidin KO mice did not show any obvious pathologies in the liver (figure 4.6.A,B). After feeding with iron–rich diet, hepcidin KO but not WT mice displayed a mild liver inflammation (Figure 4.6.D), which was confirmed by morphometric analysis (Figure 4.6.E).
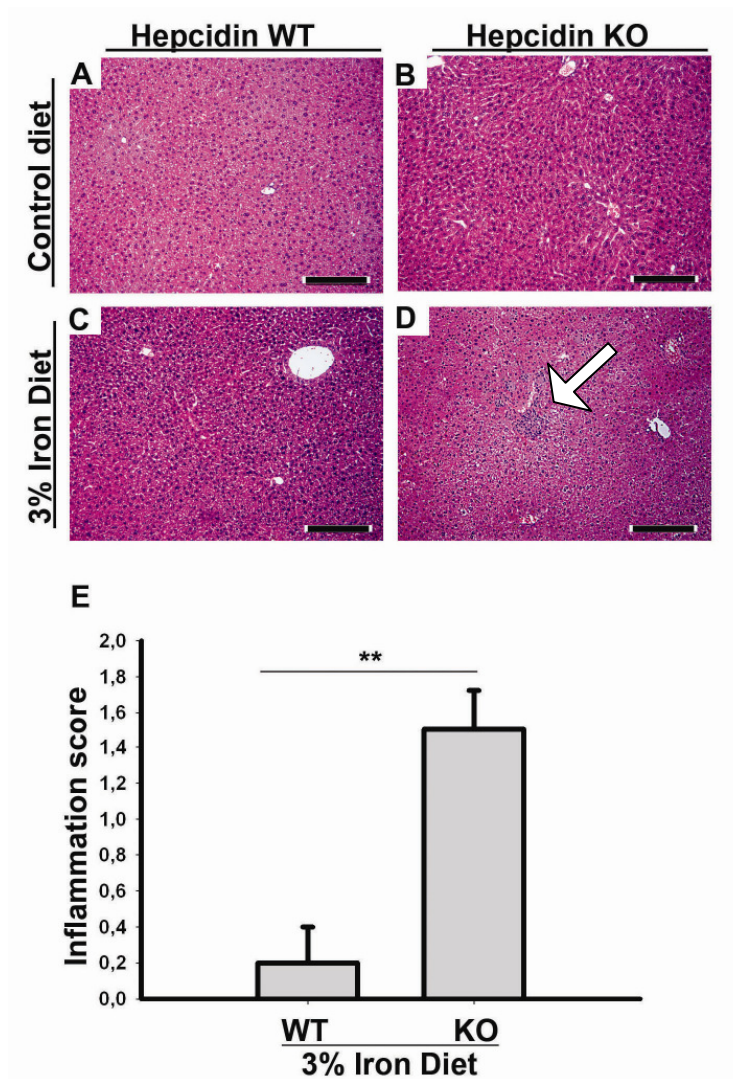

Figure 4.6. Hepcidin knockout mice fed iron-rich diet develop mild liver injury. Representative mouse liver tissues from hepcidin WT mice (A, C) and hepcidin KO mice (B, D) were fed either normal chow (A, B) or iron-rich diet (C, D) for 5 months and were stained with H&E. Scale bar 200 µm. E) Morphometric analysis of liver inflammation. Results are shown as mean ± SD (n = 5) and asterisk highlights p < 0.05. Note, that hepcidin knockouts fed with iron–rich diet develop liver injury.

4.7 6 months old hepcidin knockout mice fed iron–rich diet display a mild chronic elevated expression of inflammatory cytokines

To study the factors leading to liver inflammation in hepcidin KO animals, the expression levels of selected proinflammatory cytokines were analyzed by real time PCR. Compared to nontransgenic mice on control diet non – treated hepcidin KOs and WT mice on iron-rich diet displayed diminished MCP1 levels, while KOs on iron-rich diet displayed significant increase in MCP1 production (Figure 4.7.). Similarly, TGFβ was unaltered in mice on control diet or in WT animals fed iron–rich food, but was significantly elevated in hepcidin KO mice on iron–rich diet. Therefore, it was concluded that hepcidin knockout mice showed production of inflammatory cytokines when fed iron–rich diet.
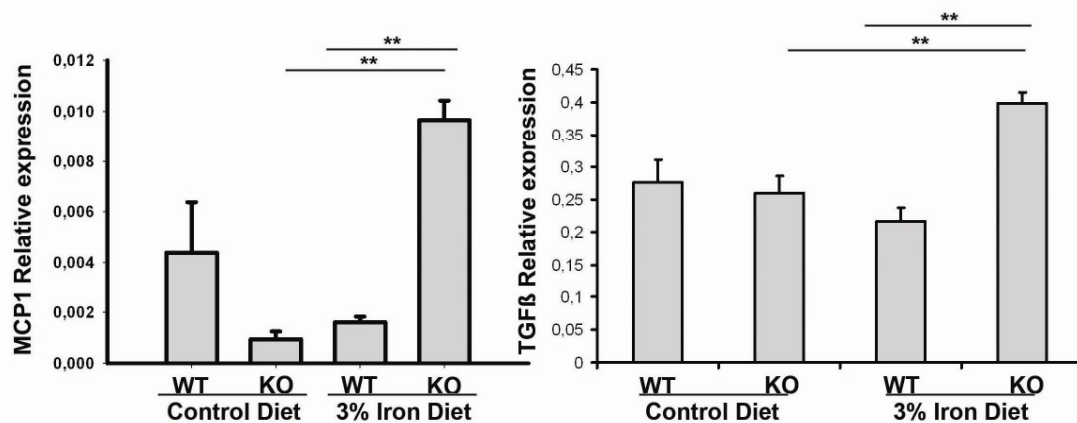

Figure 4.7. Hepcidin knockout mice on iron-rich diet display elevated expression of inflammatory cytokines. Hepcidin KO mice on iron-rich diet showed significantly increased expression of Monocyte chemoatractant protein - MCP – 1 (A) and Transforming growth factor beta - TGFß (B) as determined by real time RT - PCR. Results are shown as mean ± SD (n = 5) and double asterisk highlights $p < 0.05$.

4.8 Hepcidin knockout mice on iron–rich diet display elevated liver apoptosis

The initial histologic evaluation suggested elevated amount of apoptotic hepatocytes in hepcidin KO mice on iron–rich diet which was supported by morphometric analysis (Figure 4.8.E). To further confirm these findings, was performed IHC staining with D237 antibody (Figure 4.8.A-B), which recognizes the caspase – cleaved keratin 18 fragment [110]. Hepcidin KO mice fed iron-rich diet showed a marked increase in apoptotic level

(figure 4.8.D), while only minimal apoptosis was seen in the other groups (Figure 4.8. D). These findings were further substantiated by immunoblot analysis with the same antibody, which displayed clearly elevated apoptosis levels in hepcidin KO mice on iron–rich diet, while only moderately elevated apoptosis was seen in hepcidin KO mice on standard diet or WTs fed iron–rich chow (Figure 4.8.F).
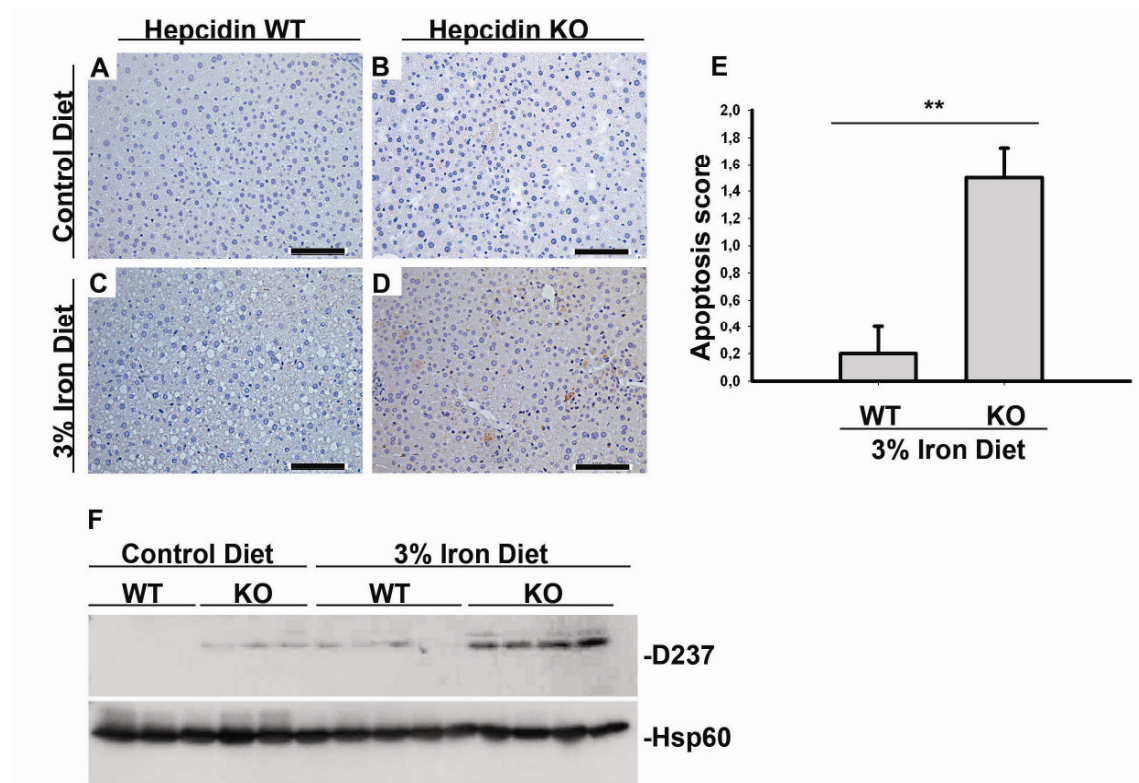

Figure 4.8. Iron-rich diet leads to activation of apoptosis in hepcidin knockout mice. Immunohistochemistry staining was carried out on liver tissues (A – D) with D237 antibody detecting a caspase – cleaved keratin 18 fragment. 6 months old hepcidin WT (A, C) and KO mice (B, D) fed normal chow (A, B) and iron-rich diet (C, D) were analyzed. Scale bar 200 µm. E) The extent of liver apoptosis was scored in H&E stained liver sections and results were presented as mean ± SD (n = 5) and asterisk highlights $p < 0.05$. Extent of apoptosis was determined by immunoblot analysis (F) using D237 antibody. Hsp 60 was used as a loading control.

4.9 6 months old hepcidin knockout mice fed iron–rich diet show signs of hepatic stellate cells activation, but no significant liver fibrosis

To test, whether hepcidin KO mice with chronic iron overload develop liver fibrosis, Sirius red staining, hydroxyproline assay, and collagen real time PCR were performed (figure 4.9.A-F). Using these methods, significant elevation of collagen expression in hepcidin knockout mice on iron - rich diet was detected (figure 4.9.F), thereby showing HSCs activation. However, 6 months old hepcidin KO mice fed iron–rich diet did not show a significant collagen deposition as confirmed by Sirius red staining and hydroxyproline assay (figure 4.9.A-E).
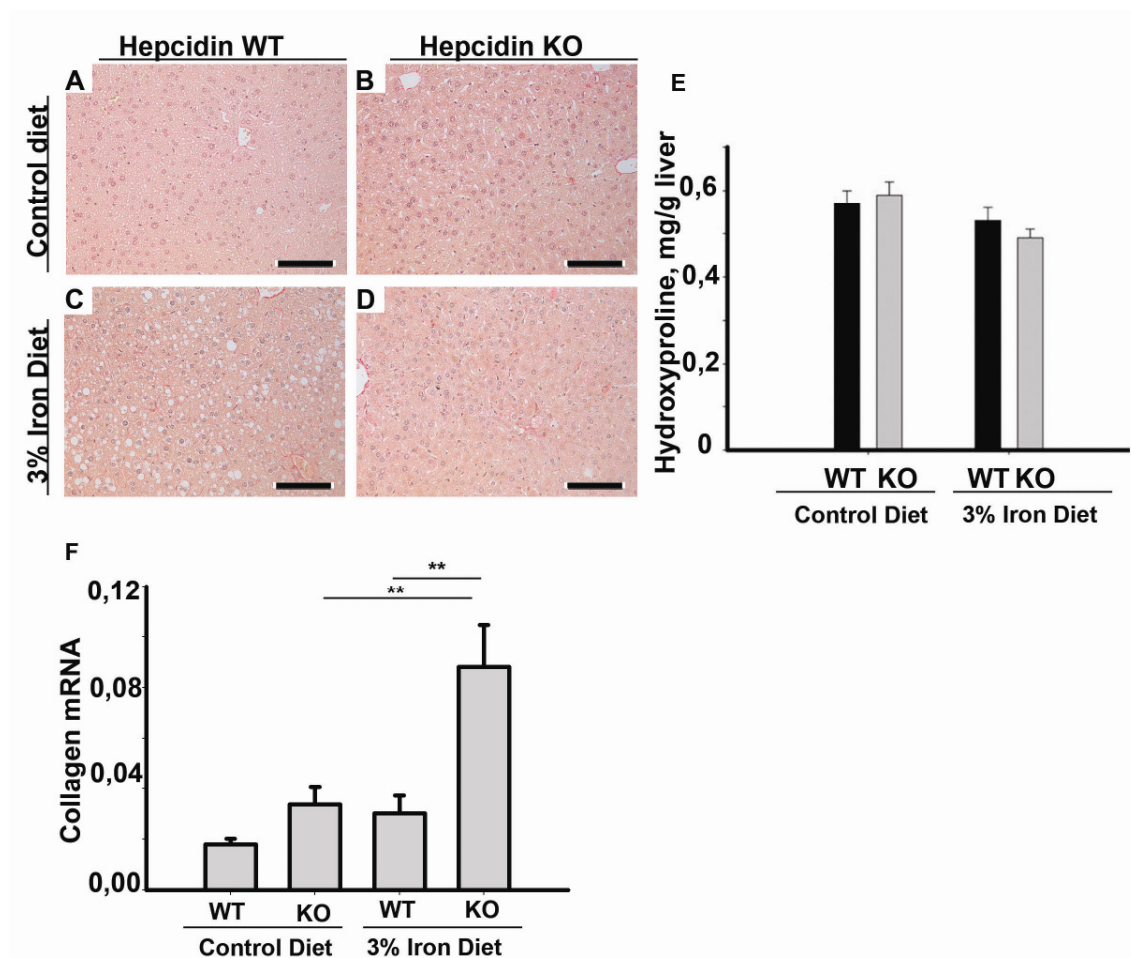

Figure 4.9. 6 months old hepcidin knockout mice fed iron–rich diet show signs of stellate cells activation, but not significant liver fibrosis development. Sirius red staining of liver sections from hepcidin WT (A, C) and KO mice (B, D) fed with iron-rich (C, D) or kept on standard chow (A, B). Scale bar 100 µm. Liver hydroxyproline content was measured in hepcidin KO and WT mice on both, iron-rich and

standard chow (E) and results were presented as mean ± SD (n = 5). Collagen mRNA level was determined using real time RT – PCR and data are shown as mean ± SD. Double asterisk highlights p < 0.05.

4.10 12 months old, iron–rich diet fed hepcidin knockout mice develop moderate liver injury

To study the effect of even more pronounced iron overload, mice were kept on iron–rich diet until the age of 12 months and serum ALT, AST and AP were measured (Figure 4.10.A, B, C). In mice on normal diet as well as in WT animals on iron–rich diet, ALT, AST, and AP levels were not grossly elevated and did not show any obvious differences between the groups. On the other hand, all parameters were clearly elevated in hepcidin KO mice kept on iron-rich diet (Figure 4.10.A, B, C). Therefore, it was concluded that hepcidin KO mice on iron-rich diet showed significant signs of liver injury.
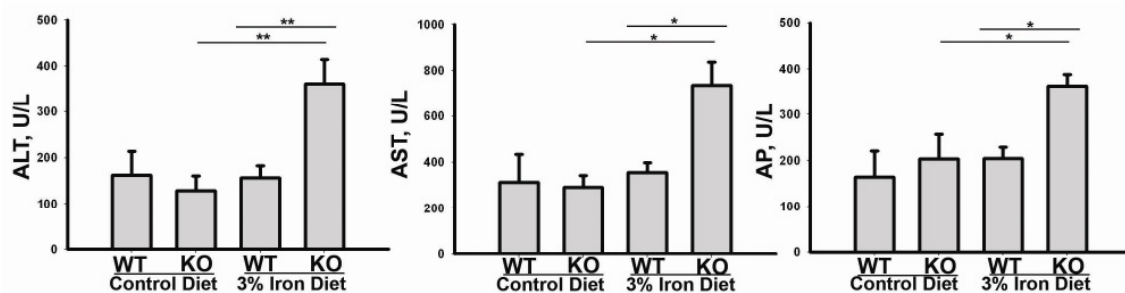

Figure 4.10. 12 months old hepcidin knockout mice fed iron–rich diet develop obvious liver injury.
Serum ALT (A), AST (B), and AP (C) levels were determinated in hepcidin WT and KO mice kept on normal or iron–rich diet. Note, that all parameters are significantly increased in hepcidin knockouts on iron–rich diet. Results are presented as mean ± SD. Asterisk and double asterisk highlights p < 0.05 and p < 0.005, respectively.

4.11 Hepcidin knockout mice develop progressive iron overload at 12 months

To evaluate the mechanism of liver injury in these animals, selected parameters of iron metabolism were quantified. Serum iron levels in mice kept on standard diet as well as WT mice on iron–rich diet remained within the normal ranges with values below 100 µM/L. However, iron-rich diet led to dramatic increase in serum iron levels in hepcidin KO mice (Figure 4.11.A). Furthermore, hepcidin KO mice and their nontransgenic littermates kept on normal diet show comparable ferritin levels. On the other hand, when fed iron–rich diet, both genotypes developed significant increase of serum ferritin (figure 4.11.B) which was more pronounced in hepcidin KO mice. Moreover, measurement of liver NTBI showed a moderate increase in NTBI levels in hepcidin KO mice on normal as well as WT mice on iron–rich diet, while grossly elevated NTBI levels were seen in hepcidin KO mice on iron-rich diet (figure 4.11.C). Taken together, hepcidin KO mice developed massive iron overload when fed with iron–rich diet over a long period of time.

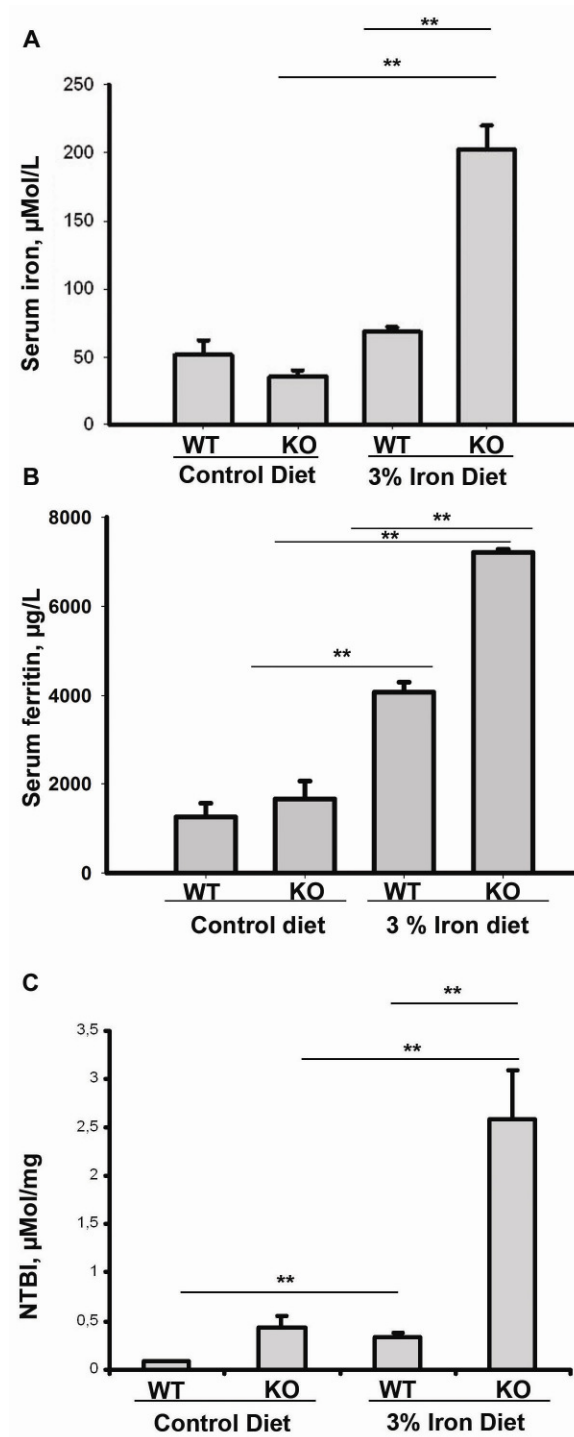**Figure 4.11. 12 months old hepcidin knockout mice kept on iron–rich diet develop massive iron overload.** Serum iron (A), serum ferritin (B), and liver NTBI (C) levels were measured in hepcidin WT and KO mice fed with iron-rich and standard chow. Hepcidin KO mice on iron-rich diet showed a dramatic increase in all iron parameters. Result are presented as mean ± SD, double asterisk highlights $p < 0.05$.

4.12 Hepcidin knockout mice show dramatic deposition of iron in liver

To evaluate iron distribution in 12 months old animals, Prussian Blue staining was performed (figure 4.12.A,C). Liver section from hepcidin WT mice on standard diet did not show any obvious iron accumulation (figure 4.12.A) and the liver non – heme iron content remained below 500 µg/mg of tissue. In contrast to that, hepcidin KO mice fed standard diet showed iron accumulation equally distributed throughout the liver lobes (Figure 4.12.B). Both genotypes subjected to iron–rich diet accumulated a significant amount of iron in their livers. As noted previously, iron accumulation in WT mice was seen in the periportal area (Figure 4.12.C), while iron accumulation was found in the whole liver in hepcidin KO mice, where a presence of big iron complexes was also noted (figure 4.12.D). Quantification of non – heme liver iron content revealed in all these experimental groups where iron leads being KO on iron–rich more than WT on iron–rich more than KO on control more than WT on control diet (Figure 4.12.E). Therefore, one can conclude that hepcidin KO mice on iron-rich diet displayed a dramatic iron accumulation in the liver.
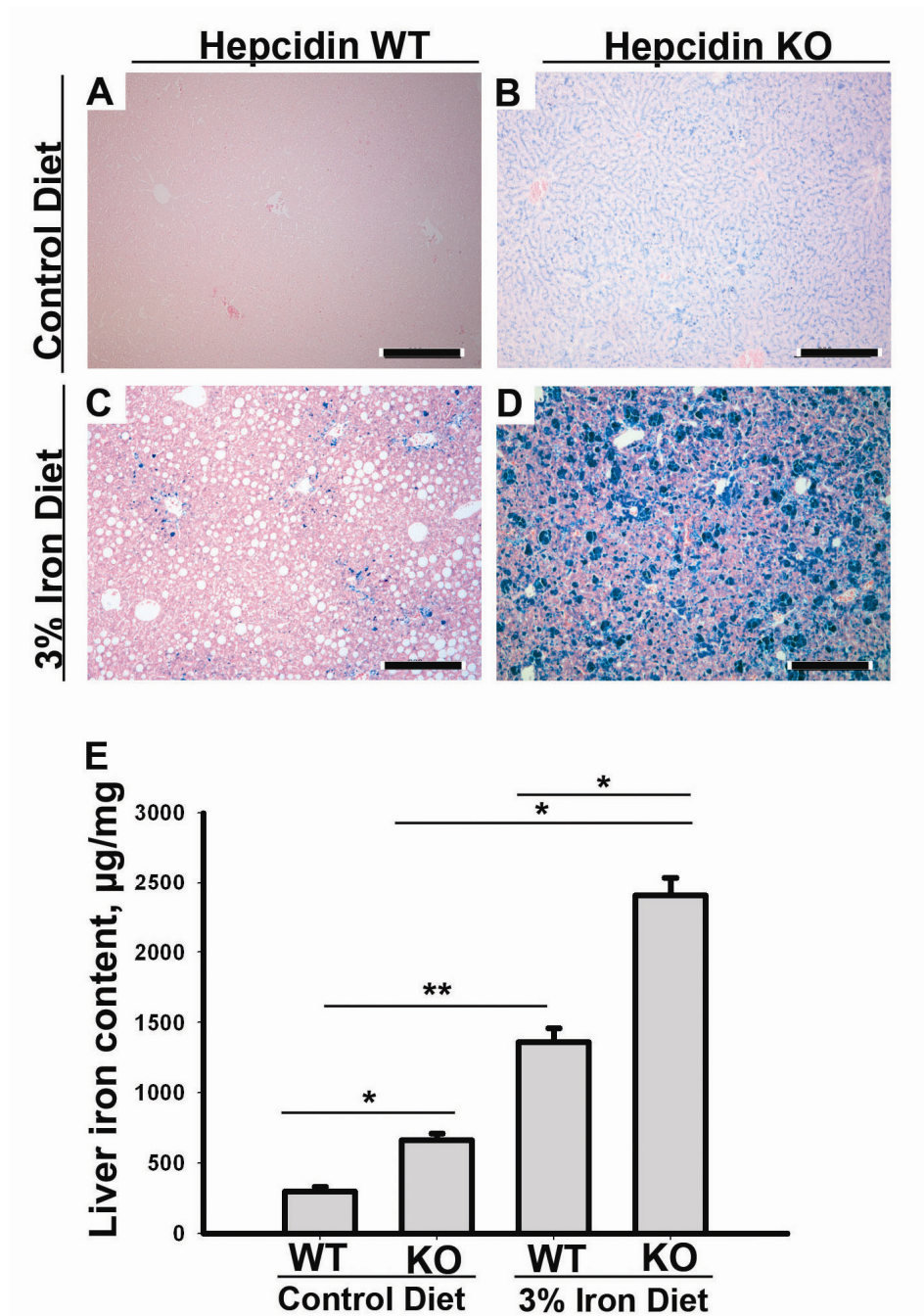
Figure 4.12. 12 months old hepcidin knockout mice fed iron–rich diet show dramatic iron accumulation in the liver. Prussian blue staining was done on liver slides of hepcidin WT (A, C) and KO mice (B, D) fed normal chow (A, B) or iron-rich diet (C, D). Hepcidin KO mice fed iron-rich diet showed presence of large iron complexes in hepatocytes. Scale bar 200 µm. E) Biochemical determination of non – heme liver iron content. Of notes, hepcidin KO mice on iron-rich diet showed dramatic elevation of liver iron content. Results are expressed as mean ± SD (n = 5). Asterisk and double asterisk highlights $p < 0.05$ and $p < 0.005$, respectively.

4.13 12 months old hepcidin knockout mice kept on iron – rich diet develop significant liver fibrosis

It was questioned, whether the chronic liver injury seen in hepcidin KO mice on iron–rich diet leads to development of liver fibrosis. The mRNA levels of several fibrogenic markers, including collagen 1 (figure 4.13.G) and TGFβ (data not shown) were significantly increased in hepcidin KO mice on iron-rich diet. Moreover, collagen deposition was markedly increased in hepcidin KO mice on iron-rich diet as shown by Sirius Red staining and confirmed by its morphometric quantification (Figure 4.13.A-E). Finally, hydroxyproline content, which is used as biochemical marker of collagen deposition, was enhanced in hepcidin KO mice kept on iron-rich diet when compared to WT mice on the same feeding regime (Figure 4.13.F). These data demonstrate that massive iron overload seen in hepcidin KO mice on iron–rich diet is sufficient to induce the development of liver fibrosis.
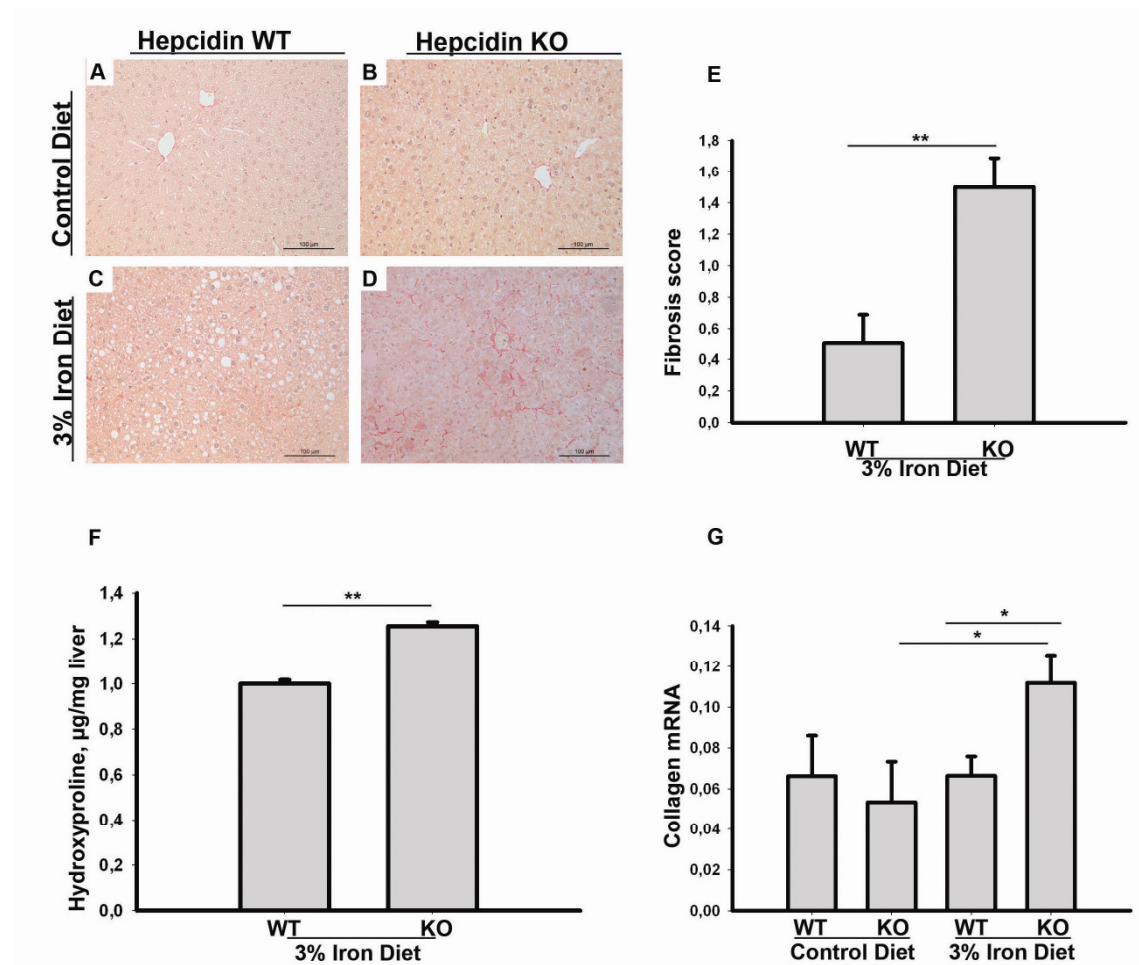
Figure 4.13. Hepcidin knockout mice develop significant liver fibrosis after feeding with iron - rich diet for 11 months. Sirius red staining was performed on liver slides of hepcidin WT (A, C) and KO (B, D) mice fed with control (A, B) and iron-rich diet (C, D). Scale bar 100 µm. Morphometric quantification of fibrosis deposits (E) seen in Sirius Red staining. Data are presented as mean ± SD (n = 5) and double asterisk highlights $p < 0.05$. Hydroxyproline content (F) was measured in livers of hepcidin KO and WT mice fed with iron–rich diet and shown as mean ± SD (n = 5). Double asterisk highlights $p < 0.05$. (G) The extent of collagen mRNA production was quantified using real time RT – PCR. Note that, hepcidin KO mice on iron-rich diet show elevation of collagen mRNA production. Results are presented as mean ± SD (n = 5) and asterisk highlights $p < 0.05$.

4.14 Hepcidin knockout mice show accumulation of iron in cytoplasm, mitochondria and lysosomes

To better understand the impact of the described observations on intracellular iron distribution, subcellular fractionation in 6 months old animals was performed (Figure 4.14.). In mice fed control diet, iron was found mainly in cytoplasm, while lower levels were found in mitochondria, nucleus, and lysosomes and similar distribution was seen in WT mice on iron–rich diet. After iron-rich diet, the situation of iron deposition in the cell is changed. However, a profound change in distribution was seen in hepcidin KO mice subjected to iron–rich diet. These animals showed significant and dramatic increase of iron within lysosomes and smaller in mitochondria, but significant increase of iron content. Finally, a marked increase of iron in nuclear fraction was observed. However, given that no/minimal iron signal in the nucleus was observed in Prussian Blue staining, one can assume that the high nucleus levels are due to precipitation of iron during the fractionation process.

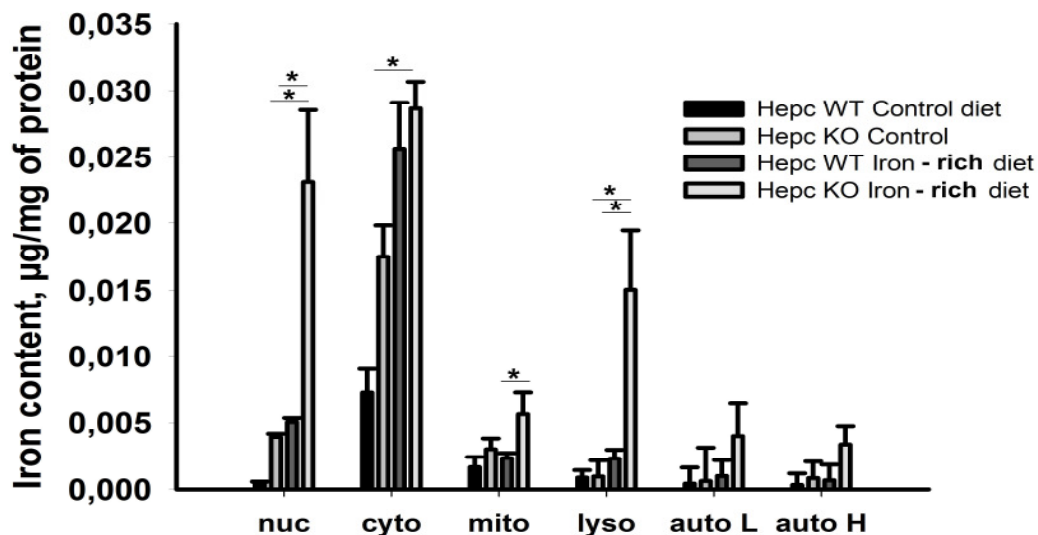**Figure 4.14. 6 months old hepcidin knockout mice kept on iron–rich diet show accumulation of iron in cytoplasm, mitochondria, and lysosomes.** Subcellular fractionation of hepcidin WT and KO mice livers obtained from animals fed normal or iron-rich diet with subsequent determination of subcellular iron content. The data are presented as mean ± SD (n = 3) and at least three mice were used per group and asterisk

highlights p < 0.05. Nuc – nuclear fraction; cyto – cytoplasm; mito – mitochondria; lyso – lysosomes; auto L – autophagosomal light fraction; auto H – autophagosomal heavy fraction.

4.15   6 months old hepcidin knockout mice fed iron–rich diet display large iron–containing complexes within lysosomes

To better characterise the large iron complexes seen in hepcidin KO mice fed iron-rich diet, high resolution Electron Microscopy was performed (figure 4.15.A and C). Increased, distributed, presumably ferritin – bound iron signal was observed in hepcidin WT mice fed iron – rich diet (figure 4.15.C), while large intralysosomal iron – containing aggregates were seen in knockout mice on iron–rich chow (figure 4.15.A). The presence of hard metal was confirmed by subcellular fractionation. To further determine the composition of the aggregates, scanning electron microscopy (SEM) was performed, which revealed several peaks corresponding to iron complexes, which were seen in hepcidin KO, but not WT mice subjected to iron–rich diet.
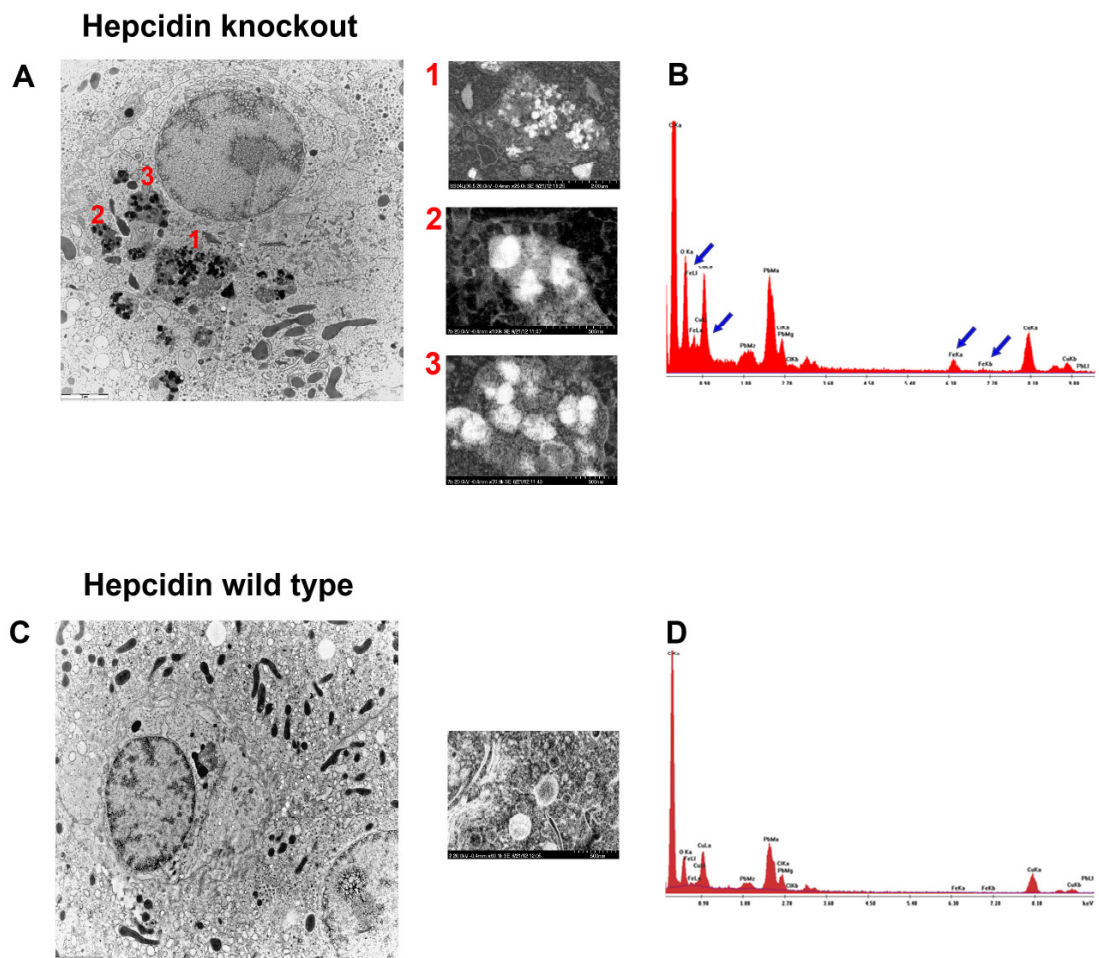
Figure 4.15. 6 months old hepcidin knockout mice fed iron–rich diet display large intralysosomal iron containing complexes. Electron microscopy was obtained from high pressure frozen liver tissues derived from hepcidin WT (A) and KO mice (B) fed iron-rich diet. Hepcidin KO, but not WT mice accumulate large iron – containing complexes in their lysosomes. Scale bar 2µm. Electron spectrum from hepcidin KO (B) and WT mouse (D), with blue arrows showing iron.

4.16 Hepcidin knockout mice show downregulation of STEAP3 and DMT1

To test, whether lysosomal iron accumulation in hepcidin KO mice is due to downregulation of genes responsible for iron transport, real time PCR from liver mRNA samples was performed. Hepcidin KO mice fed iron–rich diet for 5 months displayed downregulation of STEAP3 ferroreductase, which is responsible for iron reduction from FeIII to FeII and a diminished level of DMT1 – the known transporter of FeII from lysosomes to cytoplasm (figure 4.16 A,B). On the other hand, hepcidin WT mice fed 5 months with iron–rich diet show normal STEAP3 and decreased DMT1 levels (figure 4.16 A,B). The molecular action of both genes is summarized in figure 4.16.C-E.

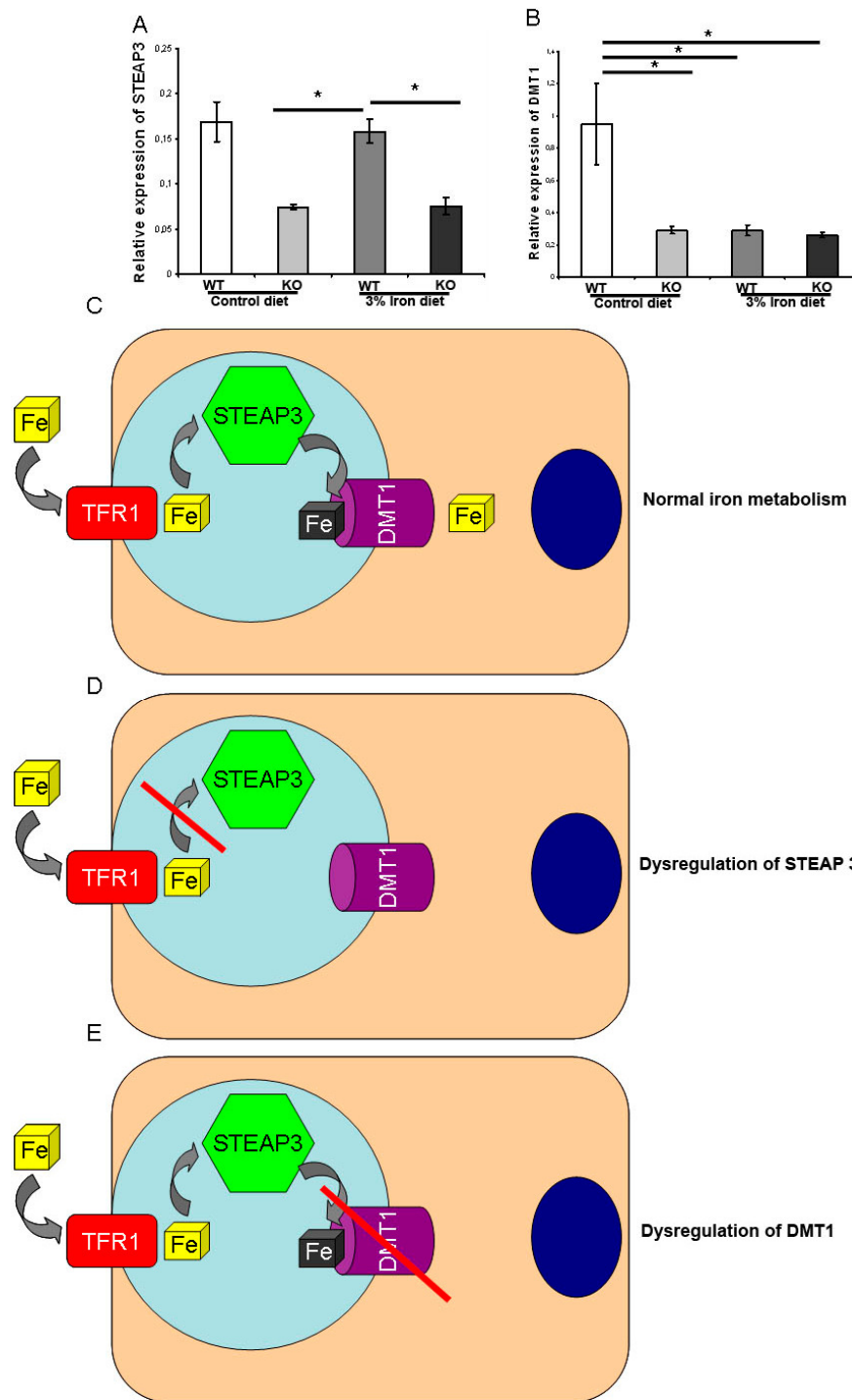**Figure 4.16. Hepcidin knockout mice show downregulation of STEAP3 and DMT1.** (A, B) Real time PCR from liver RNA samples detects diminished DMT1 and STEAP3 levels in hepcidin KO mice fed with iron–rich food for 5 months. (C-E) Schematics highlight the iron trafficking under basal conditions, as well as in situations of diminished STEAP3/DMT1 production, which both may contribute to lysosomal iron accumulation.

4.17 Hepcidin knockout mice display elevated ferritin

To test whether iron accumulation in hepcidin KO is counterbalanced by increased storage capacities immunoblotting was performed which detects the amount of the iron storing protein ferritin in total liver lysate as well as lysate from nuclear fractions. Both hepcidin KO mice on normal diet and WT animals fed iron–rich diet displayed elevated ferritin levels, but these levels were significantly lower than the ones observed in hepcidin KO mice fed iron–rich diet (Figure 4.17). Similar results, i.e. higher ferritin levels in hepcidin KO vs. WT mice kept on iron–rich diet, were seen in the nuclear fraction.
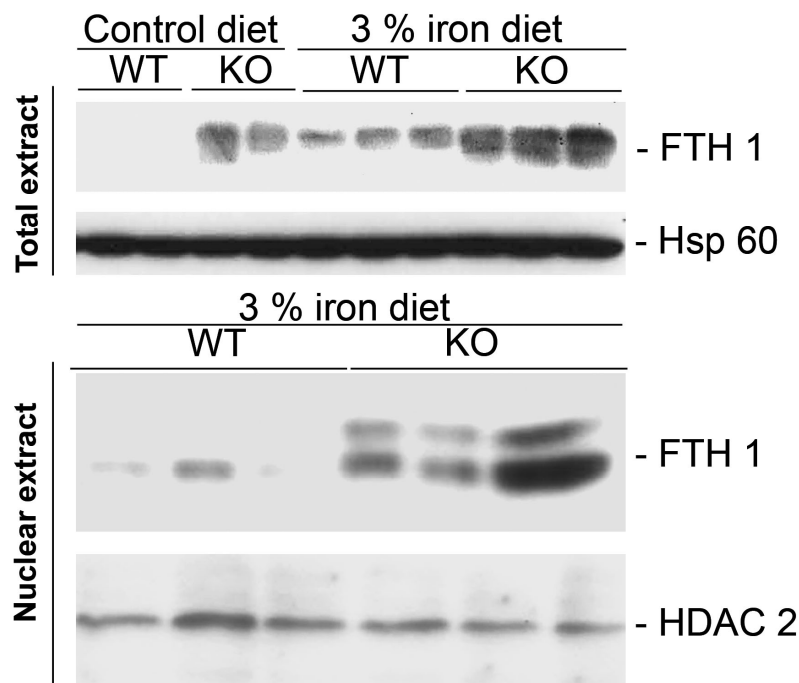

Figure 4.17. 6 months old hepcidin knockout mice show elevated ferritin levels. Ferritin immunoblot of total and nuclear protein extracts displayed elevated level of ferritin in hepcidin KO mice fed iron-rich diet. Hsp60 and HDAC2 were used as loading controls for total cell lysates and nuclear fractions, respectivetely.

4.18 Chronic iron overload leads to lysosomal damage in 6 months old hepcidin knockout mice fed iron – rich diet

Hepcidin KO mice fed iron-rich diet displayed a marked increase in mitochondrial and lysosomal iron. To test the consequences of the iron accumulation in these organelles, it was analyzed whether this leads to the release of lysosomal or mitochondrial components into the cytoplasm (Figure 4.18.). Only minimal cytochrome C levels were detected in cytoplasm of iron–rich diet fed hepcidin KO and WT mice, suggesting no gross mitochondrial leakiness in these samples. On the other hand, cytoplasmatic levels were significantly elevated in hepcidin KO mice fed iron–rich diet pointing to a lysosomal damage in these animals.

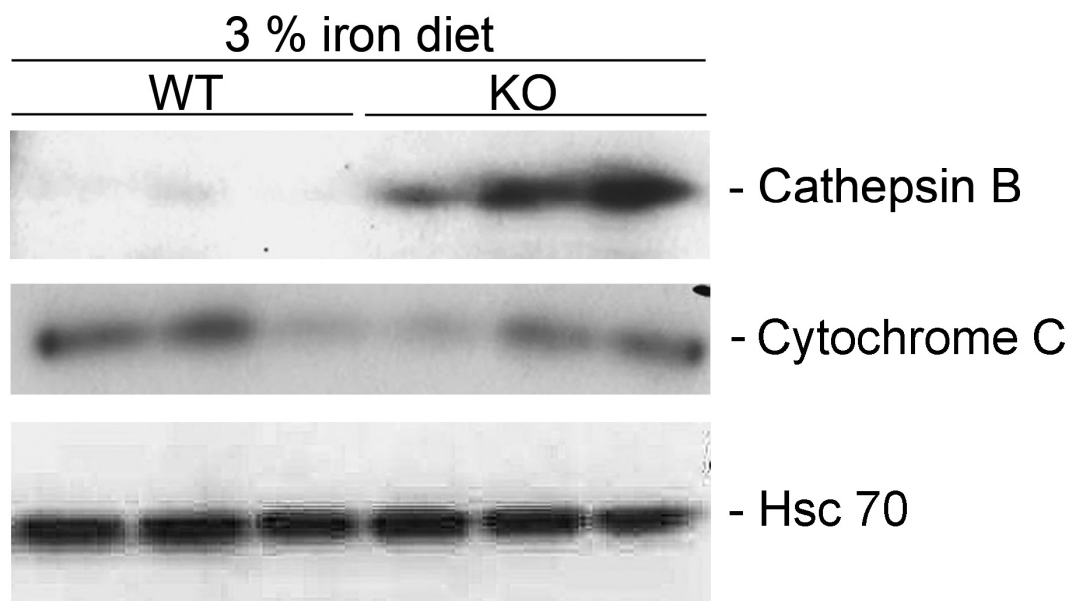**Figure 4.18. Chronic iron overload leads to lysosomal damage in 6 months old hepcidin knockout mice fed iron–rich diet.** Liver cytoplasmatic extracts were subjected to antibody against Cathepsin B (top), Cytochrome C (middle), and Hsc 70 (bottom), which was used as a loading control. Note the occurrence of Cathepsin B in cytoplasm of iron–rich diet hepcidin KO mice pointing towards a lysosomal damage.

4.19 Hepcidin knockouts fed with iron–rich diet for 5 months show an altered autophagy activation

Hepcidin KO mice fed iron – rich diet displayed a marked iron accumulation within lysosomes. To test, whether lysosomal iron accumulation affects the process of autophagy immunoblot analysis was performed on total liver lysates (figure 4.19 - top). Only hepcidin KO mice fed iron–rich diet showed increased LC3 II levels which point either to increased autophagic flux or an insufficient LC3 II clearance. The elevated p62 levels suggest that the not efficient autophagic response probably occurs in these animals (Figure 4.19 - bottom).
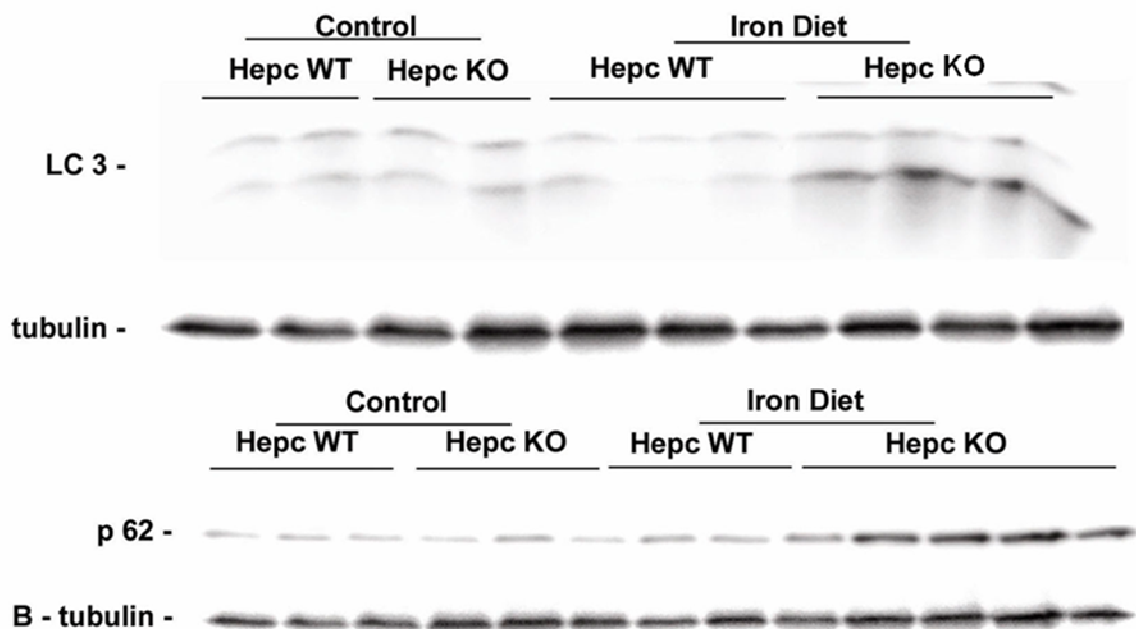
Figure 4.19. Hepcidin knockouts fed iron–rich diet for 6 months display an altered autophagic process. Liver total extracts were subjected to antibody against LC3 II (top), p 62 (bottom), and B-tubulin which was used as a loading control. Note the higher LC3 II and p62 levels, which suggest an activated, but not efficient autophagic response in hepcidin KO mice fed iron–rich diet.

4.20   Hepcidin knockout mice display an elevated oxidative DNA damage

Finally, it was of interest whether iron accumulation seen in hepcidin KO mice on iron–rich diet leads to oxidative DNA damage. Therefore, histological staining for DNA damage was performed, which was clearly present in hepcidin KO mice kept on iron–rich diet (Figure 4.20.A-D), while their nontransgenic littermates did not show oxidative DNA damage. These data demonstrate that massive iron overload seen in hepcidin KO mice on iron–rich diet is sufficient to induce oxidative DNA damage.

Figure 4.20. Hepcidin knockout mice display signs of oxidative DNA damage. Staining of liver tissues (A – D) with 'In situ Cell Death Detection Kit, POD' was performed to detect the signs of oxidative DNA damage. 6 months old hepcidin WT (A,C) and KO mice (B,D) fed normal diet (A,B) and iron–rich chow (C,D) were analyzed. Note the presence of oxidative DNA damage in hepcidin KO mice kept on iron–rich diet. Scale bar 50 µm.

5 Discussion

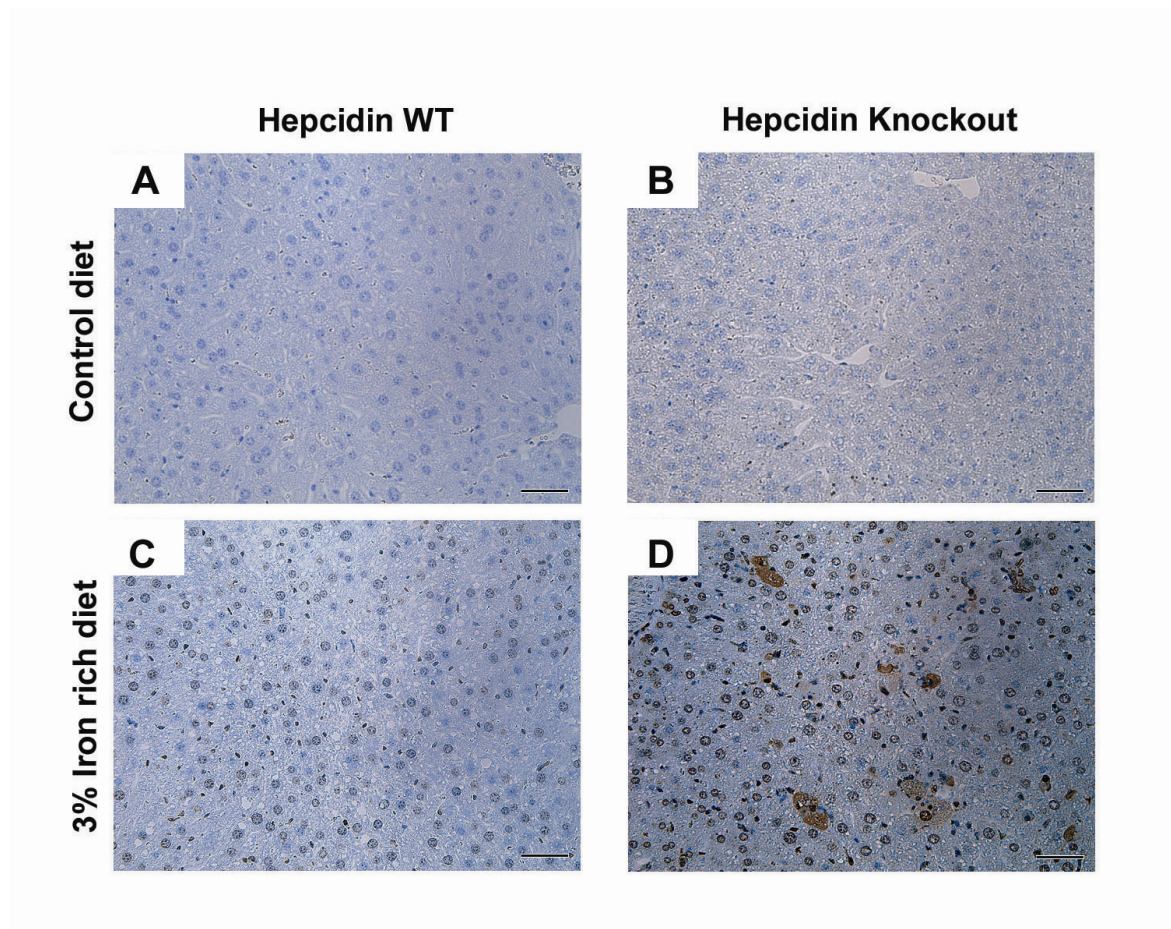In this study, hepcidin knockout mice were evaluated as a model of iron-overload associated liver injury. As was also reported previously [54], hepcidin knockout mice developed a spontaneous liver iron overload, which was even more pronounced when they were fed with iron–rich diet. In the latter group, a hepatic iron-content of approximately 45 µmol/g tissue was observed, which lies well above concentration found in most dietary-induced models of iron-overload. For example, values up to 30 µmol/g were seen in TfR2/HFE double knockout mice, hemojuvelin KO, BMP6-KO or HFE knockout mice while the HFE C282Y knock-in animals, which represent the animal counterpart of the most common hemochromatosis form, displayed even lower hepatic iron contents [121,122,123]. The high amount of iron accumulation in hepcidin knockout animals is even more remarkable given that C57BL/6 animals represent a strain which is relatively resistant to iron-overload [119]. On the other hand, comparable or even higher hepatic iron levels were reported in animals fed with ferrocene or receiving intraperitoneal supplementation with iron dextran or ferric ammonium citrate. However, these models are of limited value since they are achieved by non-physiological iron uptake mechanisms and do not mimic the chronic, slow increase of iron levels seen in hemochromatosis subjects [124,125,126,127,128,129].

Despite the massive iron overload observed in hepcidin knockout mice, the iron accumulation is comparable or even lower than the one observed in human HH subjects [130,131]. For example, HH patients can accumulate more than 1 mmol iron/g liver tissue [132,133], while in healthy subjects hepatic iron content ranges from 10 to 36 µmol/L [132,134,135]. Although the association between iron overload and liver disease development is imperfect, Adams et al showed that HH subject with hepatic iron content more than 1 mmol/g are at high risk for development of liver cirrhosis [136].

As a marker of systemic iron overload, hepcidin knockout mice fed with iron–rich diet displayed not only elevated hepatic iron content but also highly increased serum ferritin levels of approximately 5000 µg/L. Serum ferritin levels observed in hepcidin knockout mice are comparable with data seen in untreated HH patients [137]. Measurement of serum ferritin in HFE patients is of clinical importance since HH patients with serum ferritin < 1000µg/L are unlikely to display advanced liver fibrosis while ferritin values > 1000µg/L confer more than threefold higher risk for development of advanced fibrosis [137,138,139,140,141,142].

In addition, hepcidin knockouts fed iron–rich diet showed increased levels of hepatic iron and serum NTBI, i.e. approximately 1.2 µmol/mg and 10 µmol/L respectively. Therefore, observed NTBI values in this study are similar to the serum levels seen in HH subjects (mean serum NTBI = 11.9 µmol/L) [143]. On the other hand, values observed in hepcidin knockout mice fed iron–rich diet are higher than values seen in other animal models of iron overload, such as HFE KO, TFR2 KO and HFE$^{-/-}$/TFR2^{mut} [144]. For example, HFE/TFR2 double knockout mice displayed serum NTBI level of approximately 9 µM, while HFE and TFR2 knockout mice showed even lower serum NTBI of approximately 3-4 µM [144]. These differences might be particularly important since NTBIs represent the primary toxic iron species [82] and their levels correlate with the extent of liver damage. For instance, McNamara et al 1999 showed that HH patients with NTBI > 2 µmol/L displayed an inflammatory liver disease [145]. In conclusion, the particularly high extent of iron accumulation in hepcidin knockout mice which is evidenced by high NTBIs, ferritin, and liver iron levels likely contributes to the development of liver injury in hepcidin knockout mouse model as it has been observed in HH subjects [144,145].

With respect to the histological signs of liver injury, hepcidin KO mice fed with iron–rich, but not normal diet displayed mild liver inflammation, which was also observed in HFE$^{-/-}$/TFR2^{mut} mice [144]. On the other hand, no apparent inflammation was seen in HFE KO

mice and TFR2[mut] mice fed iron-rich diet [144]. Interestingly, both mouse lines showed a predominantly mononuclear infiltration, which is reminiscent of HH subjects, who present with a similar picture and in whom the presence of inflammation associates with liver fibrosis development [146,147]. While the exact reasons for the predominance of mononuclear infiltration in iron overload syndromes remain unknown, it is well in line with the important role of macrophages in iron metabolism [101,148,149].

In terms of liver injury, moderately increased liver injury marker ALT (of approximately 361 u/L) was observed in hepcidin KO mice fed iron-rich diet and this level was well above those reported in comparable animal models, such as HFE KO, TFR2 KO and HFE^{-/-}/TFR2[mut] mice [144] or in HH subjects [150,151]. Other liver injury markers such as AST and AP were also higher in hepcidin KOs fed iron-rich diet (the value of approximately 734 u/L and 362 u/L respectively) compared to HH subjects [151,152]. However, this is not surprising since it has been shown previously that mice often require a more active disease to develop significant liver alterations within their relatively short life span.

In hepcidin KO mice fed iron-rich diet, elevated apoptosis levels were observed (assessed by D237 tissue labeling and histological scoring). It has been shown previously that elevated apoptosis levels can lead to the development of chronic injury and even to liver fibrosis [153] and increased apoptosis was observed in other animal models of iron overload [153,154]. Furthermore, increased hepatic apoptosis is seen in HH subjects [155,156]. Of note, a direct correlation between liver iron amount and the extent of apoptosis was evident both in hepcidin knockout mice and in HH subjects ([155] and data not shown). Moreover, the patterns of apoptosis and iron depositions overlap which further strengthens the mechanistic link between both processes [155].

In addition to liver inflammation and hepatocellular apoptosis, hepcidin KO mice as well as HFE^{-/-}/TFR2[mut] mice showed liver fibrosis development [144]. However, both animal models displayed a chicken-wire type of fibrosis (perivenular and pericellular fibrosis)

which is characteristic for humans with alcoholic or non-alcoholic steatohepatitis but rarely occurs in HH [144,155,157]. The reason for this type of fibrosis might be the fact that hepcidin knockout mice (unlike humans) exhibit an ubiquitous iron overload with an ubiquitous liver injury while the iron accumulation and liver injury is observed predominantly in periportal area in humans [50,155]. Moreover, the higher activity of liver disease in mice versus humans might be responsible for this observation.

Given that the association between the extent of iron overload and development of liver injury is imperfect, one can hypothesize that an improper iron distribution affects the development of liver disease. In this respect, marked iron overload was detected in lysosomes of hepcidin KO mice fed iron-rich diet compared to all other treatment groups. Obviously, a loss of hepcidin alone was not sufficient to induce this accumulation, therefore, it was concluded that it is a consequence of an extreme iron overload rather than a genetic defect per se. What might be the mechanisms underlying this observation? In hepatocytes, transferrin receptor 1 represents the major way of intracellular iron uptake and after endocytosis of the iron-receptor complex, it brings iron into lysosomes [91,158]. After release from the transferrin complex, iron is reduced via STEAP3 in order to be exported to cytoplasm via DMT1 [91]. While the TfR1 levels did not change (data not shown) in hepcidin knockout mice, both STEAP3 and DMT1 levels were lower in hepcidin KO mice fed iron-rich diet suggesting that a disturbed processing and release of iron might be responsible for the observed overload. Additional studies are needed to find out whether the release of iron from transferrin complex, which represents a highly regulated process requiring acidification of lysosomes among others might also be affected [91]. Finally, iron is taken up from cytoplasm into lysosomes to remove redox-active iron [159]. In this respect, signs of elevated autophagy which likely contribute to the intralysosomal iron burden were found [160].

77

The lysosomal iron overload observed in hepcidin knockout mice is well in line with other animal models such as the feeding with ferrocene or iron carbonyl which also displayed lysosomal iron accumulation [159,161,162]. Furthermore, lysosomal iron overload of hepatocytes is commonly seen in HH patients [163,164]. Consequently, Peters and colleagues proposed that iron overload due to either primary HH or transfusional siderosis represents a form of acquired lysosomal storage disease [165].

On the other hand, hepcidin knockout mice fed iron–rich diet showed only minor changes in mitochondrial and cytoplasmatic iron content and similarly, mitochondrial iron accumulation is uncommon in HH [95] as well as in animals fed with ferrocene or iron-carbonyl containing diet [159,162]. These findings are not surprising since mitochondrial iron trafficking seems to be controlled independently on systemic iron levels and mitochondrial iron overload develops primarily due to defect in genes responsible for heme biosynthesis, iron-sulfur clusters biogenesis or mitochondrial iron transport [2,166,167]. Several mechanisms may account for the steady hepatic iron levels in cytoplasm. For example, ferroportin constitutes a potent cytoplasmatic iron exporter which is expressed in hepatocytes and becomes increasingly active in the absence of hepcidin [23]. Autophagy process may also counteract the iron accumulation in cytoplasm [160,168] and this study indicated that hepcidin knockout mice displayed signs of activated autophagy (i.e. LC3 II activation and p62 accumulation).

Besides the lysosomal iron overload, hepcidin KO mice also displayed lysosomal damage as evidenced by the release of cathepsin B into the cytoplasm as well as intralysosomal accumulation of indigestible autofluorescent material (data not shown). Similar events were shown in ferrocene and iron-carbonyl fed animals [159,162] as well as in HH patients [95]. These findings are not surprising, since lysosomes often contain iron in the form of the reactive Fe (II), which can catalyze the Fenton reaction and thereby lead to hydroxyl radical formation [160]. These hydroxyl radicals may then attack biomolecules and

interfere with their proper degradation [98]. The pronounced oxidative injury present in iron-overloaded lysosomes may in turn cause lysosomal membrane damage and release of cathepsins [160]. It has been shown previously that cathepsin release into cytoplasm can activate caspases and may therefore account for the increased apoptosis levels observed in hepcidin knockout mice [169,170].

In summary, these data suggest that hepcidin knockout mice develop chronic liver injury and liver fibrosis as a consequence of lysosomal iron overload and consequent lysosomal damage. In this respect, several other studies as well as human data showed that lysosomal damage plays an important role in development of chronic liver disease. To that end, Canbay et al reported that inactivation of cathepsin B reduced hepatic inflammation and fibrogenesis in an experimental model of cholestatic liver disease [171]. Further studies are needed to find out whether the described liver phenotype is due to hepatocellular cathepsins or whether the cathepsin expression in stellate cells, which has been shown to increase during hepatic injury, plays the pivotal role in this process [172].

Another evidence, that lysosomal injury directly contributes to development of liver disease comes from lysosomal storage disorders. They constitute a group of approximately 50 rare inherited metabolic disorders leading to lysosomal dysfunction and are typically caused by mutations in a single lysosomal enzyme such as alpha- and betta-galactosidases, alpha- glucosidase and aspartylglucosaminidase [173]. Lysosomal storage diseases typically lead to neurological abnormalities, developmental delay, but also to enlarged livers, pulmonary and cardiac as well as kidney, and skeletal phenotype [173]. Among them, Niemann-Pick type C disease represents a best characterized lysosomal storage disorder resulting in a marked liver phenotype [173]. It is caused by mutations in NPC1 or NPC2, which participate in trafficking of proteins from lysosomes [174] and leads to accumulation of several molecules such as cholesterol, glycosphingolipids, and sphingosine within lysosomes [174]. Interestingly, similar to the hepcidin knockout mice,

an increased activation of the innate immune system represents the major feature of liver phenotype while elevated apoptosis and oxidative stress are observed later on [175,176,177].

In conclusion, hepcidin knockout mice constitute a convenient model of human iron overload-associated liver disease and further support the importance of lysosomes in this process. This is well in line with human observations, which detected obvious lysosomal alterations in close proximity to the fibrotic lesions in HH subjects while there are no or only minimal mitochondrial abnormalities [163,178]. On the other hand, further studies are needed to delineate the precise relationship between the lysosomal iron overload and lysosomal dysfunction on one side and the hepatocellular apoptosis, hepatic inflammation, and liver fibrosis development on the other. In fact, there may not be only a single mechanism going on but rather a myriad of processes contributing to the observed phenotype. For example, leakage of lysosomal enzymes into the cytoplasm may lead to hepatocellular apoptosis [160] and the subsequent engulfment of apoptotic bodies may result both, in macrophage activation and a direct activation of hepatic stellate cells [156]. Furthermore, hepatocellular iron overload can also stimulate stellate cells in a paracrine way [179]. While the current evidence indicates that loss of hepcidin results in a diminished macrophage iron content, further studies are on the way to determine the macrophage and hepatic stellate cell iron content in hepcidin knockout mice fed iron-rich diet. These studies will clarify whether the observed liver phenotype is a sole consequence of hepatocellular iron overload or whether loss of hepcidin may also induce iron overload in other cell types. Last but not least, elevated serum iron may also contribute to the observed phenotype via activation of endothelial cells [180].

6 Summary

Hepcidin is the central regulatory hormone of iron metabolism. Disrupted hepcidin signalling is seen in multiple genetic disorders termed as hereditary hemochromatosis (HH) where it leads to hepatic iron overload. Acquired iron overload is observed in several chronic diseases such as hepatitis C or alcoholic liver disease and seems to promote disease progression. While the association between iron overload and development of end−stage liver disease is well established, the precise underlying mechanisms remain to be defined. Although there is a number of animal models that mimic the genetic defects found in humans, none of them replicates the iron overload-associated liver disease. To develop such a model, we analyzed hepcidin knockout (KO) and wild type (WT) mice were fed with iron-rich diet for 5 or 11 months and compared them to age matched mice kept on standard chow. Harvested livers and serum samples were used for evaluation of liver injury and fibrosis. To determine the iron localization, a subcellular fractionation and electron microscopy was performed.

Hepcidin KOs kept on standard diet developed spontaneous hepatic iron overload, which was even more pronounced in KOs fed iron-rich chow (KO:2543±114 vs. WT: 1493±136 $p < 0,005$) who reached levels similar to the ones observed in HH patients. Elevated serum liver enzymes (AST: KO 261±15, WT 142±34 $p < 0,05$), serum iron levels, mild hepatocellular inflammation (predominantly mononuclear infiltration) and apoptosis were observed in hepcidin KOs fed iron-rich diet. After 11 months of iron-rich chow, hepcidin KOs developed moderate liver fibrosis as demonstrated via Sirius red staining and increased hydroxyproline levels. The liver injury was accompanied by a marked lysosomal iron overload and lysosomal fragility with release of cathepsins (e.g. Cathepsin B) into the cytoplasm. No major differences were seen in mitochondrial morphology or injury markers. As a potential mechanism leading to lysosomal iron overload, the expression of

DMT1 and STEAP3, i.e. the molecules needed for lysosomal iron export, was greatly reduced. Increased LC3-II and p62 levels pointed towards an activated autophagy which likely contributes to the lysosomal iron overload. On the other hand, large indigestible iron complexes were found in hepcidin knockout mice fed iron-rich diet thereby suggesting a defect in protein degradation as it is observed in lysosomal storage diseases.

In conclusion, hepcidin KO mice represent an attractive animal model which mimics both iron overload and associated liver injury observed in humans with HH. Therefore hepcidin knockout mice constitute an important tool to study the mechanism of iron overload−related liver diseases and implicate lysosomal injury as a crucial event in iron hepatotoxicity.

7   References

1. Evstatiev R, Gasche C (2012) Iron sensing and signalling. Gut 61: 933-952.

2. Sheftel A, Stehling O, Lill R (2010) Iron–sulfur proteins in health and disease. Trends in Endocrinology & Metabolism 21: 302-314.

3. Lill R (2009) Function and biogenesis of iron–sulphur proteins. Nature 460: 831-838.

4. Khan AA, Quigley JG (2011) Control of intracellular heme levels: Heme transporters and heme oxygenases. Biochimica et Biophysica Acta (BBA) - Molecular Cell Research 1813: 668-682.

5. Anderson GJ, Frazer DM (2005) Hepatic Iron Metabolism. Semin Liver Dis 25: 420-432.

6. Pantopoulos K, Porwal SK, Tartakoff A, Devireddy L (2012) Mechanisms of Mammalian Iron Homeostasis. Biochemistry.

7. Zhang A-S, Enns CA (2009) Iron Homeostasis: Recently Identified Proteins Provide Insight into Novel Control Mechanisms. Journal of Biological Chemistry 284: 711-715.

8. Ganz T (2008) Iron Homeostasis: Fitting the Puzzle Pieces Together. Cell Metabolism 7: 288-290.

9. Krause A, Neitz S, Mägert H-J, Schulz A, Forssmann W-G, et al. (2000) LEAP-1, a novel highly disulfide-bonded human peptide, exhibits antimicrobial activity1 1 The nucleotide sequence data reported in this paper have been submitted to the GenBank/EBI Data Bank with accession number AJ277280. Scanning of this sequence against the data base resulted in the identification of related sequences with the accession numbers AD000684 and P81172. FEBS Letters 480: 147-150.

10. Ganz T (2003) Hepcidin, a key regulator of iron metabolism and mediator of anemia of inflammation. Blood 102: 783-788.

11. Park CH, Valore EV, Waring AJ, Ganz T (2001) Hepcidin, a Urinary Antimicrobial Peptide Synthesized in the Liver. Journal of Biological Chemistry 276: 7806-7810.

12. Nemeth E, Tuttle MS, Powelson J, Vaughn MB, Donovan A, et al. (2004) Hepcidin Regulates Cellular Iron Efflux by Binding to Ferroportin and Inducing Its Internalization. Science 306: 2090-2093.

13. Ganz T (2011) Hepcidin and iron regulation, 10 years later. Blood 117: 4425-4433.

14. Deugnier YY (2010) The iron driven pathway of hepcidin synthesis. Gastroenterol Clin Biol 34: 351-354.

15. Ganz T, Nemeth E (2011) Hepcidin and Disorders of Iron Metabolism Annual Review of Medicine 62: 347-360.

16. Camaschella C, Silvestri L (2011) Molecular Mechanisms Regulating Hepcidin Revealed by Hepcidin Disorders. The Scientific World Journal 11: 1357-1366.

17. Ganz T, Nemeth E (2012) Hepcidin and iron homeostasis. Biochimica et Biophysica Acta (BBA) - Molecular Cell Research 1823: 1434-1443.

18. Prentice AM, Doherty CP, Abrams SA, Cox SE, Atkinson SH, et al. (2012) Hepcidin is the major predictor of erythrocyte iron incorporation in anemic African children. Blood 119: 1922-1928.

19. Theurl I, Schroll A, Nairz M, Seifert M, Theurl M, et al. (2011) Pathways for the regulation of hepcidin expression in anemia of chronic disease and iron deficiency anemia in vivo. Haematologica 96: 1761-1769.

20. Leong W-I, Lönnerdal B (2004) Hepcidin, the Recently Identified Peptide that Appears to Regulate Iron Absorption. The Journal of Nutrition 134: 1-4.

21. Liu Q, Davidoff O, Niss K, Haase VH (2012) Hypoxia-inducible factor regulates hepcidin via erythropoietin-induced erythropoiesis. The Journal of Clinical Investigation 122: 4635-4644.

22. De Domenico I, Ward DM, Kaplan J (2011) Hepcidin and Ferroportin: The New Players in Iron Metabolism. Semin Liver Dis 31: 272-279.

23. Ramey G, Deschemin J-C, Durel B, Canonne-Hergaux F, Nicolas G, et al. (2010) Hepcidin targets ferroportin for degradation in hepatocytes. Haematologica 95: 501-504.

24. Luo X, Jiang Q, Song G, Liu Y-L, Xu Z-G, et al. (2012) Efficient oxidative folding and site-specific labeling of human hepcidin to study its interaction with receptor ferroportin. FEBS Journal: 3166-3175.

25. Preza GC, Ruchala P, Pinon R, Ramos E, Qiao B, et al. (2011) Minihepcidins are rationally designed small peptides that mimic hepcidin activity in mice and may be useful for the treatment of iron overload. The Journal of Clinical Investigation 121: 4880-4888.

26. Knutson MD, Oukka M, Koss LM, Aydemir F, Wessling-Resnick M (2005) Iron release from macrophages after erythrophagocytosis is up-regulated by ferroportin 1 overexpression and down-regulated by hepcidin. Proceedings of the National Academy of Sciences of the United States of America 102: 1324-1328.

27. Ramey G, Deschemin JC, Durel B, Canonne-Hergaux F, Nicolas G (2010) Hepcidin targets ferroportin for degradation in hepatocytes. Haematologica 95: 501-504.

28. Pietrangelo A (2004) Hereditary Hemochromatosis — A New Look at an Old Disease. New England Journal of Medicine 350: 2383-2397.

29. D'Alessio F, Hentze MW, Muckenthaler MU (2012) The hemochromatosis proteins hfe, tfr2 and hjv form a membrane-associated protein complex For hepcidin regulation. Journal of Hepatology 57: 1052-1060.

30. Pietrangelo A, Camaschella C (1998) Molecular genetics and control of iron metabolism in hemochromatosis. Haematologica 83: 456-461.

31. Fleming RE, Sly WS (2002) Mechanisms of iron accumulation in hereditary hemochromatosis. Annual Review of Physiology 64: 663-680.

32. Cohen AR, Glimm E, Porter JB (2008) Effect of transfusional iron intake on response to chelation therapy in β-thalassemia major. Blood 111: 583-587.

33. Tung BY, Emond MJ, Bronner MP, Raaka SD, Cotler SJ, et al. (2003) Hepatitis C, iron status, and disease severity: Relationship with HFE mutations. Gastroenterology 124: 318-326.

34. Friedman IM, Kraemer HC, Mendoza FS, Hammer LD (1988) Elevated serum iron concentration in adolescent alcohol users. Am J Dis Child 142: 156-159.

35. Porter JB (2001) Practical management of iron overload. British Journal of Haematology 115: 239-252.

36. Finberg KE (2009) Iron-Refractory Iron Deficiency Anemia. Seminars in Hematology 46: 378-386.

37. Feder JN (1996) A novel MHC class I - like gene is mutated in patients with hereditary hemochromatosis. Nat Genet 13: 399-408.

38. Merryweather-Clarke AT, Pointon JJ, Shearman JD, Robson KJ (1997) Global prevalence of putative haemochromatosis mutations. Journal of Medical Genetics 34: 275-278.

39. European Association for the Study of the L (2010) EASL clinical practice guidelines for HFE hemochromatosis. Journal of Hepatology 53: 3-22.

40. McLaren GD, Gordeuk VR (2009) Hereditary hemochromatosis: insights from the Hemochromatosis and Iron Overload Screening (HEIRS) Study. ASH Education Program Book 2009: 195-206.

41. Nadakkavukaran IM, Gan EK, Olynyk JK (2012) Screening for hereditary haemochromatosis. Pathology - Journal of the RCPA 44: 148-152.

42. Olynyk JK, Cullen DJ, Aquilia S, Rossi E, Summerville L, et al. (1999) A Population-Based Study of the Clinical Expression of the Hemochromatosis Gene. New England Journal of Medicine 341: 718-724.

43. Ajioka RS, Levy JE, Andrews NC, Kushner JP (2002) Regulation of iron absorption in Hfe mutant mice. Blood 100: 1465-1469.

44. Bacon B (1999) Molecular medicine and hemochromatosis: at the cross road. gastroenterology 116: 193-207.

45. Risch N (1997) Haemochromatosis, HFE and genetic complexity. Nat Genet 17: 375-376.

46. Nelson JE, Bhattacharya R, Lindor KD, Chalasani N, Raaka S, et al. (2007) HFE C282Y mutations are associated with advanced hepatic fibrosis in Caucasians with nonalcoholic steatohepatitis. Hepatology 46: 723-729.

47. Moodie SJ, Ang L, Stenner JMC, Finlayson C, Khotari A, et al. (2002) Testing for haemochromatosis in a liver clinic population: relationship between ethnic origin, HFE gene mutations, liver histology and serum iron markers. European Journal of Gastroenterology & Hepatology 14: 223-229.

48. Camashella (2000) The gene TFR2 is mutated in a new type of haemochromatosis mapping to 7q22. Nature Genetics 25: 14-15.

49. Chua ACG, Delima RD, Morgan EH, Herbison CE, Tirnitz-Parker JEE, et al. (2010) Iron uptake from plasma transferrin by a transferrin receptor 2 mutant mouse model of haemochromatosis. Journal of Hepatology 52: 425-431.

50. Pietrangelo A (2010) Hereditary Hemochromatosis: Pathogenesis, Diagnosis, and Treatment. Gastroenterology 139: 393-408.

51. Roetto A, Totaro A, Piperno A, Piga A, Longo F, et al. (2001) New mutations inactivating transferrin receptor 2 in hemochromatosis type 3. Blood 97: 2555-2560.

52. Roetto A, Totaro A, Cazzola M, Cicilano M, Bosio S, et al. (1999) Juvenile Hemochromatosis Locus Maps to Chromosome 1q. The American Journal of Human Genetics 64: 1388-1393.

53. Roetto A, Daraio F, Porporato P, Caruso R, Cox TM, et al. (2004) Screening hepcidin for mutations in juvenile hemochromatosis: identification of a new mutation (C70R). Blood 103: 2407-2409.

54. Lesbordes-Brion J-C, Viatte L, Bennoun M, Lou D-Q, Ramey G, et al. (2006) Targeted disruption of the hepcidin 1 gene results in severe hemochromatosis. Blood 108: 1402-1405.

55. Montosi G, Donovan A, Totaro A, Garuti C, Pignatti E, et al. (2001) Autosomal-dominant hemochrom-atosis is associated with a mutation in the ferroportin (SLC11A3) gene. The Journal of Clinical Investigation 108: 619-623.

56. Pietrangelo A (2004) The ferroportin disease. Blood Cells, Molecules, and Diseases 32: 131-138.

57. Pietrangelo A (2004) Non-HFE hemochromatosis. Hepatology 39: 21-29.

58. Galanello R, Origa R (2010) Beta-thalassemia. Orphanet J Rare Dis 21: 5- 11.

59. Higgs DR, Engel JD, Stamatoyannopoulos G Thalassaemia. The Lancet 379: 373-383.

60. Papanikolaou G, Pantopoulos K (2005) Iron metabolism and toxicity. Toxicology and Applied Pharmacology 202: 199-211.

61. Ginzburg Y, Rivella S (2011) β-thalassemia: a model for elucidating the dynamic regulation of ineffective erythropoiesis and iron metabolism. Blood.

62. Lee PL, Beutler E (2009) Regulation of Hepcidin and Iron-Overload Disease. Annual Review of Pathology: Mechanisms of Disease 4: 489-515.

63. Nai A, Pagani A, Mandelli G, Lidonnici MR, Silvestri L, et al. (2012) Deletion of TMPRSS6 attenuates the phenotype in a mouse model of β-thalassemia. Blood 119: 5021-5029.

64. Mueller S, Millonig G, Seitz HK (2009) Alcoholic liver disease and hepatitis C: a frequently underestimated combination. World J Gastroenterol 15: 3462-3471.

65. Bridle KR, Cheung T-K, Murphy TL, Walters MM, Anderson GJ, et al. (2006) Hepcidin Is Down-regulated in Alcoholic Liver Injury: Implications for the Pathogenesis of Alcoholic Liver Disease. Alcoholism: Clinical and Experimental Research 30: 106-112.

66. Harrison-Findik DD, Klein E, Crist C, Evans J, Timchenko N, et al. (2007) Iron-mediated regulation of liver hepcidin expression in rats and mice is abolished by alcohol. Hepatology 46: 1979-1985.

67. Harrison-Findik DD, Schafer D, Klein E, Timchenko NA, Kulaksiz H, et al. (2006) Alcohol Metabolism-mediated Oxidative Stress Down-regulates Hepcidin Transcription and Leads to Increased Duodenal Iron Transporter Expression. Journal of Biological Chemistry 281: 22974-22982.

68. Wu D, Cederbaum AI (2009) Oxidative Stress and Alcoholic Liver Disease. Semin Liver Dis 29: 141-154.

69. Kohgo Y, Ikuta K, Ohtake T, Torimoto Y, Kato J (2007) Iron overload and cofactors with special reference to alcohol, hepatitis C virus infection and steatosis/insulin resistance. World J Gastroenterol 13: 4699-4706.

70. Ma Y-S, Wu S-B, Lee W-Y, Cheng J-S, Wei Y-H (2009) Response to the increase of oxidative stress and mutation of mitochondrial DNA in aging. Biochimica et Biophysica Acta (BBA) - General Subjects 1790: 1021-1029.

71. Aisen P, Enns C, Wessling-Resnick M (2001) Chemistry and biology of eukaryotic iron metabolism. Int J Biochem Cell Biol 33: 940-959.

72. De Domenico I, McVey Ward D, Kaplan J (2008) Regulation of iron acquisition and storage: consequences for iron-linked disorders. Nat Rev Mol Cell Biol 9: 72-81.

73. Aisen P (2004) Transferrin receptor 1. The International Journal of Biochemistry & Cell Biology 36: 2137-2143.

74. Kawabata H, Yang R, Hirama T, Vuong PT, Kawano S, et al. (1999) Molecular Cloning of Transferrin Receptor 2. A new member of the transferrin receptor-like family. J Biol Chem 274: 20826-20832.

75. Ikuta K, Yersin A, Ikai A, Aisen P, Kohgo Y (2010) Characterization of the Interaction between Diferric Transferrin and Transferrin Receptor 2 by Functional Assays and Atomic Force Microscopy. Journal of Molecular Biology 397: 375-384.

76. van Renswoude J, Bridges KR, Harford JB, Klausner RD (1982) Receptor-mediated endocytosis of transferrin and the uptake of fe in K562 cells: identification of a nonlysosomal acidic compartment. Proceedings of the National Academy of Sciences 79: 6186-6190.

77. Eckenroth BE, Steere AN, Chasteen ND, Everse SJ, Mason AB (2011) How the binding of human transferrin primes the transferrin receptor potentiating iron release at endosomal pH. Proceedings of the National Academy of Sciences 108: 13089-13094.

78. Luck AN, Mason AB (2012) Transferrin-mediated cellular iron delivery. Curr Top Membr 69: 3-35.

79. Knutson MD (2007) Steap Proteins: Implications for Iron and Copper Metabolism. Nutrition Reviews 65: 335-340.

80. Mims MP, Prchal JT (2005) Divalent metal transporter 1. Hematology 10: 339-345.

81. Sipe D, Murphy R (1991) Binding to cellular receptors results in increased iron release from transferrin at mildly acidic pH. J Biol Chem 266: 8002-8007.

82. Brissot P, Ropert M, Le Lan C, Loréal O (2012) Non-transferrin bound iron: A key role in iron overload and iron toxicity. Biochimica et Biophysica Acta (BBA) - General Subjects 1820: 403-410.

83. Chua ACG, Olynyk JK, Leedman PJ, Trinder D (2004) Nontransferrin-bound iron uptake by hepatocytes is increased in the Hfe knockout mouse model of hereditary hemochromatosis. Blood 104: 1519-1525.

84. Trinder D, Oates PS, Thomas C, Sadleir J, Morgan EH (2000) Localisation of divalent metal transporter 1 (DMT1) to the microvillus membrane of rat duodenal enterocytes in iron deficiency, but to hepatocytes in iron overload. Gut 46: 270-276.

85. Knöpfel M, Schulthess G, Funk F, Hauser H (2000) Characterization of an Integral Protein of the Brush Border Membrane Mediating the Transport of Divalent Metal Ions. Biophysical journal 79: 874-884.

86. Gehrke SG, Riedel H-D, Herrmann T, Hadaschik B, Bents K, et al. (2003) UbcH5A, a member of human E2 ubiquitin-conjugating enzymes, is closely related to SFT, a stimulator of iron transport, and is up-regulated in hereditary hemochromatosis. Blood 101: 3288-3293.

87. Scheiber-Mojdehkar B, Sturm B, Plank L, Kryzer I, Goldenberg H (2003) Influence of parenteral iron preparations on non-transferrin bound iron uptake, the iron regulatory protein and the expression of ferritin and the divalent metal transporter DMT-1 in HepG2 human hepatoma cells. Biochemical Pharmacology 65: 1973-1978.

88. Meyron-Holtz E, Moshe-Belizowski S, Cohen L (2011) A possible role for secreted ferritin in tissue iron distribution. Journal of Neural Transmission 118: 337-347.

89. Miyazaki E, Kato J, Kobune M, Okumura K, Sasaki K, et al. (2002) Denatured H-ferritin subunit is a major constituent of haemosiderin in the liver of patients with iron overload. Gut 50: 413-419.

90. Harrison PM, Arosio P (1996) The ferritins: molecular properties, iron storage function and cellular regulation. Biochimica et Biophysica Acta (BBA) - Bioenergetics 1275: 161-203.

91. Graham RM, Chua AC, Herbison CE, Olynyk JK, Trinder D (2007) Liver iron transport. World J Gastroenterol 13: 4725-4736.

92. Drysdale J, Arosio P, Invernizzi R, Cazzola M, Volz A, et al. (2002) Mitochondrial Ferritin: A New Player in Iron Metabolism. Blood Cells, Molecules, and Diseases 29: 376-383.

93. Ramm GA, Ruddell RG (2005) Hepatotoxicity of Iron Overload: Mechanisms of Iron-Induced Hepatic Fibrogenesis. Semin Liver Dis 25: 433-449.

94. Peters TJ, Seymour CA (1976) Acid hydrolase activities and lysosomal integrity in liver biopsies from patients with iron overload. Clin Sci Mol Med 50: 75-78.

95. Seymour CA, Peters TJ (1978) Organelle pathology in primary and secondary haemochromatosis with special reference to lysosomal changes. Br J Haematol 40: 239-253.

96. Kurz T, Terman A, Gustafsson B, Brunk U (2008) Lysosomes in iron metabolism, ageing and apoptosis. Histochemistry and Cell Biology 129: 389-406.

97. Iancu TC, Shiloh H (1994) Morphologic observations in iron overload: an update. Adv Exp Med Biol 356: 255-265.

98. Terman A, Brunk UT (2004) Lipofuscin. The International Journal of Biochemistry & Cell Biology 36: 1400-1404.

99. Kalyanaraman B (2007) Iron signaling and oxidant damage. Cardiovascular Toxicology 7: 92-94.

100. Galaris D, Pantopoulos K (2008) Oxidative Stress and Iron Homeostasis: Mechanistic and Health Aspects. Critical Reviews in Clinical Laboratory Sciences 45: 1-23.

101. Pietrangelo A (1996) Metals, Oxidative Stress, and Hepatic Fibrogenesis. Semin Liver Dis 16: 13-30.

102. Britton RS (1996) Metal-Induced Hepatotoxicity. Semin Liver Dis 16: 3-12.

103. Poli G (2000) Pathogenesis of liver fibrosis: role of oxidative stress. Molecular Aspects of Medicine 21: 49-98.

104. Hübscher SG (2003) Iron overload, inflammation and fibrosis in genetic haemochromatosis. Journal of Hepatology 38: 521-525.

105. Pietrangelo A, Gualdi R, Casalgrandi G, Montosi G, Ventura E (1995) Molecular and cellular aspects of iron-induced hepatic cirrhosis in rodents. The Journal of Clinical Investigation 95: 1824-1831.

106. Penz-Österreicher M, Österreicher CH, Trauner M (2011) Fibrosis in Autoimmune and Cholestatic Liver Disease. Best Practice & Research Clinical Gastroenterology 25: 245-258.

107. Bataller R, Brenner DA (2005) Liver fibrosis. The Journal of Clinical Investigation 115: 209-218.

108. Hernandez-Gea V, Friedman SL (2011) Pathogenesis of Liver Fibrosis. Annual Review of Pathology: Mechanisms of Disease 6: 425-456.

109. Viatte L, Nicolas G, Lou D-Q, Bennoun M, Lesbordes-Brion J-C, et al. (2006) Chronic hepcidin induction causes hyposideremia and alters the pattern of cellular iron accumulation in hemochromatotic mice. Blood 107: 2952-2958.

110. Tao GZ, Li DH, Zhou Q, Toivola DM, Strnad P, et al. (2008) Monitoring of epithelial cell caspase activation via detection of durable keratin fragment formation. The Journal of Pathology 215: 164-174.

111. Wattiaux R, Wattiaux-De Coninck S, Ronveaux-dupal MF, Dubois F (1978) Isolation of rat liver lysosomes by isopycnic centrifugation in a metrizamide gradient. The Journal of Cell Biology 78: 349-368.

112. Strnad P, Tao GZ, Zhou Q, Harada M, Toivola DM, et al. (2008) Keratin Mutation Predisposes to Mouse Liver Fibrosis and Unmasks Differential Effects of the Carbon Tetrachloride and Thioacetamide Models. Gastroenterology 134: 1169-1179.

113. Desmet VJ, Gerber M, Hoofnagle JH, Manns M, Scheuer PJ (1994) Classification of chronic hepatitis: Diagnosis, grading and staging. Hepatology 19: 1513-1520.

114. Lunova M, Zizer E, Kucukoglu O, Schwarz C, Dillmann WH, et al. (2012) Hsp72 Overexpression Accelerates the Recovery from Caerulein-Induced Pancreatitis. PLoS ONE 7: e39972.

115. Walther P (2003) Cryo-Fracturing and Cryo-Planing for In-Lens Cryo-SEM, Using a Newly Designed Diamond Knife. Microscopy and Microanalysis 9: 279-285.

116. Rad AM, Janic B, Iskander AS, Soltanian-Zadeh H, Arbab AS (2007) Measurement of quantity of iron in magnetically labeled cells: comparison among different UV/VIS spectrometric methods. BioTechniques 43: 627–636.

117. Gosriwatana I, Loreal O, Lu S, Brissot P, Porter J, et al. (1999) Quantification of Non-Transferrin-Bound Iron in the Presence of Unsaturated Transferrin. Analytical Biochemistry 273: 212-220.

118. Lebeau A, Frank J, Biesalski HK, Weiss G, Srai SKS, et al. (2002) Long-term sequelae of HFE deletion in C57BL/6 × 129/O1a mice, an animal model for hereditary haemochromatosis. European Journal of Clinical Investigation 32: 603-612.

119. Fleming RE, Holden CC, Tomatsu S, Waheed A, Brunt EM, et al. (2001) Mouse strain differences determine severity of iron accumulation in Hfe knockout model of hereditary hemochromatosis. Proceedings of the National Academy of Sciences 98: 2707-2711.

120. Kautz L, Meynard D, Besson-Fournier C, Darnaud V, Al Saati T, et al. (2009) BMP/Smad signaling is not enhanced in Hfe-deficient mice despite increased Bmp6 expression. Blood 114: 2515-2520.

121. Ramos E, Kautz L, Rodriguez R, Hansen M, Gabayan V, et al. (2011) Evidence for distinct pathways of hepcidin regulation by acute and chronic iron loading in mice. Hepatology 53: 1333-1341.

122. Meynard D, Kautz L, Darnaud V, Canonne-Hergaux F, Coppin H, et al. (2009) Lack of the bone morphogenetic protein BMP6 induces massive iron overload. Nat Genet 41: 478-481.

123. Levy JE, Montross LK, Cohen DE, Fleming MD, Andrews NC (1999) The C282Y Mutation Causing Hereditary Hemochromatosis Does Not Produce a Null Allele. Blood 94: 9-11.

124. Valerio Jr LG, Petersen DR (2000) Characterization of Hepatic Iron Overload Following Dietary Administration of Dicyclopentadienyl Iron (Ferrocene) to Mice: Cellular, Biochemical, and Molecular Aspects. Experimental and Molecular Pathology 68: 1-12.

125. Dexter DT, Ward RJ, Florence A, Jenner P, Crichton RR (1999) Effects of desferrithiocin and its derivatives on peripheral iron and striatal dopamine and 5-hydroxytryptamine metabolism in the ferrocene-loaded rat. Biochemical Pharmacology 58: 151-155.

126. Golberg L, Smith JP, Martin LE (1957) The effects of intensive and prolonged administration of iron parenterally in animals. Br J Exp Pathol 38: 297-311.

127. Richter GW (1974) Effects of cyclic starvation-feeding and of splenectomy on the development of hemosiderosis in rat livers. Am J Pathol 74: 481-506.

128. Ramm GA (2000) Hemochromatosis: Cambridge University Press.

129. Moon S, Han J, Hwang H, Kim M, Lee S, et al. (2011) Establishment of Secondary Iron Overloaded Mouse Model: Evaluation of Cardiac Function and Analysis According to Iron Concentration. Pediatric Cardiology 32: 947-952.

130. Olynyk JK, Luxon BA, Britton RS, Bacon BR (1998) Hepatic iron concentration in hereditary hemochromatosis does not saturate or accurately predict phlebotomy requirements. Am J Gastroenterol 93: 346-350.

131. Bacon BR, Adams PC, Kowdley KV, Powell LW, Tavill AS (2011) Diagnosis and management of hemochromatosis: 2011 Practice Guideline by the American Association for the Study of Liver Diseases. Hepatology 54: 328-343.

132. Frazer DM, Anderson GJ, Ramm GA, Subramaniam VN, Powell LW (2008) How much iron is too much? Expert Review of Gastroenterology & Hepatology 2: 287-290.

133. Deugnier Y, Turlin B (2007) Pathology of hepatic iron overload. World J Gastroenterol 13: 4755-4760.

134. Ramm GA, Crawford DHG, Powell LW, Walker NI, Fletcher LM, et al. (1997) Hepatic stellate cell activation in genetic haemochromatosis: Lobular distribution, effect of increasing hepatic iron and response to phlebotomy. Journal of hepatology 26: 584-592.

135. Adams PC (1990) Hepatic iron in hemochromatosis. Dig Dis Sci 35: 690-692.

136. Adams PC (2001) Is there a threshold of hepatic iron concentration that leads to cirrhosis in C282Y hemochromatosis? Am J Gastroenterol 96: 567-569.

137. Waalen J, Felitti VJ, Gelbart T, Beutler E (2008) Screening for hemochromatosis by measuring ferritin levels: a more effective approach. Blood 111: 3373-3376.

138. Allen KJ, Bertalli NA, Osborne NJ, Constantine CC, Delatycki MB, et al. (2010) HFE Cys282Tyr homozygotes with serum ferritin concentrations below 1000 μg/L are at low risk of hemochromatosis. Hepatology 52: 925-933.

139. Jacobs EMG, Hendriks JCM, van Deursen CTBM, Kreeftenberg HG, de Vries RA, et al. (2009) Severity of iron overload of proband determines serum ferritin levels in families with HFE-related hemochromatosis: The HEmochromatosis FAmily Study. Journal of Hepatology 50: 174-183.

140. Pietrangelo A (2003) "Haemochromatosis.". Gut 52: ii23-ii30.

141. Maxwell KL, Kowdley KV (2012) Metals and the liver. Current Opinion in Gastroenterology 28: 217-222.

142. Barton JC, Barton JC, Acton RT, So J, Chan S, et al. (2012) Increased Risk of Death From Iron Overload Among 422 Treated Probands With HFE Hemochromatosis and Serum Levels of Ferritin Greater Than 1000 µg/L at Diagnosis. Clinical gastroenterology and hepatology : the official clinical practice journal of the American Gastroenterological Association 10: 412-416.

143. Breuer W, Ronson A, Slotki IN, Abramov A, Hershko C, et al. (2000) The assessment of serum nontransferrin-bound iron in chelation therapy and iron supplementation. Blood 95: 2975-2982.

144. Delima RD, Chua ACG, Tirnitz-Parker JEE, Gan EK, Croft KD, et al. (2012) Disruption of hemochromatosis protein and transferrin receptor 2 causes iron-induced liver injury in mice. Hepatology 56: 585-593.

145. McNamara L, Macphail A, Mandishona E, Bloom P, Paterson A, et al. (1999) Non-transferrin-bound iron and hepatic dysfunction in African dietary iron overload. Journal of Gastroenterology and Hepatology 14: 126-132.

146. Brunt EM (2005) Pathology of Hepatic Iron Overload. Semin Liver Dis 25: 392-401.

147. Bridle KR, Crawford DHG, Fletcher LM, Smith JL, Powell LW, et al. (2003) Evidence for a sub-morphological inflammatory process in the liver in haemochromatosis. Journal of Hepatology 38: 426-433.

148. Ganz T (2012) Macrophages and Systemic Iron Homeostasis. Journal of Innate Immunity 4: 446-453.

149. Pietrangelo A (1998) Iron, oxidative stress and liver fibrogenesis. J Hepatol 1: 8-13.

150. Bhavnani M, Lloyd D, Bhattacharyya A, Marples J, Elton P, et al. (2000) Screening for genetic haemochromatosis in blood samples with raised alanine aminotransferase. Gut 46: 707-710.

151. Allen KJ, Gurrin LC, Constantine CC, Osborne NJ, Delatycki MB, et al. (2008) Iron-Overload–Related Disease in HFE Hereditary Hemochromatosis. New England Journal of Medicine 358: 221-230.

152. Lin E, Adams PC (1991) Biochemical liver profile in hemochromatosis. A survey of 100 patients. J Clin Gastroenterol 13: 316-320.

153. Philippe MA, Ruddell RG, Ramm GA (2007) Role of iron in hepatic fibrosis: one piece in the puzzle. World J Gastroenterol 13: 4746-4754.

154. Takehara T, Tatsumi T, Suzuki T, Rucker Iii EB, Hennighausen L, et al. (2004) Hepatocyte-specific disruption of Bcl-xL leads to continuous hepatocyte apoptosis and liver fibrotic responses. Gastroenterology 127: 1189-1197.

155. Zhao M, Laissue JA, Zimmermann A (1997) Hepatocyte apoptosis in hepatic iron overload diseases. Histol Histopathol 12: 367-374.

156. Olynyk JK, Trinder D, Ramm GA, Britton RS, Bacon BR (2008) Hereditary hemochromatosis in the post-HFE era. Hepatology 48: 991-1001.

157. Gao B, Bataller R (2011) Alcoholic Liver Disease: Pathogenesis and New Therapeutic Targets. Gastroenterology 141: 1572-1585.

158. Hentze MW, Muckenthaler MU, Galy B, Camaschella C (2010) Two to Tango: Regulation of Mammalian Iron Metabolism. Cell 142: 24-38.

159. LeSage GD, Kost LJ, Barham SS, LaRusso NF (1986) Biliary excretion of iron from hepatocyte lysosomes in the rat. A major excretory pathway in experimental iron overload. The Journal of Clinical Investigation 77: 90-97.

160. Terman A, Kurz T (2012) Lysosomal Iron, Iron Chelation, and Cell Death. Antioxid Redox Signal 9: 9.

161. Myers BM, Prendergast FG, Holman R, Kuntz SM, LaRusso NF (1991) Alterations in the structure, physicochemical properties, and pH of hepatocyte lysosomes in experimental iron overload. The Journal of Clinical Investigation 88: 1207-1215.

162. Ward RJ, Florence AL, Baldwin D, Abiaka C, Roland F, et al. (1991) Biochemical and biophysical investigations of the ferrocene-iron-loaded rat. European Journal of Biochemistry 202: 405-410.

163. Stal P, Glaumann H, Hultcrantz R (1990) Liver cell damage and lysosomal iron storage in patients with idiopathic hemochromatosis. A light and electron microscopic study. J Hepatol 11: 172-180.

164. Iancu TC, Deugnier Y, Halliday JW, Powell LW, Brissot P (1997) Ultrastructural sequences during liver iron overload in genetic hemochromatosis. Journal of Hepatology 27: 628-638.

165. Peters TJ, Selden C, Seymour CA (1976) Lysosomal disruption in the pathogenesis of hepatic damage in primary and secondary haemochromatosis. Ciba Found Symp 9: 317-329.

166. Sebastiani G, Pantopoulos K (2011) Disorders associated with systemic or local iron overload: from pathophysiology to clinical practice. Metallomics 3: 971-986.

167. Ganz T, Nemeth E (2012) Iron Metabolism: Interactions with Normal and Disordered Erythropoiesis. Cold Spring Harbor Perspectives in Medicine 2: a011668.

168. Ramm G, Ruddell R (2010) Iron homeostasis, hepatocellular injury, and fibrogenesis in hemochromatosis: the role of inflammation in a noninflammatory liver disease. Seminars in liver disease 30: 271-287.

169. Baumgartner HK, Gerasimenko JV, Thorne C, Ashurst LH, Barrow SL, et al. (2007) Caspase-8-mediated apoptosis induced by oxidative stress is independent of the intrinsic pathway and dependent on cathepsins. American Journal of Physiology - Gastrointestinal and Liver Physiology 293: G296-G307.

170. Bröker LE, Huisman C, Span SW, Rodriguez JA, Kruyt FAE, et al. (2004) Cathepsin B Mediates Caspase-Independent Cell Death Induced by Microtubule Stabilizing Agents in Non-Small Cell Lung Cancer Cells. Cancer Research 64: 27-30.

171. Canbay A, Guicciardi ME, Higuchi H, Feldstein A, Bronk SF, et al. (2003) Cathepsin B inactivation attenuates hepatic injury and fibrosis during cholestasis. The Journal of Clinical Investigation 112: 152-159.

172. Moles A, Tarrats N, Fernández-Checa JC, Marí M (2009) Cathepsins B and D drive hepatic stellate cell proliferation and promote their fibrogenic potential. Hepatology 49: 1297-1307.

173. Platt FM, Boland B, van der Spoel AC (2012) Lysosomal storage disorders: The cellular impact of lysosomal dysfunction. The Journal of Cell Biology 199: 723-734.

174. Subramanian K, Balch WE (2008) NPC1/NPC2 function as a tag team duo to mobilize cholesterol. Proceedings of the National Academy of Sciences 105: 15223-15224.

175. Beltroy EP, Richardson JA, Horton JD, Turley SD, Dietschy JM (2005) Cholesterol accumulation and liver cell death in mice with Niemann-Pick type C disease. Hepatology 42: 886-893.

176. Cluzeau CVM, Watkins-Chow DE, Fu R, Borate B, Yanjanin N, et al. (2012) Microarray expression analysis and identification of serum biomarkers for Niemann–Pick disease, type C1. Human Molecular Genetics 21: 3632-3646.

177. Alam MS, Getz M, Safeukui I, Yi S, Tamez P, et al. (2012) Genomic Expression Analyses Reveal Lysosomal, Innate Immunity Proteins, as Disease Correlates in Murine Models of a Lysosomal Storage Disorder. PLoS ONE 7: e48273.

178. Iancu TC, Neustein HB, Landing BH (1976) The liver in thalassaemia major: ultrastructural observations. Ciba Found Symp 9: 293-316.

179. Svegliati Baroni G, D'Ambrosio L, Ferretti G, Casini A, Di Sario A, et al. (1998) Fibrogenic effect of oxidative stress on rat hepatic stellate cells. Hepatology 27: 720-726.

180. Yachie A, Niida Y, Wada T, Igarashi N, Kaneda H, et al. (1999) Oxidative stress causes enhanced endothelial cell injury in human heme oxygenase-1 deficiency. The Journal of Clinical Investigation 103: 129-135.

8 Curriculum Vitae
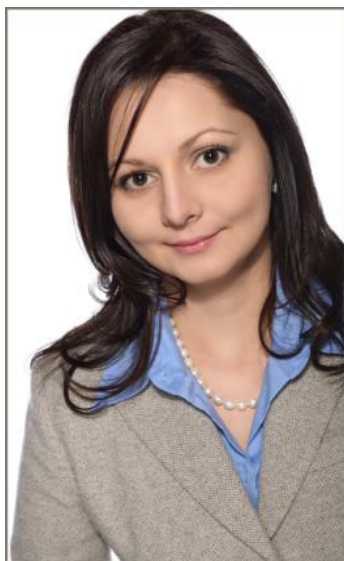
Name:	Lunova, Mariia
Current Position:	Ph.D student in the group of PD Dr. Pavel Strnad
Birth date:	July 13, 1985
Working address:	Clinic for Internal Medicine, University Hospital Ulm Albert Einstein Allee 23, D-89081 Ulm, Germany
Telefone:	working +49 (731) 500-44 553 Mobile +49 176 638 49 590

Education

6/2009- present **Ph.D student** in Clinic for Internal Medicine I Ulm, Internal medicine I, AG Strnad.

2/2009-6/2009 Volunteered in Institute of Natural Products and Clinical Pharmacology.

2007-12/2008 Worked in Ukraine as leading analyst of research laboratory at the plant "Artemovsk Winery".

2007 **Master Degree** in Chemical Sciences, Donetsk National University, Department of Organic Chemistry, Donetsk, Ukraine.

2006 **Bachelor Degree** in Chemical Sciences. Donetsk National University, Department of Organic Chemistry, Donetsk, Ukraine.

2002-2007 Student of Chemical faculty of Donetsk National University, Department of Organic Chemistry.

2002 Graduation in natural sciences class of secondary school №5 Artemosk, Ukraine.

Working experience

2009- present PhD student in Clinic for Internal Medicine I Ulm

2/2009 Volunteered in Institute of Natural products and clinical Pharmacology, Ulm.

2007-2008   Leading analyst of research laboratory at the plant "Artemovsk Winery", Artemovsk, Ukraine.

2006   Analyst of the research laboratory in research institute "Institute of physic and organic chemistry" department of "Physic and organic carbon compounds"", Donetsk, Ukraine.

2005   Analyst of laboratory of the confectionery "Kiev-Konty", Donetsk, Ukraine.

Honors and Awards

2013   Fellowship, 48th Annual Meeting of the European Association for the Study of the Liver, Amsterdam, Netherlands

2013   Honored member of EASL society 2013

2012   Fellowship, 47th Annual Meeting of the European Association for the Study of the Liver, Barcelona, Spain

2012   Honoured member of EASL society 2012

2012   Honoured member of Hepatology society 2012

2011   Fellowship, ''The Role of Notch Signalling, Intermediate Filaments and Cell Vesicle Trafficking in Cell Differentiation'', Sweeden

2007   Award "Best Scientific Work of University Students", The National Academy of Sciences of Ukraine

2001   Winner "Scientific Works in Medicine", High School Student Competition of all secondary schools of Ukraine

Research Interests

- To study the relationship between human disorders and animal models of liver disease, pancreatitis, and colitis, using different animal models, to find the potential mechanisms and corresponding treatments.

- Clinical studies of genetic disorders. Genetic mutations in human iron overload diseases

- The role of hepcidin in liver iron metabolism

- The role of heat shock proteins on pancreatitis and inflammatory liver diseases

Publications

1. Usachov V, Nahon P, **Lunova M**, Ziol M, Rufat P, Sutton A, Beaugrand M, Strnad P. Keratin 8 variants are infrequent in patients with alcohol-related liver cirrhosis and do not associate with development of hepatocellular carcinoma. BMC Gastroenterol. 2012 Oct 18;12(1):147.

2. **Lunova M**, Zizer E, Kucukoglu O, Schwarz C, Dillmann WH, Wagner M, Strnad P. Hsp72 overexpression accelerates the recovery from caerulein-induced pancreatitis. PLoS One. 2012;7(7):e39972. Epub 2012 Jul 5.

3. Strnad P, Kucukoglu O, **Lunova M**, Guldiken N, Lienau TC, Stickel F, Omary MB. Non-coding keratin variants associate with liver fibrosis progression in patients with hemochromatosis. PLoS One. 2012;7(3):e32669. Epub 2012 Mar 7.

4. **M Lunova**, S Vaulont, J Haybaeck, C. Lackner, P Strnad. Hepcidin knockout mice as a model of iron – overload associated liver fibrosis development. Journal of Hepatology vol. 56 April, 2012. p. S154-S155

5. **M. Lunova**, S Vaulont, J Haybaeck, C. Lackner, P Strnad. Hepcidin knockout mice as a model of iron-overload associated liver disease. Hepatology. 2011; volume 54, Suplement:1, pages: 928A-928A.

Selected presentations

1. **M. Lunova**, U. Wilgelmson, M. Pekny, P.Strnad. ''Loss of GFAP / Vimentin protects from DSS – induced colitis. The Role of Notch Signaling, Intermediate Filaments and Cell Vesicle Trafficking in Cell Differentiation'', GOTEBORG 2011

2. **M. Lunova**, K. Mueller, S. Vaulont, J. Haybaeck, C. Lackner, C. Trautwein, P. Strnad. "Hepcidin knockout mice develop chronic liver injury and liver fibrosis as a consequence of lysosomal iron overload", EASL 2013, Amsterdam, Netherlands

Selected posters

1. **M. Lunova**, K. Mueller, S. Vaulont, J. Haybaeck, C. Lackner, C. Trautwein, P. Strnad. Hepcidin knockout mice develop chronic liver injury and liver fibrosis as a consequence of lysosomal iron overload. GASL 2013, Hannover

2. **M Lunova**, S Vaulont, J Haybaeck, C. Lackner , P Strnad. Hepcidin knockout mice as a model of iron-overload associated liver disease. GASL 2012

3. **M. Lunova**, S Vaulont, J Haybaeck, C. Lackner, P Strnad. Hepcidin knockout mice as a model of iron-overload associated liver disease. Gastroenterologie, Viszeralchirurgie, Viszeralmedizin, 14-17 September 2011, Leipzig

4. **M. Lunova**, S Vaulont, J Haybaeck, C. Lackner , P Strnad. Hepcidin knockout mice as a model of iron-overload associated liver disease. GASL 2011

5. **M. Lunova**, U. Wilgelmson, M. Pekny, P.Strnad. ''Loss of GFAP / Vimentin protects from DSS – induced colitis. The Role of Notch Signaling, Intermediate Filaments and Cell Vesicle Trafficking in Cell Differentiation'', GOTEBORG 2011

6. Pavel Strnad, Özlem Kücükoglu, **Mariia Lunova**, Tim C. Lienau, Felix Stickel, M. Bishr Omary. ''Non-coding keratin variants associate with fibrosis progression in hemochromatosis patients. GASL 2011

7. **M. Lunova**, Özlem Kücükoglu, Eugen Zizer, Guido Adler, Martin Wagner, Pavel Strnad. Genetic Hsp72 overexpression accelerates recovery from caerulein-induced pancreatitis. Inflammatory Mechanisms and Functional Gastrointestinal Diseases: Implications for Pathophysiology, Diagnosis and Therapy, June 4th-5th, 2010, Berlin

8. P. Strnad, O. Kucukoglu, **M. Lunova**, Tim C. Lienau, Felix Stickel, M. Bishr Omary. Keratin variants associate with fibrosis progression in hemochromatosis patients. January Amsterdam, 2010

Reviewing work

2012 reviewer in Journal of Experimental Lung Research

Other activities

2004-2007 Leader of the Students Scientific Association of the Faculty of Chemistry, Donetsk National University

2005 Part-time teacher of biology and chemistry, "Erydit" school, Donetsk, Ukraine

Skils

1. Extensive expertise in animal models of human gastroenterological diseases (liver, pancreas, colon)

2. Isolation of primary cells, work with cell culture

3. Nucleic acid methods: PCR and Q-PCR, DHPLC, analysing of microarray data

4. Biochemical assays: Western Blot, ELISA, MPO measurement, oxidative stress assays, XTT/MTT cytotoxicity, immunochistochemistry and immunofluorescence, histology staining (H&E, Sirius Red, Prussian Blue), detection of iron and NonTransferinBound iron, subcellular fractionation.

5. Computer skills: MathCad, Statistica, Origin, HyperChem, ChemOffice, Sigma Plot, ImageJ, MS Office (MS-Word, MS- Excel, MS- Access, MS Power- Point etc.).

Languages

English (fluently), Russian (native), Ukrainian (native), German (limited speaking and writing skills).

References

PD Dr. Pavel Strnad

Department of Medicine III,

University Hospital Aachen,

Aachen, Germany

Tel.: +49 0241-8035324

email : **pstrnad@ukaachen.de**

Prof Dr. Thomas Simmet

Institute of Natural Products

and Clinical Pharmacology

Helmholtzstraße 20 D-89081 Ulm

Tel: (0731) 500-65600 Fax: (0731) 500-65602

email: thomas.simmet@uni-ulm.de

9 Acknowledgments

I could not imagine that time can go so fast and I am already writing this last chapter of my thesis. It would not have been possible to write this doctoral thesis without the motivation, help and support of the kind people around me.

First of all, I would like to thank my advisor PD Dr. Pavel Strnad for the great support, helpful guidance, motivation and patience all the time during my PhD work. His knowledge and advice have helped me to keep on track and work at a smooth pace.

I will newer forget huge help of Claudia Laengle, Caroline Schwarz and Claudia Goehring. In addition, I would like to thank to all of my colleagues which are still in Ulm (Nurdan, Özlem, Peggy, Elke, Anke and Katrin) and to colleagues which moved to Aachen (Kateryna, Yu Chen and Valentyn) for great time together.

I would like to thank to my family, which is now in Ukraine, and to my husband Oleg, for their understanding, patience and support.

I dedicate this thesis to my family (my husband Oleg, my mother Margarita, my father Victor and my brother Sergey) which was always with me and gave moral support.